Spring 2002

Magnetoacoustic chemical sensors based on swellable polymer microspheres

Huqun Liu
University of New Hampshire, Durham

INFORMATION TO USERS

This manuscript has been reproduced from the microfilm master. UMI films the text directly from the original or copy submitted. Thus, some thesis and dissertation copies are in typewriter face, while others may be from any type of computer printer.

The quality of this reproduction is dependent upon the quality of the copy submitted. Broken or indistinct print, colored or poor quality illustrations and photographs, print bleedthrough, substandard margins, and improper alignment can adversely affect reproduction.

In the unlikely event that the author did not send UMI a complete manuscript and there are missing pages, these will be noted. Also, if unauthorized copyright material had to be removed, a note will indicate the deletion.

Oversize materials (e.g., maps, drawings, charts) are reproduced by sectioning the original, beginning at the upper left-hand corner and continuing from left to right in equal sections with small overlaps.

Photographs included in the original manuscript have been reproduced xerographically in this copy. Higher quality 6" x 9" black and white photographic prints are available for any photographs or illustrations appearing in this copy for an additional charge. Contact UMI directly to order.

UMI®

MAGNETOACOUSTIC CHEMICAL SENSORS
BASED ON SWELLABLE POLYMER MICROSPHERES

By

Huqun Liu
B.S., Tianjin University, P. R. China, 1991
M.S., Tianjin University, P. R. China, 1996

DISSERTATION

Submitted to the University of New Hampshire
in Partial Fulfillment of
the Requirements for the Degree of

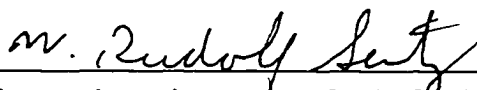Doctor of Philosophy

in

Chemistry

May, 2002

UMI Number: 3045333

UMI®
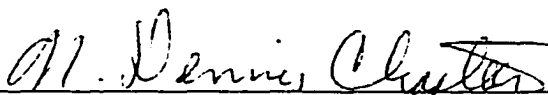
This dissertation has been examined and approved.

_____

Dissertation Director, W. Rudolf Seitz
Professor of Chemistry

_____
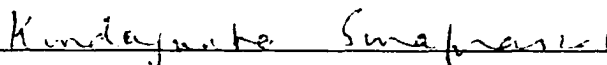
Vernon Reinhold
Professor of Chemistry

_____
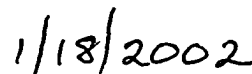
N. Dennis Chasteen
Professor of Chemistry

_____

Joseph D. Geiser
Assistant Professor of Chemistry

_____

Kondagunta Sivaprasad
Professor of Electrical and Computer Engineering

_____
1/18/2002
Date

DEDICATION

This dissertation is dedicated

to my parents, Xijie Liu and Chunhua Zhang,

my parents-in-law, Shaorong Chen and Yuanjun Zhang,

and especially to my wife, Lan Chen and our soon-to-be baby,

for their love and support.

iii

ACKNOWLEDGEMENTS

I would like to express my sincere appreciation to my research advisor, Professor W. Rudolf Seitz for his guidance, support, and encouragement throughout my years at UNH. It is he who helped me make all the important decisions.

I wish to thank the following:

Dr. Craig A. Grimes of Pennsylvania State University for developing and providing the Resonance Meter and K. G. Ong and P. G. Stoyanov for their help in instrument operation.

Nancy Cherim, UNH Instrument Center, for her help with Scanning Electron Microscopy and CHN.

Dr. Todd S. Gross in the Department of Mechanical Engineering for his help with Dynamic Mechanical Analyzer.

Edward T. Norton Jr. in the Material Science Program for his help with Alpha-Step 100 to measure film thickness.

the technicians in the Space Center Machine Shop at UNH for making the parts of the spectrometer and the Resonance Meter.

Professor Hongxiu Yang and Professor Zhujun Zhang, my advisors in the People's Republic of China, for their guidance and education in science.

my committee members, all other faculty and staff in the Chemistry Department, especially Cindi Rohwer, Peggy Torch, Amy Lindsay, Bob Constantine, and Sabrina Kirwan for their support and encouragement.

all my labmates, past and present, and my friends in New Hampshire.

Finally, my special thanks go to my wife for her love, understanding, and caring support.

TABLE OF CONTENTS

v

LIST OF TABLES

LIST OF FIGURES

x

ABSTRACT

MAGNETOACOUSTIC CHEMICAL SENSORS

BASED ON SWELLABLE POLYMER MICROSPHERES

By

Huqun Liu
University of New Hampshire, May 2002

The goal of this dissertation was to investigate chemical applications of magnetoacoustic sensors based on swellable polymer microspheres. The magnetoacoustic sensor was used to monitor viscosity of starch solution, water loading, and 2-hydroxyethyl methacrylate polymerization.

Poly(vinylbenzyl chloride) (polyVBC) microspheres were prepared by suspension polymerization and then derivatized to introduce dicarboxylate groups onto the polymer backbone. Poly(vinylbenzyl chloride-trichlorophenyl acrylate) (polyVBC-TCPA) microspheres were prepared by dispersion polymerization and then derivatized to introduce amine groups onto the polymer backbone. These derivatized polymer microspheres swell and shrink with changing pH. They were entrapped in a hydrogel membrane and the membrane turbidity was investigated by UV/Vis spectrophotometry. Membrane turbidity increased with pH from 6.0 to 8.0 for entrapped aminated polyVBC-TCPA microspheres, and decreased with pH from 2.0 to 8.0 for entrapped dicarboxylated

polyVBC microspheres. The change in turbidity with pH was subject to hysteresis that decreased with increasing water content of the hydrogel membrane.

A magnetoelastic ribbon coated with a layer of hydrogel membrane with entrapped aminated polyVBC-TCPA or dicarboxylated polyVBC microspheres was used to monitor pH. A thin layer of polyurethane was pre-coated on the ribbon to prevent it from rusting and increase its adhesion to the pH sensitive membrane. The resonance frequency of the sensor increased as pH changed from 6.0 to 8.0 when aminated polyVBC-TCPA microspheres were used, or decreased as pH changed from 2.0 to 8.0 when dicarboxylated polyVBC microspheres were used. The magnitude of the frequency shift was linearly proportional to the particle concentration in the hydrogel membrane.

Poly(vinyl alcohol) (PVA) and HYPAN hydrogels were used to make hydrogel membranes. HYPAN hydrogels are hydrophilic acrylate derivatives. They are good for magnetoacoustic sensors due to their high water content, high mechanical strength, and good adhesion to the polyurethane coated ribbon.

The new magnetoacoustic sensors do not require any physical connections to the sensing elements. They are ideally suited for applications where physical connections are undesired or not possible.

xv

CHAPTER 1

INTRODUCTION

1.1 Chemical Sensors

A sensor is a device that can continuously and reversibly record a physical parameter.[1,2] Although some devices called probes can be used only once, they have also been considered as sensors. If the recorded physical parameter is related to the quantity of a chemical species, this device is called a chemical sensor. An ideal chemical sensor can be used directly inside the sample and responds rapidly to concentration changes. There is growing interest in developing real-time, automatically operated chemical sensors.

Generally, a chemical sensor consists of a physical transducer and a chemically selective membrane, film or layer at the sensing tip.[3] The performance of the chemical sensor, such as sensitivity, lifetime, and response time, depends on the composition of the sensitive layer. Usually, ligands or functional groups that are contained in this sensitive layer recognize the analyte and produce signals. The recognition process can be a surface interaction or a bulk interaction depending on how the analytes partition between the sample phase and the sensor. Selectivity is defined as the ability of a sensor to respond to the analyte in the presence of other chemical species.

In the 1930s, the first true chemical sensor was developed. This was the glass electrode selective for hydronium ions. In the 1960s, other ion-selective electrodes and

1

semiconductor detectors appeared. In 1970, the ion-sensitive field-effect transistor

(ISFET) was developed through the union of microelectronics and chemical sensor

science. In 1980, Peterson introduced the first optical fiber sensor to detect changes in

pH. There are many advantages to optical fiber sensors, such as remote sensing. In

1982, a surface plasmon resonance sensor was used to analyze anesthetic gases. When a

sample gas absorbed on a gold coated sensor surface, the resonance angle shifted. In

1983, the first international conference on chemical sensors was held in Fukuoka. A

number of books, journal reviews, and conference proceedings that concentrate on

chemical sensors have been appeared since the mid- 1980s. Journals, such as *Sensors*

and Actuators B (chemical sensors) and *Biosensors and Bioelectronics*, are devoted to

sensor technologies.[4,5] A series of papers written by Janata[6] since 1988 has closely traced

the recent development of chemical sensors. They reviewed the new trends, features, and

distribution of effort in the entire chemical sensor field. Clearly, great progress in both

the theoretical and practical aspects of the chemical sensor field has been made and will

continue in the future.

1.2 Classification of Chemical Sensors

Generally, chemical sensors are classified according to the transduction principle

as thermal, electrochemical, optical, or mass sensors.[3] Sometimes, the term "acoustic

wave sensor" is used instead of "mass sensor", but it refers to the same kind of sensor.[4]

2

1.2.1 Thermal sensor

The analytical information obtained from thermal sensors is the heat absorbed or evolved by a chemical reaction. According to the first law of thermodynamics, the generated heat is related to the changes of the internal energy of the system. Usually the chemically sensitive layer is placed on the top of a thermal probe to measure the temperature changes of the sensing element or the heat flux through the sensing element. This is a nonequilibrium process and the measurement is taken in a steady-state situation.[3]

1.2.2 Electrochemical sensor

The analytical information obtained from electrochemical sensors is voltage, current, or conductivity. Therefore, electrochemical sensors are divided into potentiometric sensors that measure voltage, amperometric sensors that measure current, and conductimetric sensors that measure conductivity. These devices are the largest and oldest group of chemical sensors. Their measurement process is based on chemically modulated electrode reactions. The charge transport can be electronic, ionic, or mixed.[3]

1.2.3 Optical sensor

When light interacts with matter, it can be partially or totally transmitted. If it is absorbed, its intensity will decrease. It can be reflected, refracted, or scatted at an interface. It can also coupled to other nonoptical effects, for example, changes of temperature, pressure or electrical conductivity. All of the above phenomena can be used to design optical sensors. The general strategy is to guide the light beam out of the

3

spectrophotometer to interact with the sample and then back to the spectrophotometer for processing. A typical optical sensor consists of a source, monochromator, chopper, sample space, detector, and other modules. Light is guided with cylindrical optical fibers or planar waveguides between different modules.[2,3]

1.2.4 Mass sensor

Piezoelectric materials have the property of producing an electric potential if mechanical stress is applied. Conversely, these materials will mechanically deform if an electric potential is applied across them.[4] A wide range of technologies has used these two properties, such as quartz crystal oscillators in timepieces and strain gauges in seismometers. In chemistry, they have been used in microscopic devices to precisely position a probe and in mass sensors. Thompson and Stone have provided the history of the development of piezoelectric devices.[4] Based on their description, Table 1-1 summarizes landmarks in the development of acoustic wave devices, and Table 1-2 summarizes landmarks in the development of acoustic wave devices as chemical sensors. There are two kinds of acoustic wave chemical sensors: bulk acoustic wave (BAW) sensors and surface acoustic wave (SAW) sensors. They differ in their two-dimensional and three-dimensional structure. BAW sensors are also called thickness-shear mode (TSM) sensors and quartz crystal microbalance (QCM). King[7] first introduced the BAW sensor in 1964 as a detector in gas chromatography. Thompson[4,8] and co-workers reviewed the applications of BAW sensors in contact with gas and liquids. O'Sullivan and Guilbault[9] have reviewed commercial quartz crystal microbalances in an article that included theory, applications, and recent developments. Moreover, the main

4

commercially available quartz crystal microbalances were compared. Wohltjen and Dessy[10] first reported a gas sensor based on SAW in 1979. Kowalski[11,12] and co-workers first studied arrays of polymer-coated TSM resonators in 1986. Albert[13] and co-workers reviewed developments in this field. Grate[14] presented a more detailed review on acoustic wave microsensor arrays for vapor sensing.

The analytical information obtained with mass sensors is mass changes when chemical species interact with the sensors.[3] Therefore, mass sensors are sometimes called microbalances. However, standard scales and balances used in laboratories are not regarded as sensors. In recent years, it has been recognized that the response of the sensor is related to the properties of the film and their mass, for example, conductivity and elasticity of the deposited films on the sensor surface.[15,16] There are many advantages of mass sensors, such as small size, light weight, simplicity of construction and operation, low power requirement, high sensitivity, stability, and relatively low cost. Frequency shift measurements are very accurate compared with measurement of other physical parameters.[3] But the physics is so complex that it is sometimes difficult to obtain a simple relationship between the mass changes and the output signals. Especially in the liquid phase, frictional effects at the sensor-liquid interface in addition to the mass effects affect the energy loss which influences the output signal of the sensors.

Table 1-1.Landmarks in the development of acoustic wave devices

Year	Scientist	Landmark
1880	P. Curie; J. Curie	First announcement of confirmation of piezoelectricity by recording electrical effects through applying pressure on various crystals, including quartz
1881	W. G. Hankel	First introduce the term piezoelectricity
1881	G. Lippmann	Prediction of the converse piezoelectric effect
1881	P. Curie; J. Curie	Verification of crystal mechanical deformation through the application of electrical energy
1885	Lord Rayleigh	Confirmation of the existence of elastic vibrations of the surface of the surface of solid materials
1890	W. Voight	A rigorous theory involving electric vectors and elastic tensors
1893	Lord Kelvin	A theory of piezoelectricity based on thermodynamic concepts
1921	W. G. Cady	Produced the piezoelectric resonator
1937	A. Langevin; A. Moulin	One of the first piezoelectricity applications showed that piezoelectric plates emitted and received acoustic waves propagating under water. Led to ultrasonics as a discipline.
1950s		Development of bulk wave devices based on Love, Lamb, or Stonely waves
1960s		Combination of piezoelectricity with microelectronics
1965	R. M. White; F. W. Voltmer	Deposit interdigital transducer using photolithographic techniques on piezoelectric substrates to excite and couple surface waves. Initiated surface acoustic wave engineering

6

Table 1-2.Landmarks in the development of acoustic wave devices as chemical sensors

Year	Scientist	Landmark
1895	Marie and Pierre Curie	The first application of piezoelectric material as a chemical sensor, which was termed as "quartz electric balance", during the discovery of the new element radium
1959	G. Sauerbrey	Directly deposited films on the surface of a bulk acoustic wave (BAW) sensor. Introduced the Sauerbrey Equation.
1960s - 1970s	See Reference [10]	A number of gas phase and liquid phase theoretical models on BAW sensors were published.
1964	W. H. King	The first application of a BAW device as a selective analytical sensor.
1979	H. Wohltjen; R. Dessy	First application of a surface acoustic wave (SAW) chemical sensor with a deposited sorptive film
1980	T. Nomura; G. J.Bastiaans	Firstly successfully used a BAW sensor in contact with a liquid

7

1.2.4.1 Bulk acoustic wave sensor

Figure 1-1 shows the configuration of a quartz crystal microbalance with a pair of facing metal film electrodes placed on opposite sides of the crystal.[1,17] Thickness shear mode mechanical oscillations are excited between the electrodes and propagate through the bulk of the material. The oscillations are perpendicular to the parallel faces of the thin quartz crystal piezoelectric element. They cause the atomic displacements parallel to the crystal surface. The chemically sensitive films are placed on the surfaces of the crystal or the metal films where they interact with the species of interest to cause some change that can be detected by the sensor. These changes include mass, viscosity, and modulus. The sensor response is a result of the frequency shift. Sauerbrey[1,4] first quantitatively investigated the response of a BAW sensor. He found that the acoustic wavelength at resonance increased as the device thickness increases. Based on this, he derived the following relationship between the frequency shift and the mass change:

$$\Delta f = -\frac{2f_0^2}{\sqrt{\mu_s \rho_s}} * \frac{m_s}{A} \qquad (1\text{-}1)$$

In this relationship, Δf (Hz) is the frequency shift, f_0 (Hz) is the fundamental resonance frequency of the unloaded piezoelectric crystal, μ_s is the shear modulus of the crystal, ρ_s is the crystal density, A (cm^2) is the surface area of one face of the crystal, m_s is the total mass of the rigid thin film that deposited on the crystal. After calculating the constants and letting $\Delta M = m_s/A$, the following equation results:

$$\Delta f = -C_1 * \Delta M \qquad (1\text{-}2)$$

Equation (1-2) shows that the frequency shift is linearly proportional to the mass change. This is the reason that bulk acoustic wave sensors are also called quartz crystal

8

microbalances. The negative sign means that the frequency decreases as the added mass increases. The proportionality constant is calculated under the assumption that the film is thin and mechanically rigid enough to neglect any changes in these characteristics when it binds with analytes. Recently, a number of theoretical models have been published to consider the acoustic impedance of the added film.[17,18]

If the crystal is in contact with liquid, the viscosity of the liquid has to be considered. Kanazawa and Gordon[19-22] derived an equation to express the oscillation frequency shift of a quartz crystal when the quartz crystal contacts a liquid.

$$\Delta f = -f_0^{3/2} \left(\frac{\rho_l \eta_l}{\pi \mu \rho} \right)^{1/2} \qquad (1\text{-}3)$$

In this relationship, Δf is the resonance frequency shift, f_0 is the resonance frequency for the dry crystal, μ is the elastic modulus of the quartz crystal, ρ is the density of the quartz, η_l is the absolute viscosity of liquid, and ρ_l is the density of the liquid. Equation (1-3) considers the viscosity and density of the liquid, but not the interfacial effects.[23] Thompson[8] reviewed and compared a number of the bulk acoustic wave sensors in the liquid phase.

BAW sensors have been used for chemical vapor sensing by coating a sensitive film on the crystal surface. This film selectively binds the species of interest and causes its mass to change, which can be detected by the sensors.[24,25] Various gases in ambient air, such as sulfur dioxide, ammonia, hydrogen sulfide, hydrogen chloride, carbon monoxide, phosgene, have been detected using BAW sensors.[26] Recently molecularly imprinted polymers have been used as sensitive films.[27,28] Ji et al.[29,30] developed piezoelectric odor sensors to detect 2-methylisoborneol. Haupt et al.[31] developed an

9

selective acoustic sensor to detect S-propranolol. After coating the crystal with a layer of derivatized silica substrate with aminopolycarboxylate ligand, Cox[32] detected lead (II) and silver (I) in aqueous solution using a BAW sensor. Shana[22] fabricated a novel continuous flow cell to monitor liquid viscosity.

1.2.4.2 Surface acoustic wave sensors

In 1965 using photolithographic techniques, White and Voltmer[4] deposited interdigital transducers on piezoelectric substrates to excite and couple to elastic surface waves. This initiated the new field of surface acoustic wave engineering. The simplest form is to induce oscillating electrical fields between a pair of electrode fingers. This results in atomic displacement in a piezoelectric material of correct crystal orientation. The signal is a surface acoustic wave (SAW) that possesses longitudinal and shear components. A second interdigital transducer is used to detect the wave. Surface acoustic wave sensors have great design flexibility. Their sensing parts, which are the waveguides, are separate from the piezoelectric transducer/receiver. In 1979, the first SAW chemical sensor was developed.[10] Because the SAW sensors can be operated at a higher frequency, typically in a range from 30 to 160 MHz, they have higher mass sensitivity than bulk sensors.[1]

Figure 1-2 shows the configuration of a SAW sensor.[1,17] The input end is a pair of electrodes that are adjacent and separated by ¼ of the acoustical wavelength. An AC potential bias is applied between the electrodes to produce undulatory surface oscillations, i.e., surface waves. The oscillations propagate toward the output end that is a pair of electrodes similar to that in the input end. Their speed is determined by the

10

properties of the crystal and by the sample mass added on the crystal in the region between two sets of electrodes. Any changes in the surface wave propagation rate are detected as changes in the resonance frequency. The response of the sensor is given as:[33]

$$\Delta f = -\kappa C_m f_0^2 h \rho \qquad (1\text{-}4)$$

In this relationship, Δf is the frequency shift, f_0 is the unperturbed oscillation frequency, h is film thickness, and ρ is the film density. C_m is a constant representing the mass sensitivity of the device. $\kappa = 1$ when the entire surface area of the device is covered with a film. The film in equation (1-4) is thin, rigid, nonpiezoelectric, and nonconducting. Its thickness is small compared to the acoustical wavelength. If it is thicker, its elastic properties may affect the frequency shift.[33] The frequency shift may also be affected if the film has appreciable elasticity or the film elasticity changes after binding the target molecules.

SAW sensors have a wide variety of applications in analytical chemistry. Ballantine[1] studied the elastic properties of thin polymer films by varying temperatures spanning the polymer glass transition temperatures. Frye[1] studied thin-film properties, such as diffusion, surface area, and pore size distribution, by measuring the mass changes due to N_2 absorption on thin porous sol-gel glass films. Galipeau[34] studied water uptake and release using both cured and uncured polyimide films on the crystal surface. The results suggested the possibility of using a SAW sensor as a cure indicator and a humidity sensor. Many inorganic gases and organic vapors have been selectively detected with SAW sensors.[4] The future development of SAW sensors will proceed in several directions, such as reducing sensor noise and temperature drift, increasing sensitivity by using higher frequency SAW devices, and developing new selective films.[4]

11
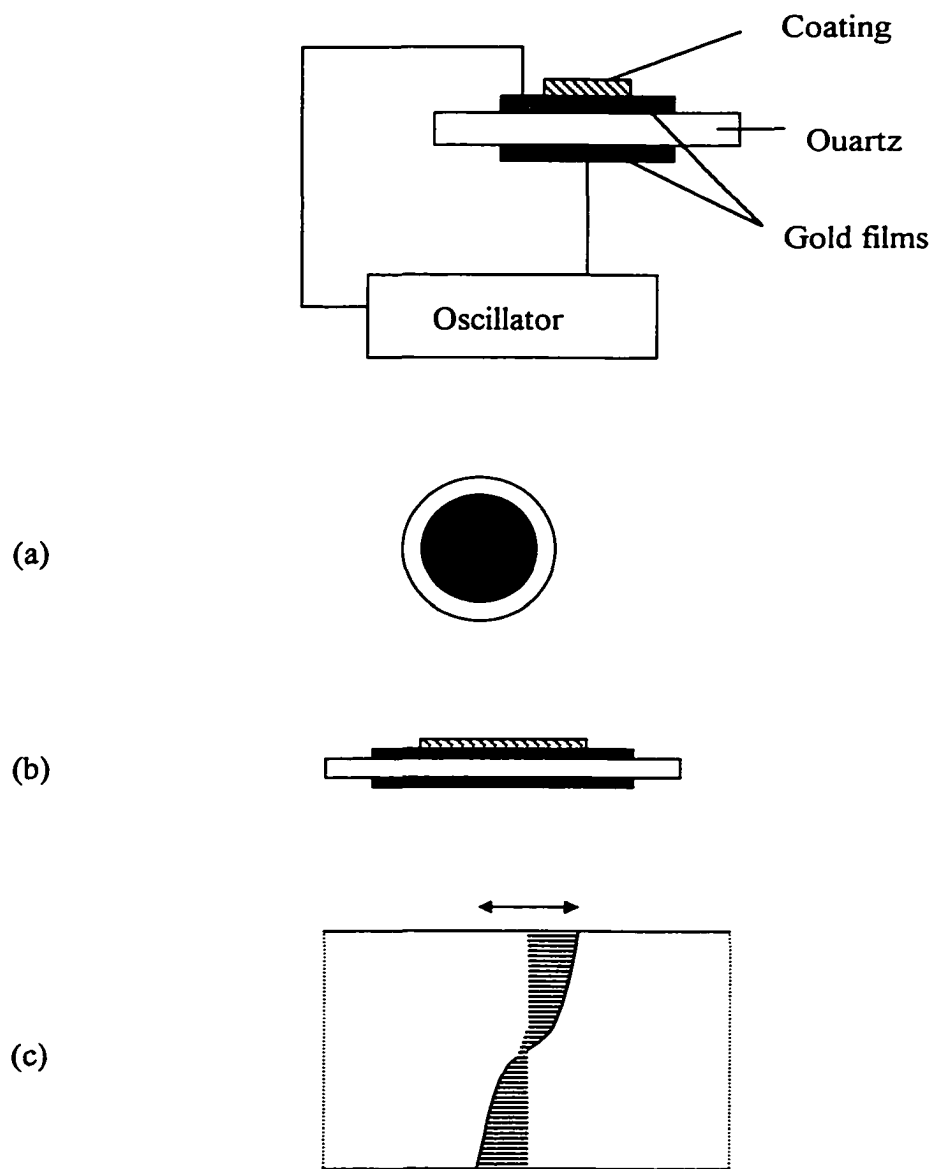
Figure 1-1 Quartz crystal microbalance configuration. (a) top view, (b) side view, (c) side view of wave mode

12

Input   Output

(a)

Selective layer

(b)

(c)
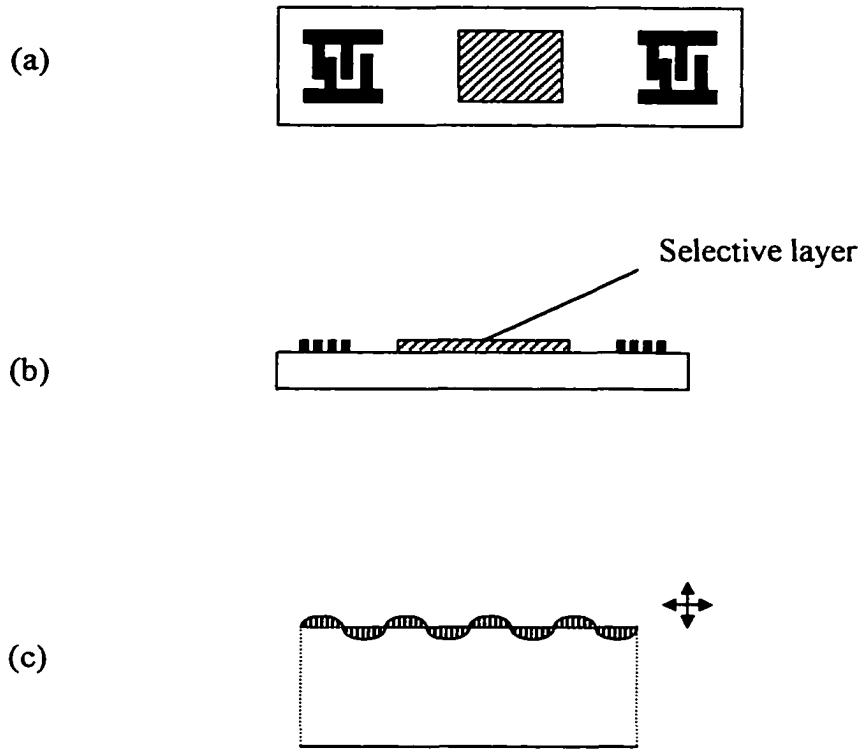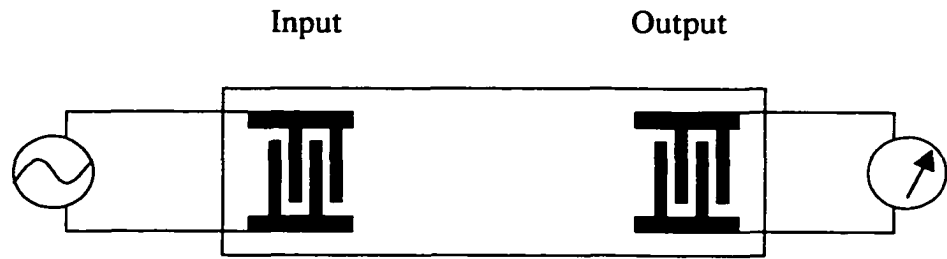
Figure 1-2 SAW sensor configuration. (a) top view, (b) side view, (c) side view of wave mode

13

1.3 Chemical Sensors Based on Polymer Swelling

A cross-linked polymer swells rather than dissolving in a compatible solvent. It reaches an equilibrium between the swelling forces arising from solvation and the retractive forces arising from the cross-linked polymer network. The extent of swelling depends on the affinity of the polymer backbone for the solvent if the polymer is uncharged. Additional swelling caused by the electrostatic repulsion forces should be considered if the polymer contains charged sites. Considering swelling as an osmotic pressure effect, the difference in the charge density of the polymer network and the solution is equalized by solvent entering the network. This occurs if the charge density on the polymer is higher than the charge density of the solution, i.e. the ionic strength.[35]

Seitz[35] has recently reviewed swellable polymer microspheres for chemical transduction. This kind of work has been carried out in our research group for several years.[36-40] Derivatized lightly cross-linker polymers swell and shrink as a function of analyte concentration. They can be prepared as membranes[41,42] or microspheres[43,44], and coupled to different transduction methods, such as optical fiber sensors based on changes in refractive index,[45-48] and pressure sensors based on changes in physical displacement.[49] Dispersion polymerization, suspension polymerization, and seeded emulsion polymerization have been used to prepare 0.3 to 3 μm diameter microspheres.[35] These microspheres include poly(vinylbenzyl chloride), (poly(4-acetoxy-styrene), and co-polymers of 2,4,5-trichlorophenylacrylate (TCPA) and vinylbenzyl chloride (VBC). The purpose of adding TCPA units into polyVBC microspheres is to increase hydrophilicity and porosity of the polymer after the microspheres are aminated. In this case, the chloromethyl group of VBC is converted to an amine that is pH sensitive. The TCPA is

14

converted to an amide that is hydrophilic, which causes the polymer to swell slightly in aqueous media introducing microporosity. Additional microporosity is introduced in the polymer after a small amine group displaces the large leaving group 2,4,5-trichlorophenol. Increasing microporosity and hydrophilicity in the backbone of the polymer results in fast diffusion of analyte in the microspheres, which in turn results in fast sensor response.[50]

Most of the chemical transducers in our group have been used for pH.[45-48] For example, polyVBC microspheres are derivatized with diethanolamine or diethylamine to introduce amine groups on the polymer backbone. The amine groups are protonated at low pH and deprotonated at high pH. If the derivatized microspheres are entrapped in a hydrogel membrane, in most cases, swelling causes the refractive index of the microsphere to decrease so that it is closer to the refractive index of the hydrogel membrane. This results in a decrease in membrane turbidity, which can be measured either as a change in transmitted or reflected intensity. Figure 1-3 illustrates the sensing principle.[35] For example, the hydrogel membrane is polyvinyl alcohol (PVA) with a refractive index of 1.34. The swellable microspheres are diethanolamine derivatized polyVBC. They swell in acid with a refractive index of 1.43 and shrink in base with a refractive index of 1.46. Because diethanolamine derivatized polyVBC microspheres swell over a pH range from 6.5 to 7.8, they can be used for many applications including biological measurements. Swellable polymers can also be implemented for metal ion sensing.[40] One approach is to change the charge density on the polymer backbone through binding with metal ions. Another approach is to combine ion pairing chemistry with polymer swelling. This is demonstrated using poly(4-hydroxy,3-nitrostyrene)

15

microspheres containing dibenzo-18-crown-6 (DB18C6) to detect potassium in a pH 7.0 buffer. The formation of potassium DB18C6 complex is accompanied by deprotonation of the hydroxy group on the polymer backbone, which causes the microspheres to swell.

In this dissertation, we explored the use of the swellable microspheres in magnetoacoustic sensors in collaboration with Dr. Craig Grimes and his research group at Pennsylvania State University. Figure 1-4 illustrates the sensing element configuration. A layer of hydrogel membrane containing swellable microspheres is coated on a magnetic ribbon that can be interrogated remotely. The polyurethane layer is used to prevent the ribbon from rusting and improves the adhesion of the hydrogel membrane to the ribbon. The changes of the magnetic properties of the ribbon during membrane swelling and shrinking are measured as a change of the frequency shift.
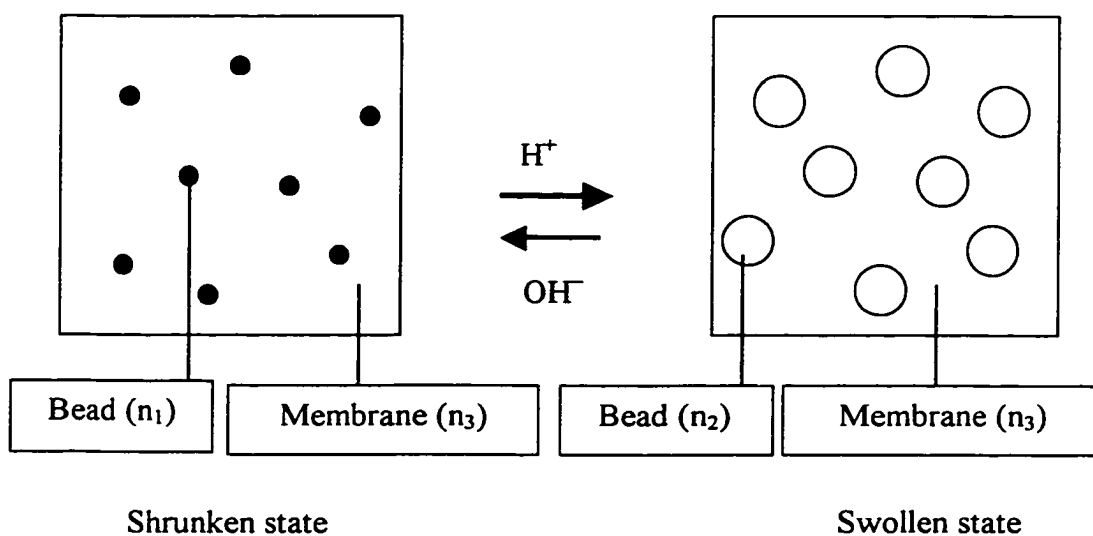
Figure 1-3 Schematic of sensing response mechanism. For diethanolamine derivatized polystyrene, n_1 and n_2 is 1.46 and 1.43, respectively. For PVA membrane, n_3 is 1.34.
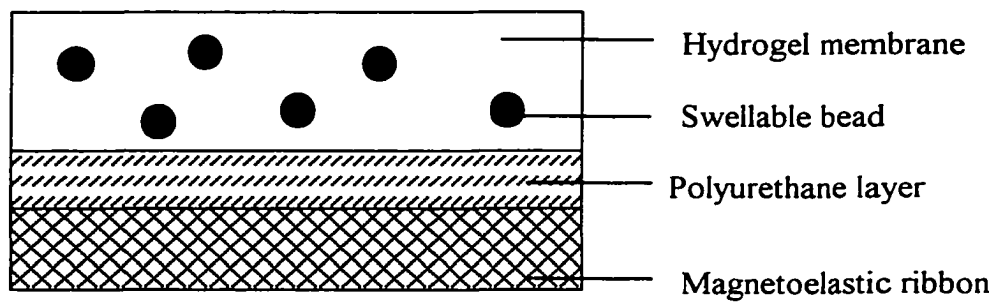
Figure 1-4 Side-view of the sensing element configuration for magnetoacoustic sensor

17

1.4 Summary of Work

The primary objective of my work was to develop a new kind of magnetoacoustic sensors to monitor pH. Because this is a completely new research field, we have compared the principles of magnetoacoustic sensors with those of acoustic wave sensors. Based on the introduction provided in this chapter, we know that some aspects of acoustic wave sensors have only recently been applied in the liquid phase. Therefore, we have proposed models to study possible factors affecting frequency shift with magnetoacoustic sensors. These models indicate that viscosity, mass loading, and configuration of the sensing element are all involved components. In configuring sensing elements, we should consider the types of pH sensing particles, modulus of the sensitive membranes, concentration of particles, types of hydrogel membranes, adhesion of the sensing membrane on the ribbon, thickness of sensitive membrane, corrosion of the ribbon, positions of the sensitive membranes on the ribbon, and ribbon bending that could be caused by swelling and shrinking of the sensitive membranes. One successful model is that used to monitor HEMA polymerization. The resonance frequency peaks disappear and appear according to our predictions.

Making pH sensitive microspheres is the first important step. These become the sensing reagents for the magnetoacoustic sensors. Two kinds of microspheres, polyTCPA-VBC containing amine groups and polyVBC containing carboxylic groups, were prepared by dispersion and suspension polymerization, respectively. A new technique called Shirasu Porous Glass (SPG) emulsification has been introduced to prepare a monomer emulsion. These pH sensitive microspheres are entrapped in a hydrogel to make a pH sensitive membrane. The optical properties of the membrane are

18

studied using UV/Vis spectrophotometer. Response is based on the change of the membrane turbidity that is caused by a change in the refractive index of the microspheres as they swell. If a magnetoelastic ribbon is coated with a layer of pH sensitive membrane, it can be used as chemical sensor to monitor pH.

In this dissertation, Chapter 2 provides the background on magnetoacoustic sensors, including theory and instrument setup. Background on polymer chemistry and radical polymerization techniques used in this dissertation are also discussed. Chapter 3 discusses experimental methods to make and study pH sensitive microspheres. Chapter 4 studies the optical properties of pH sensitive microspheres and the effects that hydrogel membranes have on the optical measurements. Chapter 5 considers the application of a resonance meter as a sensor for monitoring viscosity, mass changes, and polymerization. Many factors that affect the frequency shifts are studied in this chapter. Chapter 6 describes the results of using the resonance meter as a chemical sensor to monitor pH changes. The configuration of the sensor elements, sensor response, and frequency shift factors are all considered. Chapter 7 summaries the entire work of this dissertation. Appendix A, B, and C presents detailed information and operating instructions for the resonance meter.

19

CHAPTER 2

THEORY

2.1 Magnetoacoustic Chemical Sensors

When a time varying alternating-current (AC) magnetic field is applied to thick-film ribbons of magnetoelastic amorphous ferromagnetic alloys, the magnetic energy is converted into elastic energy that deforms the material greatest along the length of the ribbon. This mechanical deformation exhibits a resonance vibration at a frequency that is inversely proportional to the length of the ribbon. It also excites a magnetic flux inside magnetostrictive materials that are widely used as disposable identification and antitheft markers. Recently a new remote query sensor was developed using these magnetostrictive ribbons.[51] Figure 2-1 shows a schematic drawing of the sensor measurement system.[52,53] The whole system can be divided into two main circuits: the driving coil circuit and the pick-up coil circuit. The driving coil circuit consists of the signal generator, AC amplifier, ammeter, DC power supply, and a pair of driving coils. The driving coils include a pair of Helmholtz coils that apply a constant 5.5Oe DC field, and a pair of wire coils that apply a 50 mOe AC field sweeping over a pre-determined frequency range. The DC field is used to offset the ribbon's magnetic anisotropy and enhance the magnetoelastic properties of the sensor. All devices are controlled with a programmed computer. The magnetoelastic ribbon used as the sensing element is located in the test region, the center of the pick-up coil. Figure 2-2 illustrates the operational

20

principle of magnetoelastic sensors.[53] An externally applied AC magnetic field excites

magnetoelastic waves in the magnetostrictive ribbon, which, in turn, emits a magnetic

flux. The time rate of change of the emitted magnetic flux is monitored with a pick-up

coil. The response is transferred to a low noise preamplifier, lock-in amplifier, and the

computer. We measure the resonance frequency of the sensor instead of the relative

amplitude of the measured response. Figure 2-3 is a picture of the sensor measurement

system. The standing unit holds all meters. The driving coils and pick-up coil are placed

on the bench. Figure 2-4 is a picture of the driving coils, pick-up coil, and bucking coil.

The pair of big circles is the driving coils, including a pair of AC drive coils and a pair of

DC bias field coils. The upper square coil is the pick-up coil. The sample is placed in

the center of the pick-up coil.

A magnetoelastic resonance occurs when the frequency of the AC field is equal to

the frequency of the mechanical resonance of the sensor. For a thin, strip-like ribbon

vibrating in its basal plane the resonance frequency is given by[51]

$$f_n = \sqrt{\frac{E}{\rho(1-\sigma^2)}} * \frac{n\pi}{L} \qquad (2\text{-}1)$$
$$n = 1,2,3,\ldots\ldots$$

In this relationship, f_n is the resonance frequency, E is elastic modulus, ρ is the density of

the ribbon material, σ is the Poisson ratio, L is the long dimension of the ribbon, and n

denotes an integer. Elastic modulus is a ratio of the stress to the stain, which is a

measurement of the stiffness of the material. Stress δ is defined as the applied force F

per unit of area A in the x direction, in which direction the material is stretched. Strain ε is

defined as the length in the x direction (L-L_o) divided by the initial sample length L_o.

Their relationships are shown in the following equations:[54]

21

$$\delta = \frac{F}{A}$$

$$\varepsilon = \frac{L - L_0}{L_0} \qquad (2\text{-}2)$$

$$E = \frac{\delta}{\varepsilon}$$

The definition of Poisson ratio can be described as following. When a sample is stretched in the x direction, its cross-sectional area decreases. This means that the sample has a negative strain in the y direction, which is perpendicular to the stretching direction. Here the Poisson ratio σ is defined as the ratio of the strain in y direction to that in the x direction, shown in the equation:[54]

$$\sigma = -\frac{\varepsilon_y}{\varepsilon_x} \qquad (2\text{-}3)$$

In most cases, we only measured the fundamental resonance frequency where n is equal to 1 because of the larger amplitude. A mass load on the sensor surface also affects the resonance frequency of the magnetoacoustic sensor. Crimes and Stoyanov studied the response of the sensor to mass loading and derived the following relationship:[51,52]

$$\Delta f = -\frac{f_0}{2} * \frac{\Delta m}{M} \qquad (2\text{-}4)$$

In this case, $\Delta f \, (= f_n - f_0)$ is the frequency shift, f_0 is the resonant frequency of a bare sensor, M is the mass of the sensor, Δm is the mass loading that is less than M. $\Delta f < 0$ means that the frequency shift is downward.

When immersed in liquid, the frequency shift is correlated with the square root of the liquid viscosity and density product as shown in Equation (2-5).[51,52]

$$\Delta f = -\frac{\sqrt{\pi f_0}}{2\pi \rho d} (\eta \rho_l)^{\frac{1}{2}} \qquad (2\text{-}5)$$

22

In this relationship, Δf is the frequency shift, f_0 is the resonance frequency of a bare sensor, ρ is the sensor material density, ρ_l is the liquid density, d is the thickness of the sensor ribbon, η is the coefficient of dynamic viscosity of the liquid. It is noticed that equation (2-4) and (2-5) are similar to equation (1-2) and (1-3), respectively. For mass load, the frequency shift is linearly proportional to the mass change. For liquid contact, the frequency shift is proportional to the square root of the liquid viscosity and density product. This similarity reminds us that these new sensors are similar to acoustic wave sensors that have been studied for many years.

The important advantage of the magnetoacoustic sensor is that no physical connection to the sensing element is required. The sensor response is remotely monitored with a pick-up coil located outside the testing area. Therefore, this kind of sensor is ideal for applications where physical connections are undesirable or not possible, such as monitoring gastric pH, bloodstream glucose levels, or chemical concentration in a sealed container.[55,56] In addition, the whole measurement system is low cost. The magnetoelastic ribbon is very cheap and can be used on a disposable basis. At a result, magnetoacoustic sensors promise new applications for remote query sensor technology.

23

Digital ammeter

DC power supply

Audio amplifier

Computer

Preamplifier

Signal generator

IEEE 488 bus

Lock-in amplifier

Ref in

AC drive coils (Helmholtz configuration)

DC bias field coils (Helmholtz configuration)

Compensated pick-up coil + Bucking coil
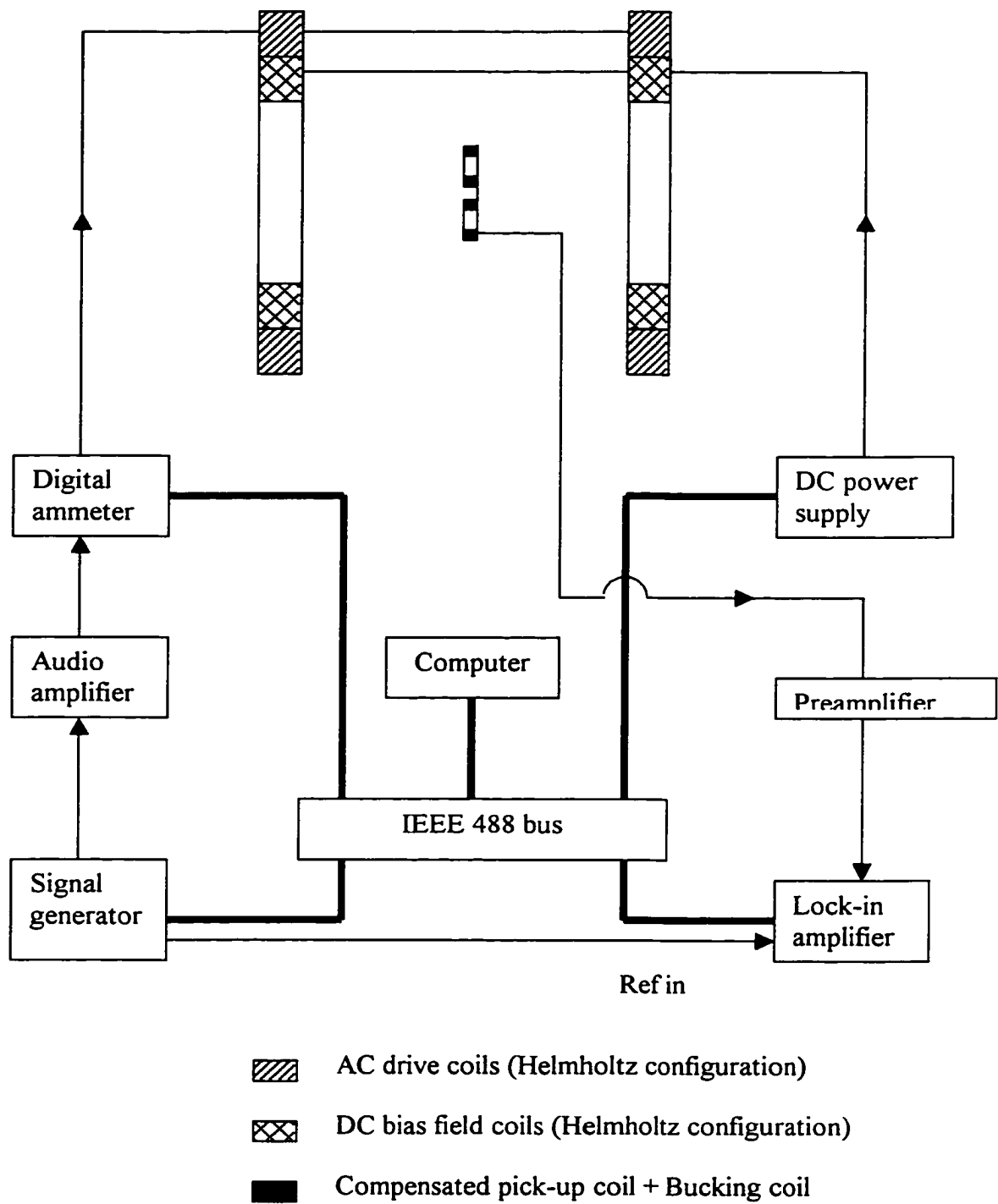
Figure 2-1 Schematic drawing of the sensor measurement system

24
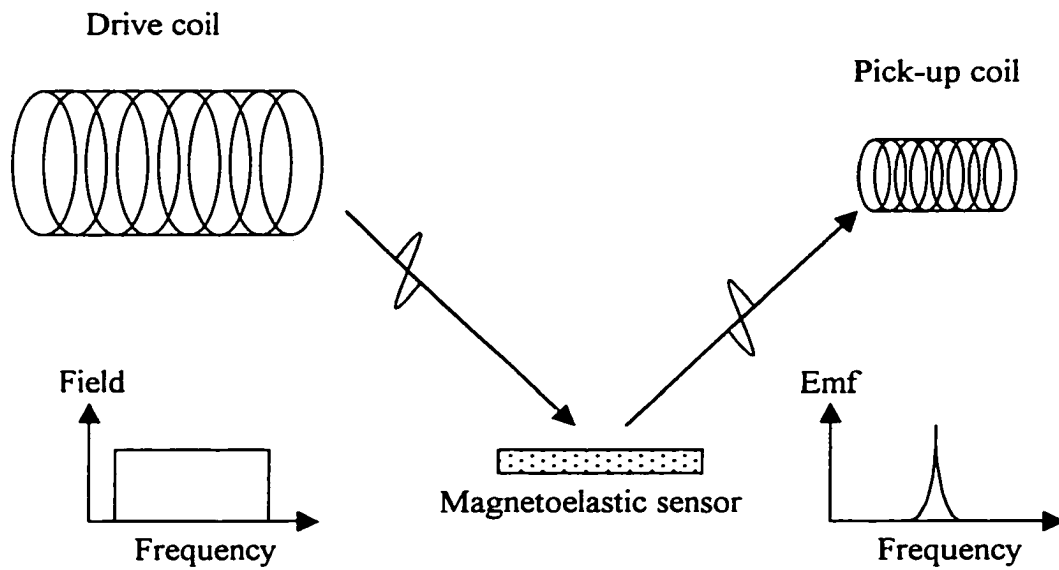
Figure 2-2 Schematic drawing demonstrates operating principle of magnetoelastic sensors.

25

Figure 2-3 Picture of the sensor measurement system.

26
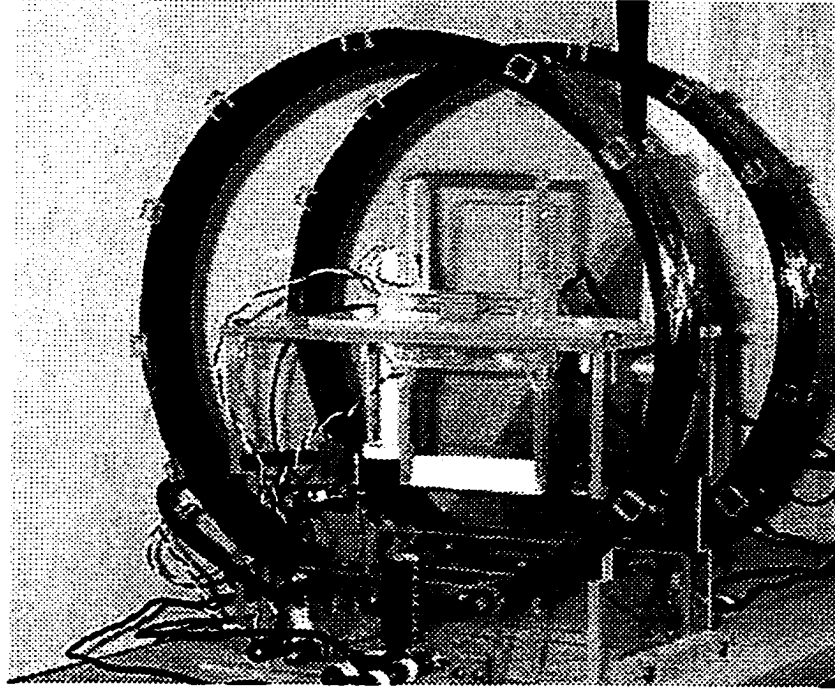
Figure 2-4 Picture of the driving coils, pick-up coil, and bucking coil.

27

2.2 Polymer Chemistry

A polymer is a large molecule that is made up of simple repeating units. The word "polymer" combines the Greek "poly", meaning "many", with "mer", meaning "part". Simple molecules that form the repeating units are called monomers, and the process that synthesizes the polymer is called polymerization.[57] The molecular weights of polymers vary from several thousand to several million atomic mass units.

A homopolymer is a polymer prepared from a single monomer. A copolymer is a polymer prepared from two or more monomers. Copolymers are divided into random, alternating, and block polymers, where the monomeric units are distributed randomly, in alternating fashion, and in blocks, respectively. A graft polymer consists of a polymer branching from the backbone of another polymer. These type polymers are illustrated in Figure 2-5 with A and B representing different monomers.[57] Polymers can also described as linear, branched, and network as shown in Figure 2-6.[57] A network polymer is formed by covalently crosslinking linear or branched polymer chains.

Traditionally, polymers are classified as addition polymers and condensation polymers based on whether the repeating unit of the polymer and monomer have the same atoms.[54,57] If the atoms are same, the polymer is called an addition polymer and corresponding synthesis is called addition polymerization. If the polymer contains fewer atoms, it is called a condensation polymer and the corresponding synthesis is called condensation polymerization.

Currently, the polymerization mechanisms are classified as step-growth and chain-growth.[54,57] In step-growth polymerization, monomer molecules react with each other to form low-molecular-weight polymers, which in turn react with each other to

form the polymer chains in a stepwise fashion. In chain-growth polymerization, polymer chains are built up by adding monomer molecules to the active centers of growing chains. According to the nature of the active centers, chain-growth polymerization is further classified as radical, cationic, anionic, and coordination.[58] Our work will focus on radical polymerization that takes place in three distinct steps, initiation, propagation, and termination. Usually the free radical initiators used in initiation step are classified into four major types: peroxides and hydroperoxides, azo compounds, redox initiators, and photoinitiators. The three steps in radical polymerization are shown in Figure 2-7 using styrene as the monomer and benzoyl peroxide as the initiator.[37,58] The initiation step consists of two elementary reactions. First, benzoyl peroxide is thermally decomposed into benzoyloxy radicals that then break down into phenyl radicals and carbon dioxide. Second, the phenyl radicals react with vinyl groups on the styrene to form active centers. In the propagation step, monomer molecules rapidly add to the active centers to from growing chains. In the termination step, the polymer chain radicals are destroyed by combination or by disproportionation. In combination termination two chain radicals combine together to form an inactive chain. In disproportionation termination one chain radical gives its unpaired electron to the other and both polymer chains become inactive.[54]

29

-A-A-A-A-A-A-A-A-   Homopolymer

-A-B-B-A-B-A-A-B-   Random copolymer

-A-B-A-B-A-B-A-B-   Alternating copolymer

-A-A-A-A-B-B-B-B-   Block copolymer

-A-A-A-A-A-A-A-A-   Graft copolymer
         |
         |
        B-B-B-B-B-

Figure 2-5 Structure of homopolymer and copolymer

(a)

(b)

(c)
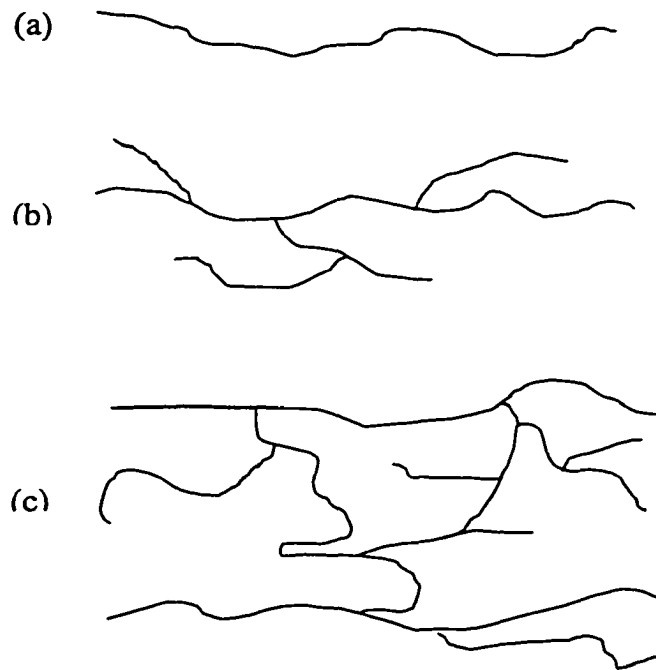
Figure 2-6 Structures of (a) linear, (b) branched, and (c) network polymers.

30
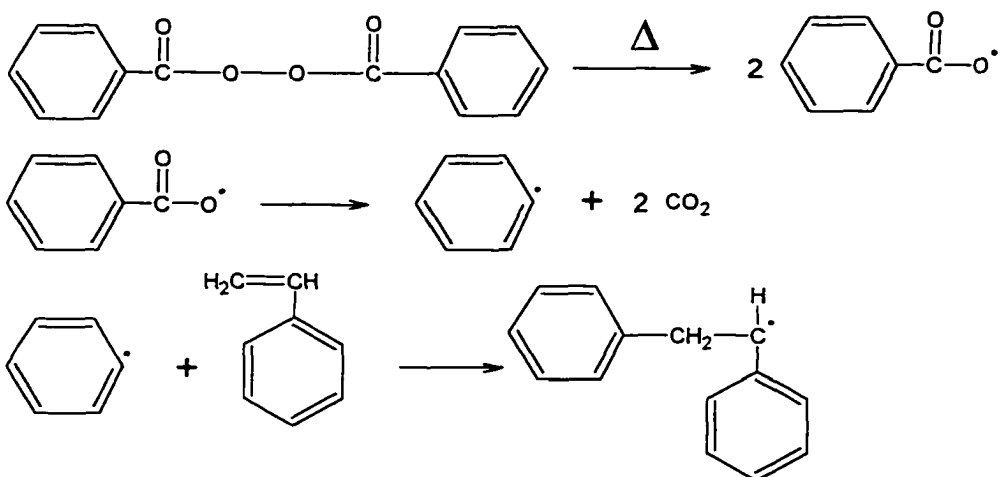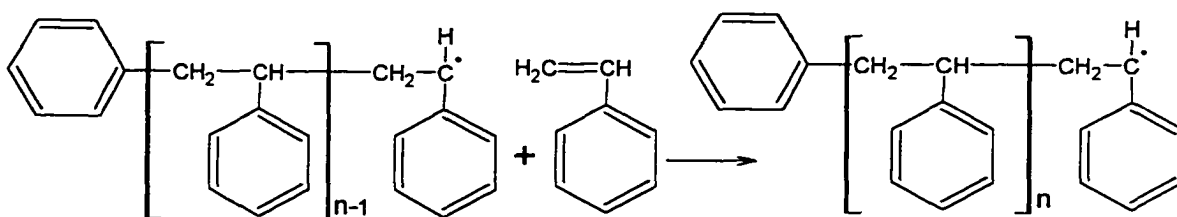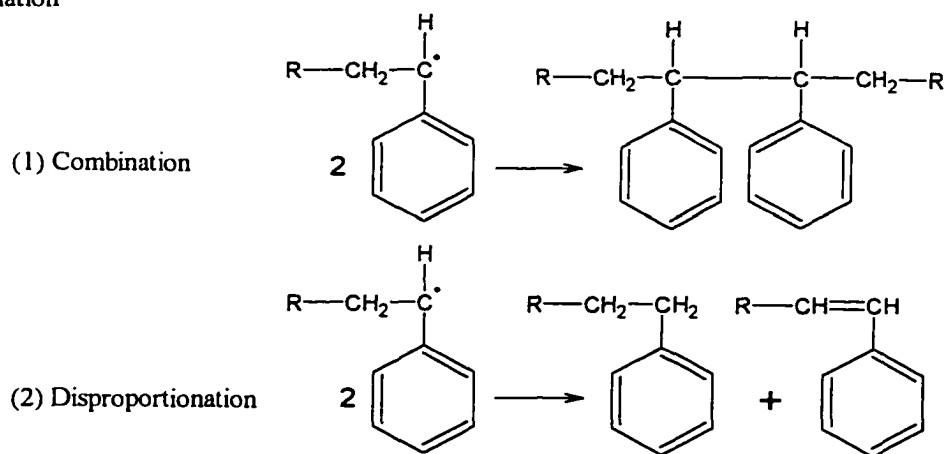
Figure 2-7 Free radical polymerization of styrene using benzoyl peroxide as the thermal initiator

31

2.3 Techniques of Free Radical Polymerization

Polymer microspheres with uniform sizes are receiving considerable attention in the industries of chemistry, biology, medicine, and electronics. For example, they can be used as stationary phases packed in chromatographic columns.[59,60] Free radical polymerization is divided into homogeneous and heterogeneous systems.[57,61] Homogeneous polymerization means the initiator, monomer, and polymer are all mutually soluble in a single phase. Heterogeneous polymerization means the initiator, monomer, and polymer are not mutually soluble and the polymer forms a discrete separate phase. Homogeneous polymerization includes bulk polymerization and solution polymerization. In the former case the initiator, monomer, and polymer are mixed together in one phase without adding solvent. In the latter case an inert solvent is used to lower the viscosity of the system and help to remove heat. Heterogeneous polymerization includes suspension, emulsion, inverse emulsion, and dispersion polymerization. In suspension polymerization, the monomer is dispersed by vigorous stirring into the continuous phase as droplets typically 100 μm to 10 mm in diameter.[61] The continuous phase usually contains small amounts of stabilizer to prevent droplets from coagulating. Oil-soluble initiator is used to initiate polymerization in the monomer droplets. Emulsion polymerization differs from the suspension polymerization in several ways. The most important characteristic is that the water-immiscible monomer is emulsified in an aqueous continuous medium using an oil-in-water emulsifier. The initiator is water soluble. The monomer droplets are from 0.05 to 5 μm in diameter, but the final polymer particles are usually smaller that 0.5 μm. Inverse emulsion involves dispersing an aqueous solution of monomer in a nonaqueous phase using a water-in-oil

32

emulsifier. In dispersion polymerization, the monomer, oil-soluble initiator, and polymeric stabilizer are dissolved in an organic solvent to form a homogeneous solution. The polymerization starts as a solution polymerization but becomes heterogeneous, because the polymer particles are insoluble in the oil medium and precipitate out to form a colloidal dispersion with the aid of the stabilizer. The polymer particles are in the size range in diameter from 1 to 5 μm.[35] This covers the particle size gap between emulsion and suspension polymerization. They can be monodisperse or in a narrow size distribution under favorable conditions. Dispersion and suspension polymerization were used in this work to prepare polymer microspheres.

2.4 Shirasu Porous Glass (SPG) Emulsification Technique

In suspension polymerization, the particle size and distribution are important quality parameters. They are extremely dependent on reactor geometry and agitation.[62] Reactors are classified as batch, semibatch, tubular, homogeneous continuous-flow stirred-tank, and semicontinuous reactors depending on existing flow conditions.[54] The batch reactors in our laboratory are round three-neck glass flasks, in which all reagents are charged initially and polymerization is carried out to the desired time. Usually a round three-neck flask with a magnetic stirring bar works very well for dispersion polymerization. However, for suspension polymerization, a flask with rough inner surface is needed. A mechanical stirring motor with high rotating speed and a specially shaped stirring rod are also required. The requirements for suspension polymerization are based on its reaction mechanism. Vigorous stirring and high frictional force are

33

needed to break the dispersed phase into small drops. The stirring speed affects not only

the product shapes but also the molecular weight distribution.[62]

Considering an attractive approach, a stable monomer emulsion can be made

before all materials are put into the reactors. Here the reactor requirements for

suspension polymerization are less stringent. In this research, a new technique called

Shirasu Porous Glass (SPG) was used to make monomer emulsions.[63-65] SPG is actually

a microporous glass membrane made from $CaO-Al_2O_3-B_2O_3-SiO_2$ by washing out CaO-

B_2O_3 with acid leaving $Al_2O_3-SiO_2$ to form uniform microporous structures. Under

applied pressure, the dispersion phase permeates through the membrane into the

continuous phase to produce an emulsion of uniform particle size. Figure 2-8 shows the

relationship between the applied pressure and droplet formation.[66] In Figure 2-8, P_a is the

applied pressure. P_c, called the critical pressure, refers to a pressure under which the

dispersion phase just permeates into the continuous phase. There are three situations that

are a consequence of applied pressure: $P_a < P_c$, $P_a = P_c$, and $P_a > P_c$. When Pa is smaller

than P_c, the dispersion phase can't pass through the membrane. When Pa is larger than

P_c, the dispersion phase passes through the micropores and forms emulsion droplets. The

following equation describes the critical pressure P_c.[66]

$$Pc = \frac{4\gamma \cos\theta}{D_m} \qquad (2\text{-}6)$$

In this relationship, γ is the interfacial tension θ is the interface contact angle, and D_m is

the micropore size. When using the same membrane, the most important factor is the

composition of the continuous phase and dispersion phase. This determines the

interfacial tension and then the critical pressure. Usually we set the applied pressure

slightly higher than the critical pressure. The flux of the dispersion phase increases with

the applied pressure. The emulsion is transferred to a three-neck flask and suspension

polymerization starts when the emulsion is heated to 70 °C.

Continuous phase

Emulsion droplet

Microporous membrane

Dispersion phase

(a) $P_a < P_c$ (b) $P_a = P_c$ (c) $P_a > P_c$
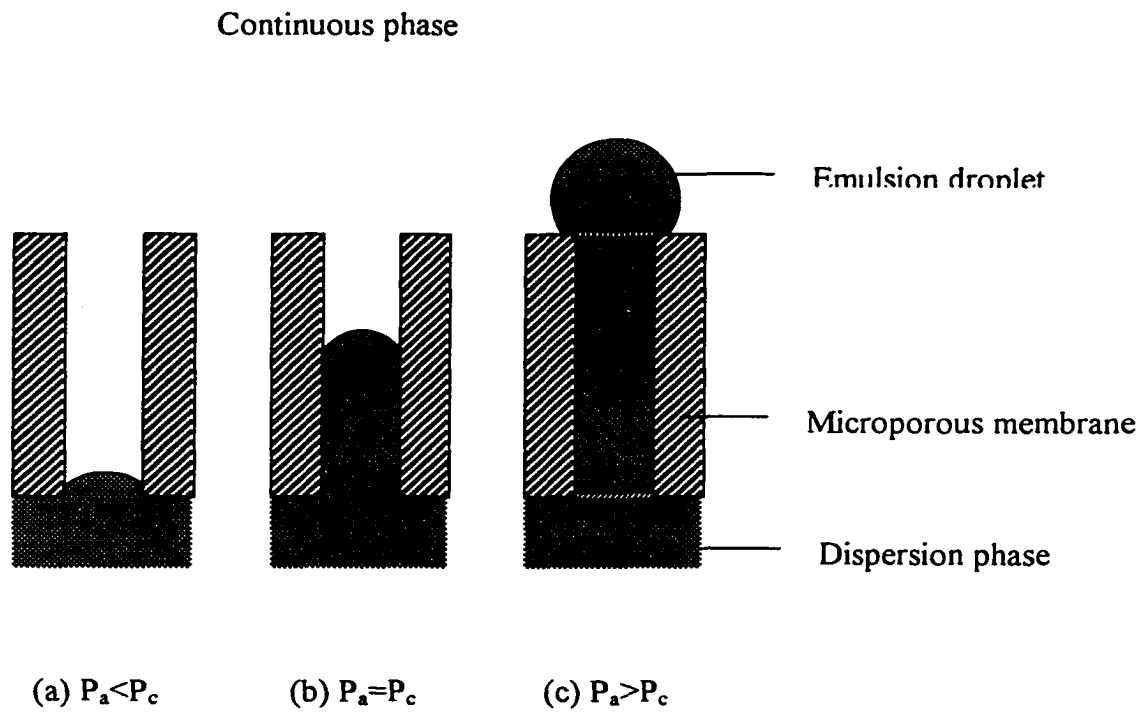
Figure 2-8 Relationship between the applied pressure and droplet formation

35

CHAPTER 3

EXPERIMENTAL

3.1 Regents

<u>Aldrich Chemical Company, Inc., Milwaukee, WI 53233</u>

Acryloyl chloride, F.W. 90.51, b.p. 72-76°C

2,4,5-Trichlorophenol (TCP), F.W. 197.45, m.p. 67-69°C

Divinylbenzene (DVB), 55% mixture of isomers, remainder mainly 3- and 4-

ethylbenzene, F.W. 130.19, b.p. 195°C

Poly(vinyl alcohol) (PVA), 100% hydrolyzed, Av. M.W. 14,000

Poly(vinyl alcohol), 87-89% hydrolyzed, Av. M.W. 85,000-146,000

2,2-Azobisisobutyronitrile (AIBN), 98%, F.W. 164.21, m.p. 103-105°C

2,2-Dimethoxy-2-phenyl-acetophenone (DMPAP), 99%, F.W. 256.30, m.p.67-70°C

Ethylene glycol dimethacrylate (EGDMA), 98%, F.W. 198.22, b.p. 98-100°C

2-Hydroxyethyl methacrylate (HEMA), 97%, F.W. 130.14, b.p. 67°C

Diethylamine, 98%, F.W. 73.14, b.p. 170°C

Toluene, 99%, F.W. 92.14, b.p. 110.6°C

Methyl sulfoxide (DMSO), 99%, F.W. 78.13, b.p. 189°C

Acetic acid

2-Hydroxyethyl acrylate (HEA), 96%, F.W. 116.12, b.p. 90-92°C

N-(2-acetamido)-2-aminoethansulphonic acid (ACES), F.W. 182.20

36

Dichloromethane (CH$_2$Cl$_2$), 99%, F.W. 84.93, b.p. 40°C

Starch powder, soluble up to 10% in cold water

Schweizerhall Inc., 3001 Hadley Rd., S. Plainfield, NJ 07080

Triethylamine, 99%, F.W. 101.19, b.p 88.8°C

Sigma Chemical Company, P.O. BOX 14508, St. Louis, MO 63178

Polyvinylpyrrolidone (PVP), Av. M. W. 40000,

The Dow-Chemical Company, Midland, MI 48674

Vinylbenzyl Chloride (VBC), mixture of 3- and 4- isomers, F.W. 152.62, b.p.229°C

Fisher Scientific Company, Fair Lawn, NJ 07410

Glutaraldehyde, 50% w/w solution in water, F.W. 100.12

Sodium bicarbonate, ACS, F.W. 84.01

Acetone, F.W. 58.08, b.p. 56.01°C

Sodium acetate, F.W. 82.03, m.p. 324°C

Sodium hydroxide

Hydrochloric acid

Sodium chloride, F.W. 58.44, m.p. 801°C

HYMEDIX International, Inc, Dayton, NJ 08540

HYPAN HN30, HN50, and HN80 Structural Hydrogel

Bayer Corporation, Pittsburgh, PA

Bayhydrol 110 waterborne polyurethane

Unless otherwise specified, two series of buffers are used. One is 0.1 M buffer

concentration with 0.3 M ionic strength, and the other is 0.05 M buffer concentration

37

with 0.05 M ionic strength. All ionic strength is adjusted with sodium chloride. Doubly deionized distilled water is prepared with a Corning Mega-Pure distillation apparatus.

3.2 Apparatus

A Fisher laboratory centrifuge (3400 rpm) was used to separate polymer microspheres. A Branson model 1210 sonicator was used to suspend the particles in water when cleaning them, or in dimethyl sulfoxide when making HYPAN hydrogel membranes. An Orion 901 digital analyzer with an Orion 91/55 combination pH electrode was used to measure pH when preparing buffers. An Amray 3300FE scanning electron microscope (SEM) was used to measure microsphere diameters. A Perkin-Elmer Model 2400 CHN analyzer was used to determine the carbon, hydrogen, and nitrogen content of the derivatized microspheres. X-ray photoelectron spectroscopy spectra were obtained with a Kratos Axis HS XPS. A Cary 500 UV/Vis/NIR spectrophotometer was used for turbidity measurements. Plastic membrane holders for Cary 500 UV/Vis/NIR spectrophotometer and testing cells for resonance meter were fabricated by the Machine Shop in the University of New Hampshire. A 400 Watt UV lamp was used for photo-polymerization of the HEMA and HEA. Brookfield viscometer (Model DV-I+, Version 2.0) with UL Adapter from Brookfield Engineering Laboratories, Inc. was used to measure viscosity. 500 ml three neck reaction vessels, mechanical stirring apparatus, and hot plates with magnetic stirring system were purchased from VWR. A Specialty Coating Systems Spin Coater Model P6204-A was used for coating membranes on ribbons.

38

A set of SPG emulsification apparatus was purchased from SPG Technology Co., Ltd in Miyazakiken, Japan. The pore sizes of porous membranes are 0.1 μm, 0.2 μm, 0.5 μm, and 1.5 μm, respectively.

A Resonance Meter that is the measuring system of the magnetoacoustic sensor was fabricated in Dr. Craig Grimes' research group in Department of Electrical Engineering at the Pennsylvania State University. Magnetoelastic ribbons are METGLAS® magnetic alloy 2826MB (iron nickel-based) from Honeywell which were cut to a 38.0 x 12.5 x 0.035 mm size with a pair of scissors.

3.3 Procedures

3.3.1 Preparation of 2,4,5-trichlorophenyl acrylate (TCPA) monomer[38,39]

Figure 3-1 shows the reaction of 2,4,5-trichlorophenol (TCP) and acryloyl chloride to make TCPA. In this case, 0.25 mol TCP and 75 ml dichloromethane are mixed in a 500 ml of three-neck flask that is immersed in an ice bath and stirred with a magnetic stirrer until TCP is completely dissolved. Dropping funnels are put on the two necks of the flask, one containing a mixture of 0.25 mol of triethylamine and 75 ml of dichloromethane, and the other containing a mixture of 0.25 mol of acryloyl chloride and 75 ml of dichloromethane. The two solutions are added dropwise while stirring. This step may take about 40 minutes. After mixing all reagents, the solution is stirred in an ice bath for 3 hours and then at room temperature for 6 hours. The raw product is filtered through glass wool to remove the precipitated triethylammonium chloride salt. The filtrate is washed in a 1000 ml separatory funnel with 100 ml deionized water, 100 ml saturated sodium bicarbonate, and 100 ml deionized water. The solution is dried

39

overnight with anhydrous sodium sulfate in a capped flask. After that, the product is filtered to remove sodium sulfate. The filtrate is put in a rotary evaporator to remove dichloromethane and obtain solid TCPA. The solid TCPA is re-crystallized with ethyl acetate. The final product is dried in a vacuum oven overnight at 35 °C, and stored in a capped bottle.
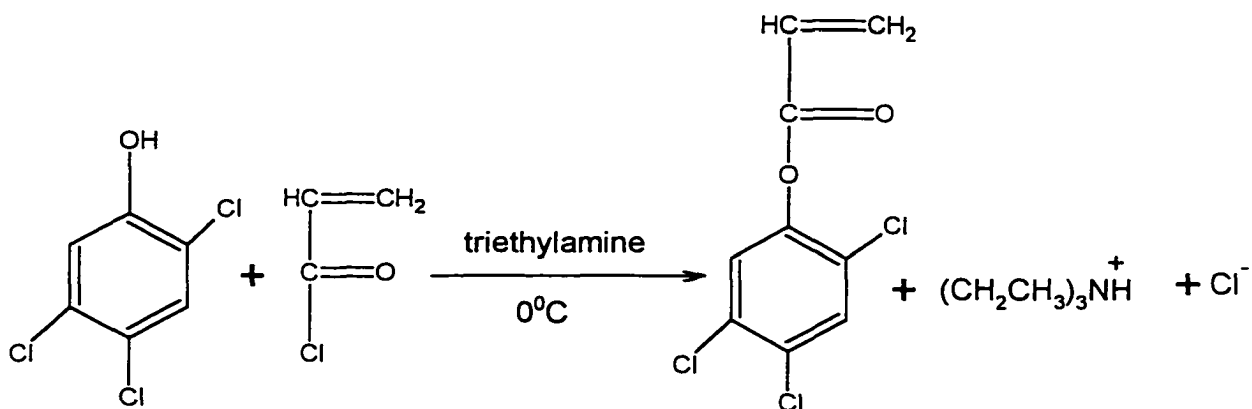
Figure 3-1 Synthesis of 2,4,5-trichlorophenyl acrylate (TCPA) monomer

40

3.3.2 Preparation of poly(vinylbenzyl chloride)-(2,4,5-trichlorophenyl acrylate) (polyVBC-TCPA) microspheres by dispersion polymerization[50]

PolyVBC-TCPA microspheres were made by dispersion polymerization. Table 3-1 shows a typical formula for a 500 ml batch size. VBC and TCPA are used as co-monomers in a 1:1 mole ratio. AIBN is the initiator, polyvinylpyrrolidone (PVP) is the steric stabilizer, and ethanol is the solvent. All reagents are placed in a 500 ml three-neck flask and stirred with a magnetic stirrer until the TCPA completely dissolves. This reaction mixture is purged with nitrogen for about 10 minutes, and then the flask is put in a water bath at 70±2 °C. It takes about 8 hours for the polymerization to finish. Figure 3-2 shows the reaction of polymerization of VBC and TCPA.

Table 3-1 A typical formula for synthesis of polyVBC-TCPA microspheres

Reagent	Amount
VBC	4.70 g
TCPA	7.70 g
DVB	0.32 g
PVP	2.88 g
AIBN	0.25 g
Ethanol	240 ml

41
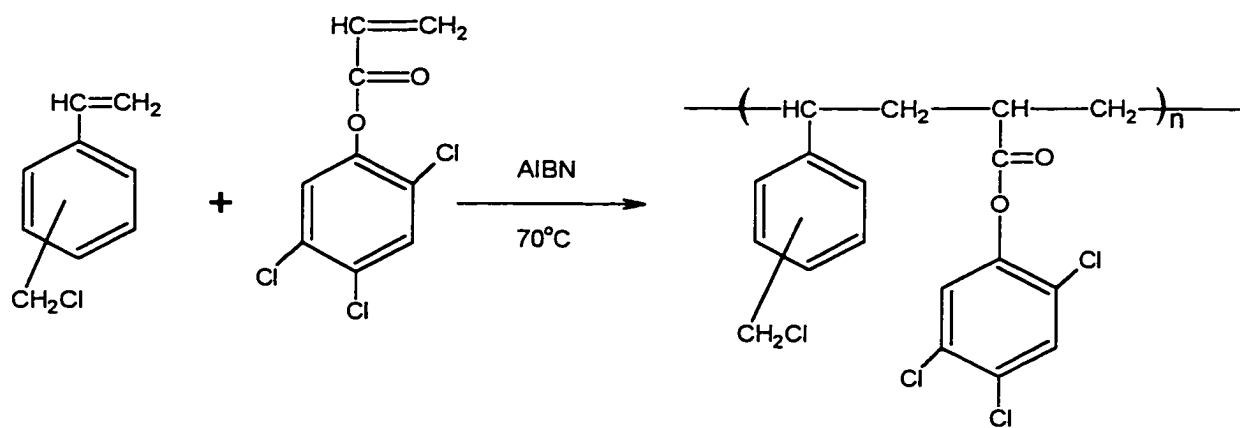
Figure 3-2 Polymerization of VBC and TCPA

42

3.3.3 Operation of the SPG apparatus to make Oil/Water emulsion[66]

A porous membrane is placed in a large test tube filled with deionized water and sonicated to drive air from the porous membrane which must be completely wetted before starting the SPG. The water-wetted porous membrane tube is installed inside the membrane module sheath, as shown in Figure 3-3. The dispersion phase is placed in the dispersion phase storage tank and continuous phase in the emulsion tank. The nitrogen gas inlet valve and the gas-releasing valve are opened a little. The dispersion phase gradually fills in the space between and membrane module sheath and the porous membrane tube. Both gas valves are closed when the dispersion phase starts coming out of the gas-releasing valve. Those two valves are closed for 5 minutes under a small pressure. It indicates no leakage for the dispersion phase circulation system if the reading of the applied pressure gauge doesn't change during this period of time. The circulation pump is then turned on. The applied pressure is gradually increased until it is slightly higher than the critical pressure. As defined in equation (2-6), the critical pressure refers to a pressure under which the dispersion phase just permeates into the continuous phase. In practice it is the pressure point at which the continuous phase becomes slightly milky. When the dispersion phase passes through the porous membrane, the continuous phase becomes milky and an emulsion is formed with uniform droplet size. After emulsification, the emulsion is directly poured into a three-neck flask to start the suspension polymerization. The porous membrane tube is removed and cleaned separately. Other parts are circulated with water 3 times and methanol once to clean the system.

43
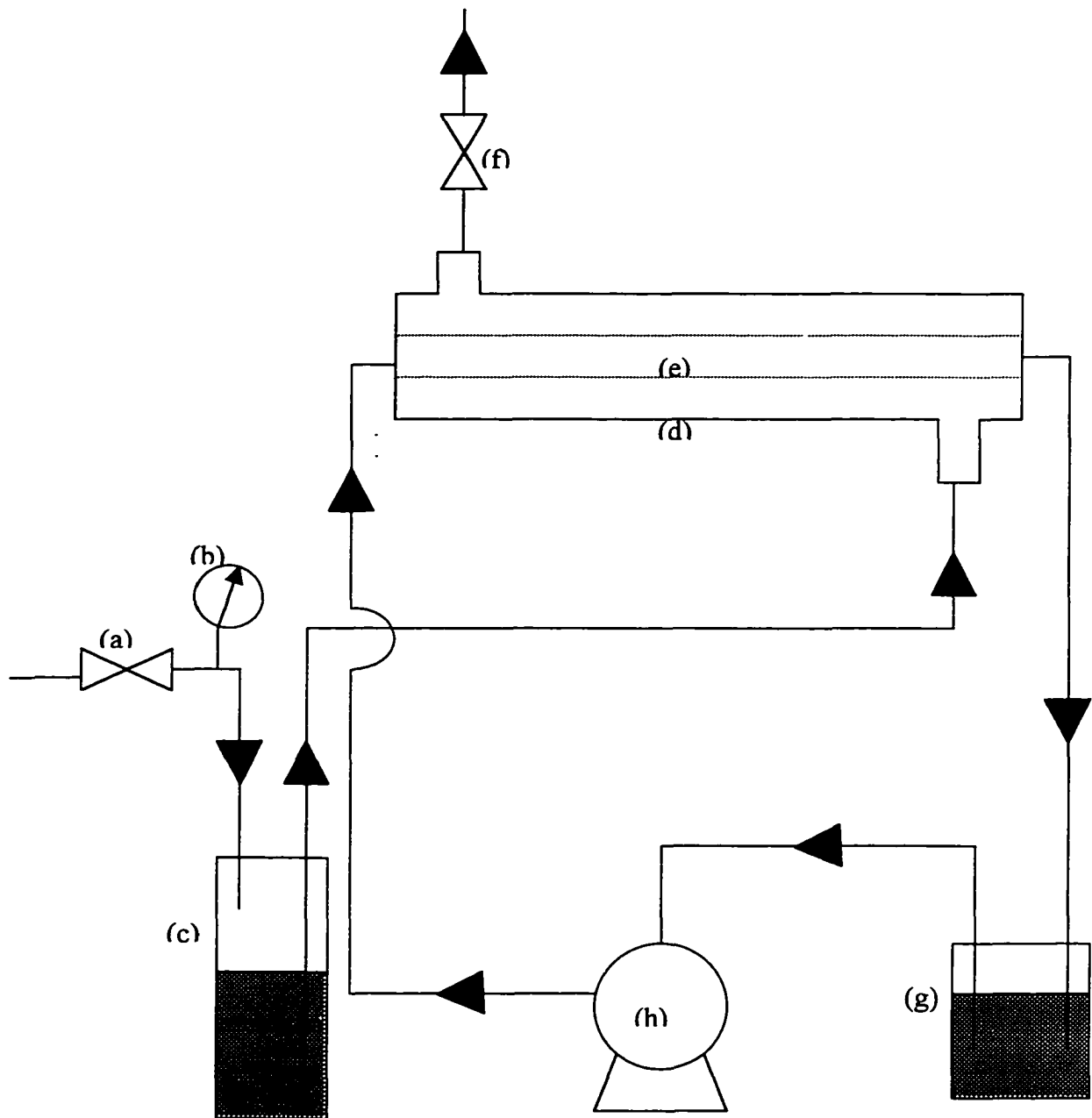
(a) Nitrogen gas inlet valve   (e) Porous membrane tube
(b) Applying pressure gauge   (f) Gas releasing valve
(c) Dispersion phase storage tank   (g) Emulsion tank
(d) Membrane module sheath   (h) Circulation pump

Figure 3-3 Schematic diagram of SPG emulsification apparatus

44

3.3.4 Cleaning procedure of the SPG porous membrane[66]

A completely cleaned porous membrane is essential to make emulsions with uniform droplet size. Hydrophilic membranes are cleaned with water and methanol. Membranes are placed in a capped test tube filled with water or methanol and sonicated for 10 minutes. The membranes are washed 3 times with water, methanol, and water. A clean membrane means no residual dispersion phase and air bubbles inside the micropores. The cleaned membrane is stored in a capped test tube filled with water.

3.3.5 Preparation of poly(vinylbenzyl chloride) (polyVBC) microparticles by suspension polymerization[44]

An emulsion of VBC and DVB in water was made using the SPG technique. The dispersion phase includes VBC, DVB, BPO, xylene, and dodecane. A typical formulation is shown in Table 3-2. These materials were mixed in a 50 ml beaker and stirred with a magnetic stirring bar until BPO was completely dissolved. Then the dispersion phase was transferred to the dispersion phase storage tank. The continuous phase includes SDS, Na_2SO_4, 0.5% wt/wt PVA, and water. The applied pressure is set 0.05 kgf/cm^2 higher than the critical pressure depending on the composition of the dispersion and continuous phases. In this experiment, the applied pressure is 1.50 to 1.80 kgf/cm^2 for a porous membrane with 0.5 μm pore sizes. It takes about 30 minutes to finish the emulsification of 50 ml of dispersion phase.

The emulsion was placed in a three-neck flask equipped with a mechanical stirrer at the center neck. The other two necks were stopped with plastic stoppers. Before polymerization, the emulsion was purged with nitrogen gas for 15 minutes to remove

dissolved oxygen. Then the flask was placed in a water bath heated to 70±2 °C.

Polymerization was continued for 12 hours.

3.3.6 Microparticle cleaning

After polymerization and derivatization procedures, all particles are cleaned with water, methanol, and water repeatedly. The basic method is to isolate the particles from solution matrix using a centrifuge and re-suspend them into water or methanol by sonication. The particles are dried in an oven at 40 °C and then stored in a glass bottle.

3.3.7 Derivatization of polyVBC-TCPA microspheres with diethylamine[37,38]

PolyVBC-TCPA microspheres are pre-swollen in acetone for one hour. Then a mixture of diethylamine and acetone in a 1:1 volume ratio is added and stirred at room temperature for three days. Figure 3-4 shows the derivatization reaction. The diethylamine displaces the phenolic ester and the chloride from the chloromethyl carbon. After the microspheres are washed with water and methanol, they are washed with 0.1 M HCl to remove un-reacted diethylamine. Finally they are washed with water and stored in a glass bottle. Some particles are dried in an oven at 35 °C and used for the magnetoacoustic pH measurements.

46

Table 3-2 A typical formula for making polyVBC particles by suspension polymerization

Dispersion phase		Continuous phase	
VBC	40.28 g	PVA	2.50 g
DVB	1.37 g	SDS	0.17 g
BPO	0.62 g	Na_2SO_4	0.11 g
Xylene	8.60 g	Water	500 ml
Dodecane	3.75 g		
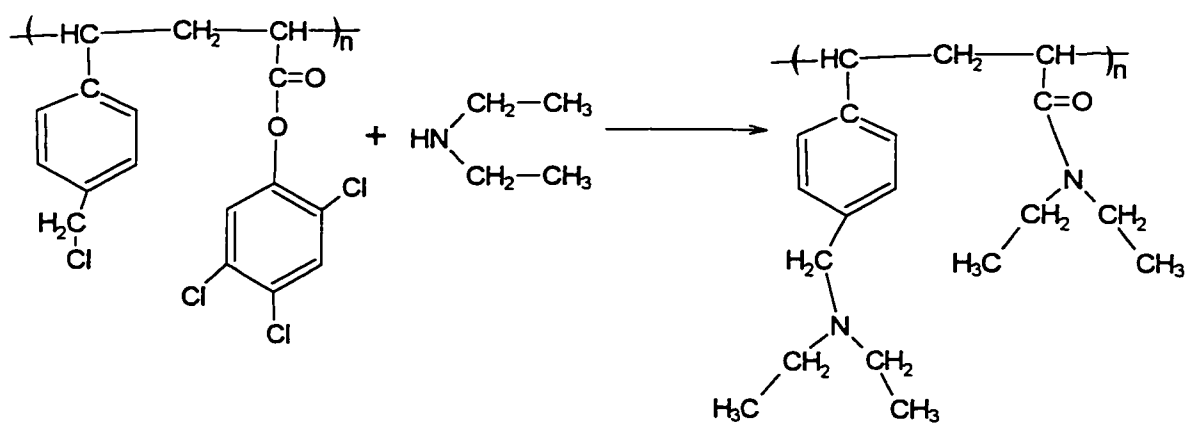
Figure 3-4 Derivatization of polyVBC-TCPA microspheres with diethylamine

48

3.3.8 Derivatization of polyVBC particles with diethyl malonate

Derivatization of polyVBC with diethyl malonate was based on previous work.[67]

11.2 g of diethyl malonate and 60 ml of N, N-dimethylformamide (DMF) are added to a 125 ml addition funnel. This funnel is inserted into a 500 ml three-neck flask containing 1.5 g of sodium hydride and 140 ml of DMF. The mixture of diethyl malonate and DMF is added dropwise to the flask. The solution is stirred at 60 °C for 1 hour followed by addition of 4.0 g of polyVBC particles and stirred at 80 °C for 3 days. Figure 3-5 shows the derivatization reaction. After derivatization, the particles are centrifuged and washed with ice-cooled distilled water, hot distilled water, and methanol.

3.3.9 Hydrolysis of diethyl malonate derived polyVBC particles

Many methods of hydrolyzing dicarboxylic esters have been reported.[68-71] The hydrolysis can be done in water or a mixed aqueous - organic solvent. The organic solvents include dimethyl sulfoxide (DMSO), ethanol, acetonitrile, and dioxane. Usually acid or base is added to the solution as a catalyst. Here we hydrolyzed diethyl malonate derived polyVBC particles in water-DMSO using NaOH as the catalyst. A typical batch of mixture contained 0.5 g of derived particles, 8 ml of DMSO, and 32 ml of 6 M NaOH. The mixture was refluxed at 50 °C for 3 days. After hydrolysis, the particles were centrifuged and washed with distilled water 3 times. The cleaned beads were dried in an oven at 50 °C.

49
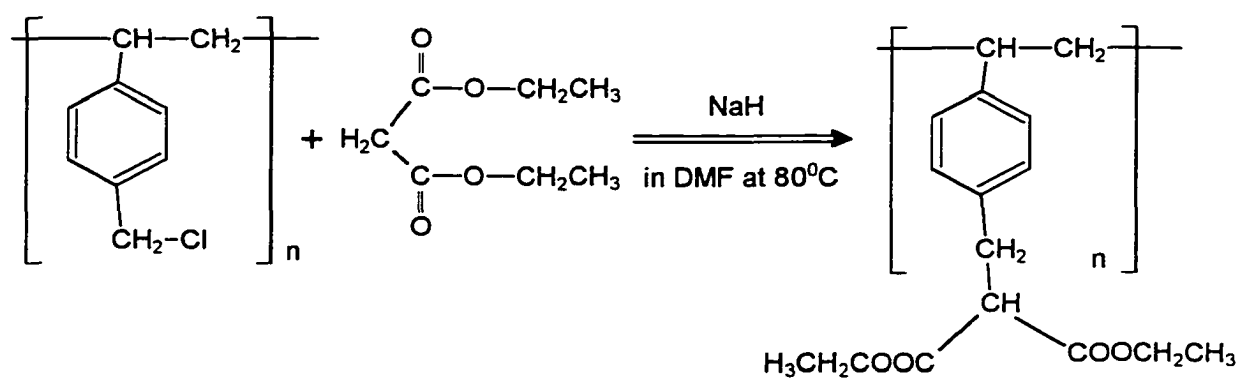
Figure 3-5 Derivatization of polyVBC particles with diethyl malonate

50

3.3.10 Polymerization of HEMA

14.75 g of HEMA, 0.222 g of EGDMA, and 0.225 g of DMPAP were added to a glass bottle. HEMA is the monomer and EGDMA is the crosslinker. Polymerization was initiated under a 400 Watt mercury lamp using DMPAP as the photo-initiator. Figure 3-6 shows the structures of HEMA, EGDMA, and DMPAP. The polymerization was monitored magnetoacoustically.

3.3.11 Preparation of hydrogel membranes

3.3.11.1 Poly(vinyl alcohol) membranes

A 10% (wt/wt) PVA solution was prepared by dissolving 5 g of PVA (MW 14,000) in 45 g of water. A 10% glutaraldehyde solution was prepared by diluting from a 50% stock solution. These two solutions were stored in plastic bottles at room temperature. Figure 3-7 shows the structures of PVA and glutaraldehyde. First, 1.0 ml of the PVA solution, 25 µL of glutaraldehyde, and an appropriate amount of particles were mixed together in a small beaker. This mixture was sonicated to get a homogeneous suspension of particles. Second, 50 µL of 4 M HCl was added to this suspension to initiate PVA crosslinking. This polymer solution was quickly transferred to a mold, which was made of two microscope slides and a piece of Teflon tape. The Teflon tape, which center had been cut out, was placed on one microscope slide to form a cavity. This cell was covered with another microscope slide after it was filled with the polymer solution. It took about 30 minutes to finish the crosslinking. The membranes were easily removed from the mold when they were put in water. The thickness of the membrane was controlled by the thickness of the Teflon tape. There are two kinds of Teflon tapes

51

that were used in our group. One is 76 μm, and the other one is 51 μm. Unless otherwise specified, the 51 μm thick Teflon tape was used in all experiments.

3.3.11.2 PolyHEA membranes

The same mold for making PVA membranes was used for making HEA membranes. DMPAP (1.5wt% HEA), HEA, and EGDMA (1.5mole% of HEA) were mixed together in a small glass bottle. Figure 3-6 and Figure 3-7 show the structures of EGDMA, DMPAP, and HEA. This mixture was added to the mold, and then placed under a 400 Watt mercury lamp for 10 minutes to induce polymerization.

3.3.11.3 HYPAN polymer membranes

For the preparation of HYPAN polymer membrane, 0.0020 g of dry particles were added to 0.2000 g of DMSO in a small glass bottle, and sonicated to form a homogeneous suspension. Then 0.8000 g of 10% HYPAN polymer solution in DMSO was added to this bottle. This mixture was continuously stirred with a magnetic stir bar until a homogeneous suspension of particles formed. This suspension was transferred to the same mold used to make PVA membranes. However, instead of covering the Teflon cell with another microscope slide, the polymer mixture in the cavity was leveled with a razor blade. The cell was quickly immersed into water in a beaker. HYPAN membranes formed in water and easily came out of the cavity.

Monomer
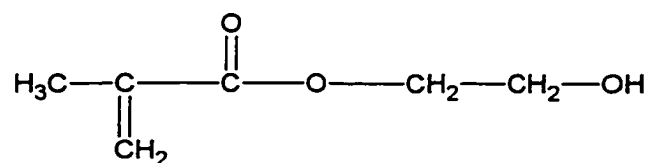
2-Hydroxyethyl methacrylate (HEMA)

Crosslinker
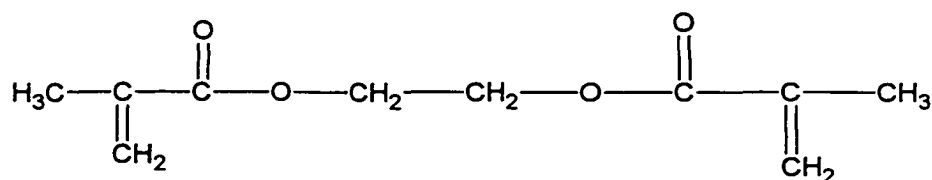
Ethylene glycol dimethacrylate (EGDMA)

Photoinitiator
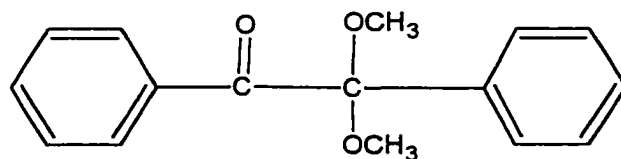
2,2-Dimethoxy-2-phenylacetophenone (DMPAP)

Figure 3-6 Structures of HEMA, EGDMA, and DMPAP used for HEMA polymerization

53

Monomer

H—C——C——O——CH₂—CH₂—OH (with O double-bonded to second C, and CH₂ double-bonded to first C)

2-Hydroxyethyl acrylate (HEA)

—(CH₂—CH)ₙ— (with OH group on CH)
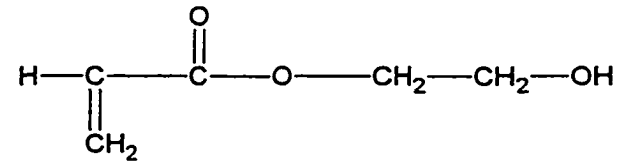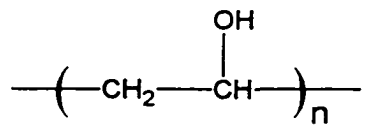
Poly(vinyl alcohol) (PVA)

Crosslinker for PVA

H—C——CH₂——CH₂——CH₂——C—H (with O double-bonded to each C)
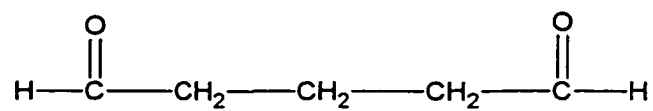
Glutaraldehyde

Figure 3-7 Structures of HEA, PVA, and glutaraldehyde

54

3.3.12 Spin-coating sensing membranes on magnetoelastic ribbons

A magnetoelastic ribbon was sonicated in 2% Micro-90 water solution for 15 minutes. Then it was washed with distilled water 3 times and acetone 3 times. The ribbon was blown dry with nitrogen gas. One side of the ribbon was spin coated with a layer of polyurethane waterborne dispersion and dried in an oven at 50 °C for 20 minutes. This step was repeated to coat polyurethane on the other side of the ribbon. 0.040 g of dry particles were suspended in 1.000 grams of 4% HYPAN polymer solution in DMSO. This suspension was spin coated on one side of the polyurethane-coated ribbon. The coated ribbon was dried in air for 24 hours. The spin coater was set at a speed of 2500 rpm with quick start and stop of acceleration for 20 seconds. Sometimes, experience plays an important role to make a good sensitive ribbon, especially when spin-coating the sensitive membrane. Due to the rapid evaporation of DMSO, the suspension of the HYPAN and microspheres becomes viscous quickly. Therefore, it requires quickly transferring the suspension from the glass bottle to the ribbon surface. The transferred amount should be enough to coat the whole ribbon surface, but not so much as to form droplets at the ends of the ribbon. Usually 0.5 ml of the suspension was transferred. Care should be taken to avoid air bubbles in the membrane.

3.4 Characterization

3.4.1 Scanning electron microscopy (SEM)

A drop of the particle suspension in ethanol was placed on the surface of graphite SEM platform and left to dry in air. Then a layer of gold/palladium alloy was coated on the particle layer to a thickness of about 300 Å under vacuum.

3.4.2 CHN analysis

The aminated microspheres were washed with 0.1 M HCl and deionized water to remove unreacted diethyl amine. Then they were dried in an oven at 35 °C overnight. The dried microspheres were ground with a mortar and pestle and submitted for analysis.

3.4.3 Membrane thickness measurements

A layer of waterborne polyurethane dispersion was spin-coated onto the surface of a magnetoelastic ribbon and dried in an oven at 150 °C for 20 minutes. One third of the polyurethane layer was carefully scratched off using a razor blade to obtain a sharp edge. The thickness was measured with Alpha-Step 100 profilometer.

3.4.4 Optical microscopy

A drop of SPG emulsion was placed between two microscopy slides during or after emulsification. The sizes of the emulsified monomer droplets and their distribution were observed using a Nikon optical microscope.

3.4.5 Turbidity measurements

A piece of hydrogel membrane with entrapped swellable microspheres was tightly held in a plastic holder. This holder was then placed in a standard cuvette. A piece of blank hydrogel membrane without microspheres was also held with the same kind of holder and placed in a cuvette. This blank membrane was used as the reference. A Cary 500 UV/Vis spectrophotometer was used to measure the turbidity changes of the sample membrane when changing pH. The wavelength was scanned from 400 nm to 1000 nm.

.

56

3.4.6 Operation of the resonance meter

A resonance meter was used to monitor viscosity, mass load, curing polymerization, and pH. Appendix A describes the unit functions of the resonance meter. Appendix B describes the button functions of the operational program MERM 3.03b. Appendix C describes the operational instruction for the resonance meter. A typical measurement is as follows. First, turn on all units: DC power supply, Mackie power amplifier, SR 830 Lock-in Amplifier, Keithley 2000 Voltmeter, Hewlett-Packard Function Generator, Earthworks preamplifier. The right toggle switch on the Earthworks Preamplifier is turned to the ON position. All units are warmed up for 15 minutes before measurements. Second, the controlling computer is turned on. The operational program MERM 3.03b is loaded. Usually we accept most of the default values in the program except for the Start and Stop Frequency, Points, and Time Control. The Start Frequency is the starting frequency for the measurement, and the Stop Frequency is the stopping frequency for the measurement. The Points indicates how many data points will be collected. These three values determine the response rate and accuracy of the measurement because the current resonance meter in our group can only sweep a pre-determined frequency range one frequency at a time. In order to set a narrow frequency range to decrease the response rate, we always run a preliminary measurement to determine the shift between the resonance frequencies at lowest and highest analyte concentrations. The resonance frequency shift is less than 2 kHz in most of cases. As an example, we can set 56 kHz at Start Frequency, 58 kHz at Stop Frequency, and 400 measurement points. Running time is about 3 minutes for these parameters. There are two buttons, Start and Time Start, in the Control Panel. Start is clicked if we sweep the

57

pre-determined frequency range only once. We prefer to use this function to find out the rough resonance frequency shift. Time Start is clicked if we would like to run multiple scans for a period of time. We can designate how long we want to run the scans in the Time Control. Mechanical vibrations of the workbench should be avoided during the measurement. All metallic parts should be moved away from the pick-up coil area. All saved data during measurements can be re-opened using KaleidaGraph 3.09 from Synergy Software. The resonance frequency can be read from the data point series or from the maximal peak.

3.4.7 pH monitoring with resonance meter

Two kinds of microspheres were used for pH measurements. One was diethylamine derivatized polyTCPA-VBC. The other one was carboxylate derivatized polyVBC. A suspension containing 4% beads in 4% HYPAN polymer in DMSO was used to prepare the sensitive membrane. The membrane was conditioned by placing it in low and high pH buffers twice. This causes the water content of the polymer to be repeatable. Then the membrane was placed in a Teflon cell, which in turn was placed at the center of the pick-up coil of the Resonance Meter.

3.4.8 Viscosity measurement

The viscosities of the starch solutions were measured at 28 °C with a YULA-15 UL spindle. The viscometer speeds were programmed into the standard DV-I+. In this study, the speed was 100 RPM.

58

3.4.9 Mass change monitoring with resonance meter

DMPAP (1.5 wt% HEA) was dissolved in a mixture of HEA and EGDMA (1.5 mole% of HEA) in a 25 ml glass bottle. PolyHEA membranes were prepared using two microscope slides as shown in Figure 3-8. The surfaces of the two slides were covered with Teflon tape. A piece of Teflon tape was cut in the center to form a frame. This Teflon frame was placed on one slide of a microscopy slide to form a cell. The depth of the cell was 51 µm. 0.5 ml of solution was added into the cell. The second slide was put on the frame. The two slides were tightly held with two clamps, and exposed to a 400 W mercury lamp for 10 minutes to form a polyHEA membrane. After polymerization, the membrane was put in distilled water for one hour to swell. A piece of 5x37 mm swollen polyHEA membrane was cut and bonded to the magnetoelastic ribbon with Superglue. The resonant frequency of the sensor was monitored after adding water to a bare ribbon and a ribbon coated with polyHEA.
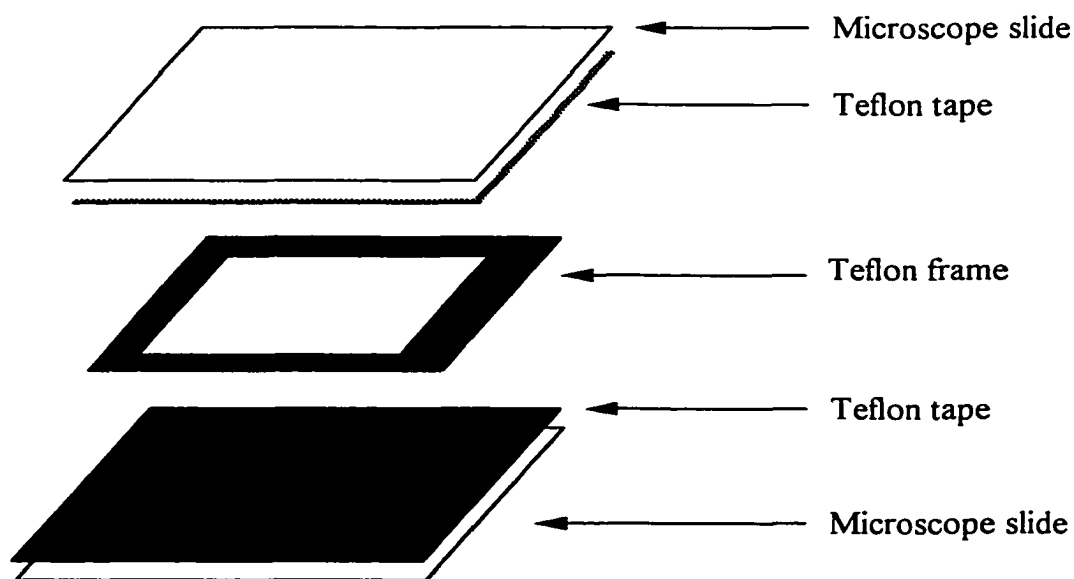
Figure 3-8 Schematic of mold for polymer membrane preparation

59

CHAPTER 4

PREPARATION AND OPTICAL PROPERTIES OF pH SENSITIVE
MICROSPHERES

4.1 Introduction

The goal of this dissertation was to develop a new kind of magnetoacoustic

chemical sensor. The first objective was to develop a chemical response system. This

was then combined with the Resonance Meter to create a new kind of magnetoacoustic

chemical sensor. This chapter describes the development of a chemical response system.

We started with a relatively simple but very important chemical response system:

measuring solution pH. The method of measuring solution pH is based on polymer

microspheres swelling and shrinking with changing solution pH. The principles of this

method have been discussed in Chapter 1. The first pH sensitive microspheres that we

describe in this chapter are polyTCPA-VBC prepared by dispersion polymerization.

These microspheres were derivatized with diethylamine to introduce amine groups on the

microspheres. The aminated microspheres change from their swollen state to shrunken

state when the pH changes from 6.0 to 8.0. Later, dicarboxylated microspheres were

prepared to measure gastric pH from 2.0 to 8.0. We prepared polyVBC particles by

suspension polymerization. These particles were derivatized with diethyl malonate and

then hydrolyzed to introduce carboxylate groups. The derivatized particles responded to

pH from 2.0 to 8.0. There are two new developments involved in making polyVBC

60

particles. First, we use suspension polymerization rather than dispersion polymerization to make the polyVBC particles. This allows us to use a porogen during polymerization to form micropores inside the particles. Porous particles respond more rapidly to pH changes. Second, we use the SPG technique to make the emulsion which overcomes some drawbacks in the traditional method of making emulsions, resulting in large particle sizes and broad size distribution.

The pH responses of all derivatized microspheres were tested by turbidity measurements as described in Section 3.4.5. These results helped us to understand the properties of the derivatized particles before we applied them to the resonance meter. They also helped us to identify possible problems if we failed to obtain responses from the resonance meter. Finally, these results can be compared with those obtained with the resonance meter when we make the magnetoacoustic chemical sensors.

Different hydrogel membranes were used to investigate possible membrane effects on the pH responses of derivatized particles. These hydrogels include PVA and different HYPAN polymer types. The composition of HYPAN hydrogels is discussed in detail in Section 6.2.2. HYPAN polymers are plasticized with water. Therefore, it is a simple process to convert the HYPAN polymer solution into a high-performance hydrogel. There is no chemical reaction involved in the coagulation step. The mold with the filled polymer solution is quickly immersed into a water bath. This process must be performed very carefully to prevent air bubbles from adsorbing at the surface of the coagulated film. Both the hard and soft blocks in the HYPAN polymer are solvated in the solvent. The solvent is replaced by water during the coagulation process. Water solvates the soft blocks, but precipitates the hard blocks. These hard blocks form a new

61

phase and cause the polymer to solidify. HYPAN polymers keep their properties after multiple hydration-dehydration cycles.

Unless otherwise specified, the pH 2.0 buffer was made from chloroacetic acid. Buffers from pH 3.0 to 5.0 were made with acetic acid. Buffers from pH 6.0 to 8.0 were made with N-(2-acetamido)-2-aminoethansulphonic acid (ACES). The buffer concentrations were 0.05 M. The ionic strengths of buffers were adjusted to 0.05 M with NaCl.

4.2 Preparation and Derivatization of PolyTCPA-VBC Microspheres

Figure 4-1 is a SEM picture of the polyTCPA-VBC particles prepared by dispersion polymerization. These particles were small and uniform, which is consistent with results usually obtained from dispersion polymerization.[39,50] The average particle sizes was about 0.3 μm. This size is good for magnetoacoustic chemical sensors because we want to entrap these microspheres in the hydrogel membrane and increase the membranes adhesion to their substrates. The TCPA to VBC mole ratio is 1:1. The particles are lightly crosslinked with DVB at 2% (mole/mole monomer). As described in Section 1.3, the purpose of preparing copolymer of TCPA and VBC is to increase the hydrophilicity and porosity of the polymer after the microspheres are aminated. When derivatizing the particles with diethylamine, the secondary amine displaces a chloride on the VBC group to form a pH sensitive tertiary amine. The secondary amine also displaces the 2,4,5-trichlorophenol to form an amide. Table 4-1 shows the CHN analysis of the diethylamine derivatized polyTCPA-VBC particles. The nitrogen percentage is 8.55% in theoretical calculation and 5.94% in CHN experiment. Therefore, it shows that

62

about 69%, i.e. the experimental value over the calculated value, of the functional groups have been aminated.
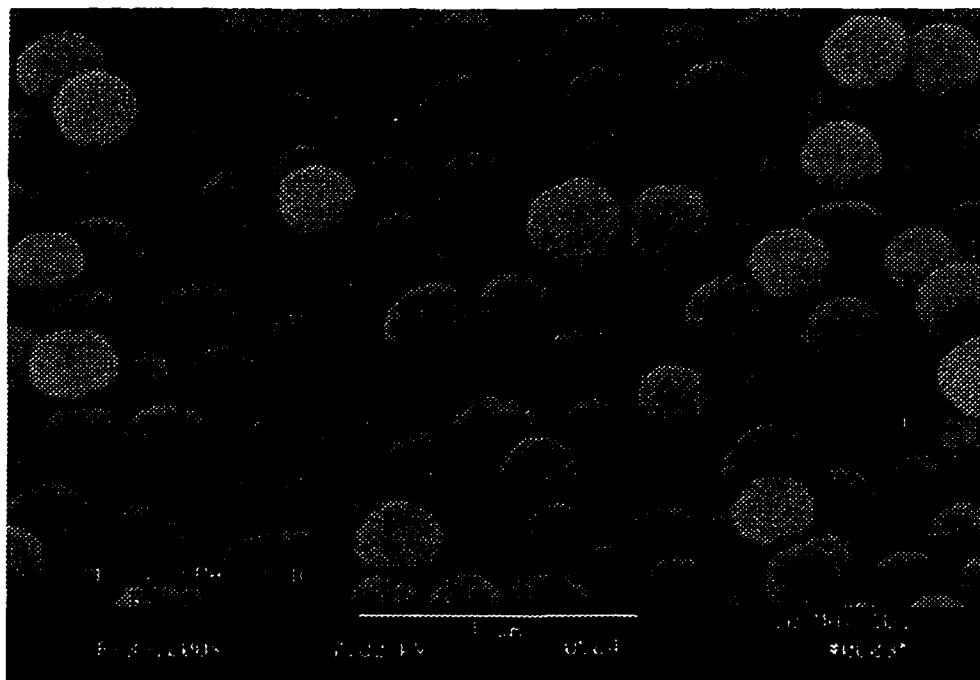
Figure 4-1 SEM picture of the polyTCPA-VBC microspheres prepared by dispersion polymerization

Table 4-1 CHN analysis of the diethylamine derivatized polyTCPA-VBC particles

Content	Theoretical Calculation	CHN Experiment
C%	74.52	63.20
H%	10.49	9.37
N%	8.55	5.94

63

4.3 Optical Properties of Diethylamine Derivatized PolyTCPA-VBC Microspheres

4.3.1 pH effects on the turbidity measurements

Figure 4-2 shows protonation of the aminated polyTCPA-VBC particles. It should be noted that only the tertiary amine on the VBC groups are protonated. 2,4,5-trichlorophenol, a large leaving group, is displaced with smaller diethylamine to introduce microporosity into particles. This decreases the response time. Figure 4-3 shows the turbidity changes of the sensitive membrane as a function of pH. The reference was a particle free HYPAN HN50 hydrogel membrane. Turbidity was measured as absorbance at 400 nm. The instrument was zeroed at pH 6.0. The sample membrane was prepared from a suspension of 0.2% microspheres in 8% HYPAN HN 50 solution in DMSO. In curve (a) un-derivatized polyTCPA-VBC microspheres were entrapped in the sample membrane. The turbidity of this membrane does not change as the pH changes. In curve (b) diethylamine derivatized polyTCPA-VBC microspheres were entrapped in the sample membrane. The turbidity of this membrane increases as the pH increases. The reason is that the derivatized microspheres deprotonate with increasing pH. They gradually shrink and lose water, which causes their refractive index to increase. Therefore, the swellable microspheres are responsible for the turbidity changes.
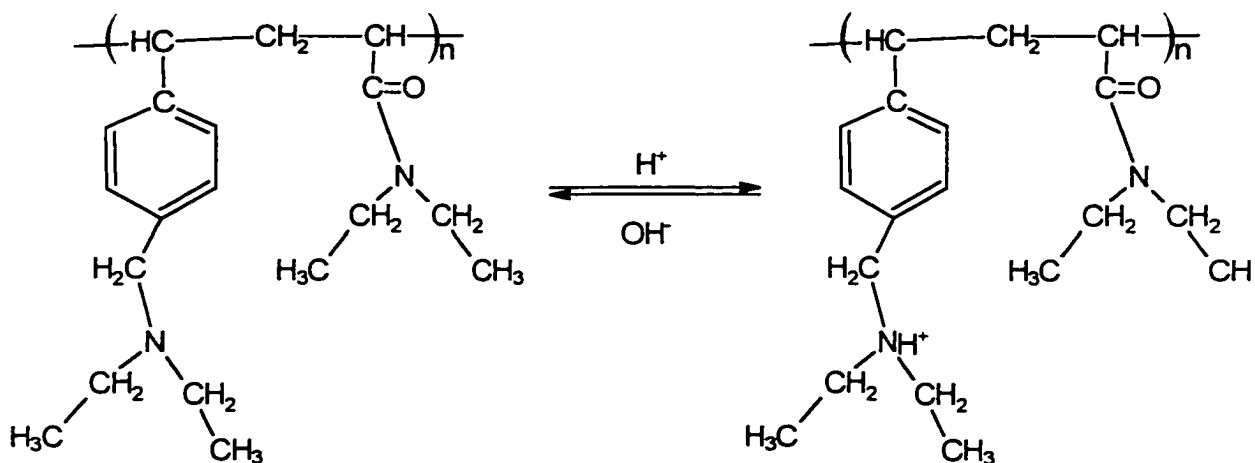
Figure 4-2 Protonation of the diethylamine derivatized polyTCPA-VBC particles.
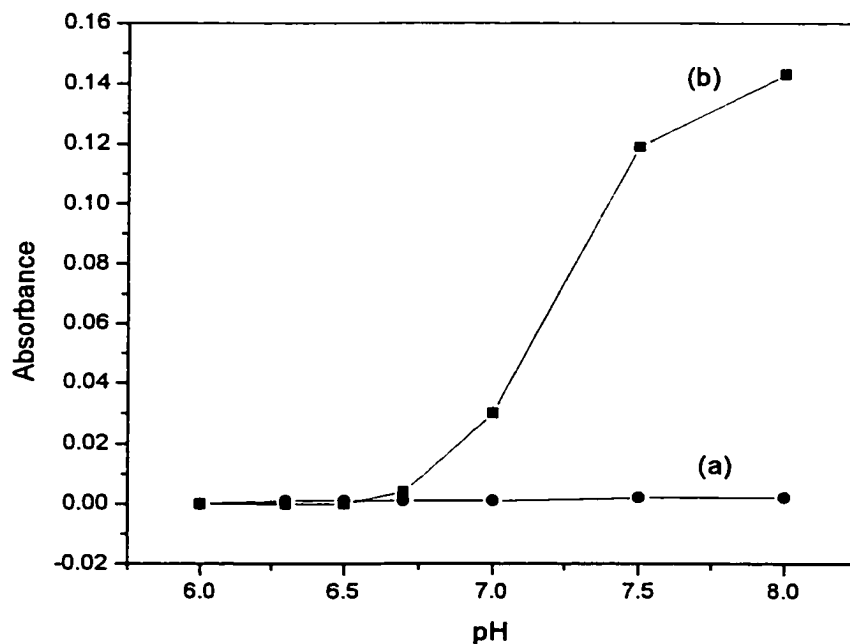
Figure 4-3 Turbidity measurements using HYPAN HN 50 membranes with entrapped (a) underivatized and (b) diethylamine derivatized polyTCPA-VBC microspheres.

65

4.3.2 Effects of different HYPAN types on turbidity measurements

During the pH measurements, we found that the swelling curve differs from the shrinking curve. This phenomenon is called hysteresis. Figures 4-4, 4-5, 4-6 show pH measurements using different HYPAN types as the hydrogel membrane. The pH sensitive particles are diethylamine derivatized polyTCPA-VBC. The sensitive membranes are prepared from a suspension of 0.2% particles in 8% HYPAN solution in DMSO. These figures clearly show that hysteresis is lowest when using HYPAN HN 80. HYPAN HN 80 has the smallest elastic modulus and largest water content of these three HYPAN polymers. We use the percentage of hysteresis to describe the effects of different HYPAN types. The percentage of hysteresis is defined as a ratio of the shrinking and swelling turbidity difference at a specified pH to the total turbidity gap. The total turbidity gap is defined as the turbidity difference between pH 8.0 and pH 6.0. Figure 4-7 shows the relationship between the percentage of hysteresis and water content of the HYPAN membrane. The percentage of hysteresis decreases as the water content of the membrane increases. Figure 4-7 also shows that the hysteresis at pH 7.0 is larger than at pH 7.5.

Figures 4-4 through 4-7 show that membrane response is subject to hysteresis. The degree of hysteresis increases as the water content of the membrane decreases. The dependence of hysteresis on membrane properties indicates that this is a mechanical effect. When a particle swells, it has to push against the outside membrane. Membranes with lower water contents are stiffer with higher elastic moduli. These membranes do not reach mechanical equilibrium in the time scale of the measurements described here. The hysteresis at pH 7.0 is larger than the hysteresis at pH 7.5 because the particles are more

66

highly protonated at the lower pH. Therefore, the equilibrium degree of swelling is greater.
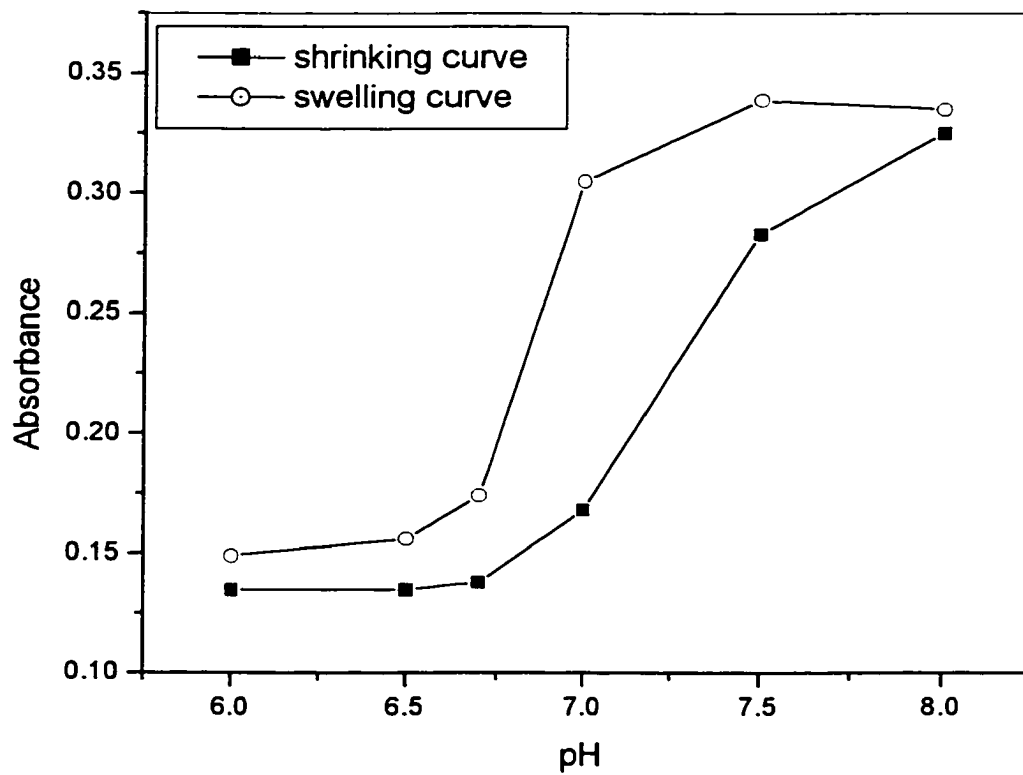
Figure 4-4 pH measurements using HYPAN HN 30 as the hydrogel membrane

67
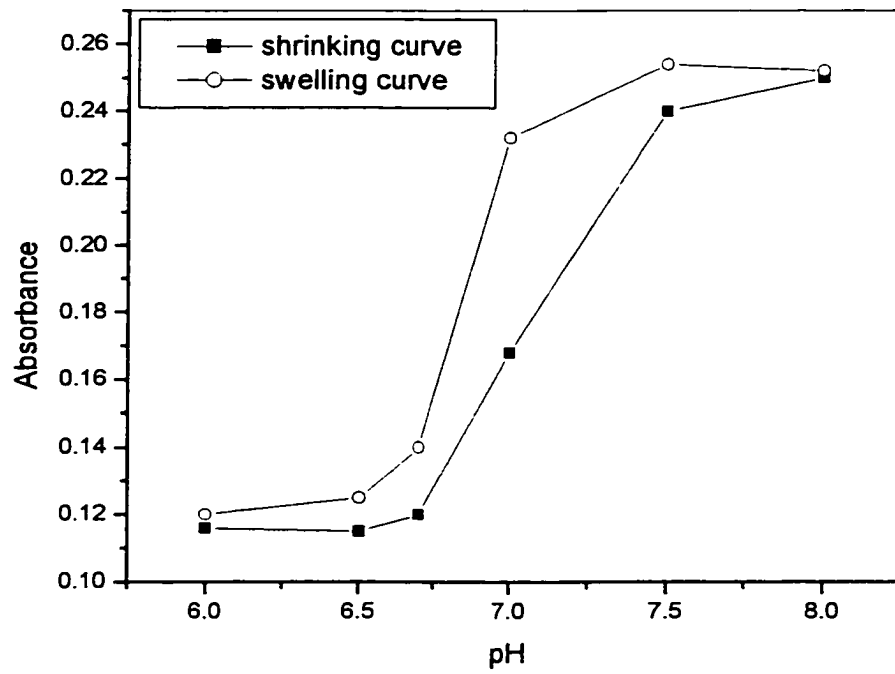
Figure 4-5 pH measurements using HYPAN HN 50 as the hydrogel membrane

68
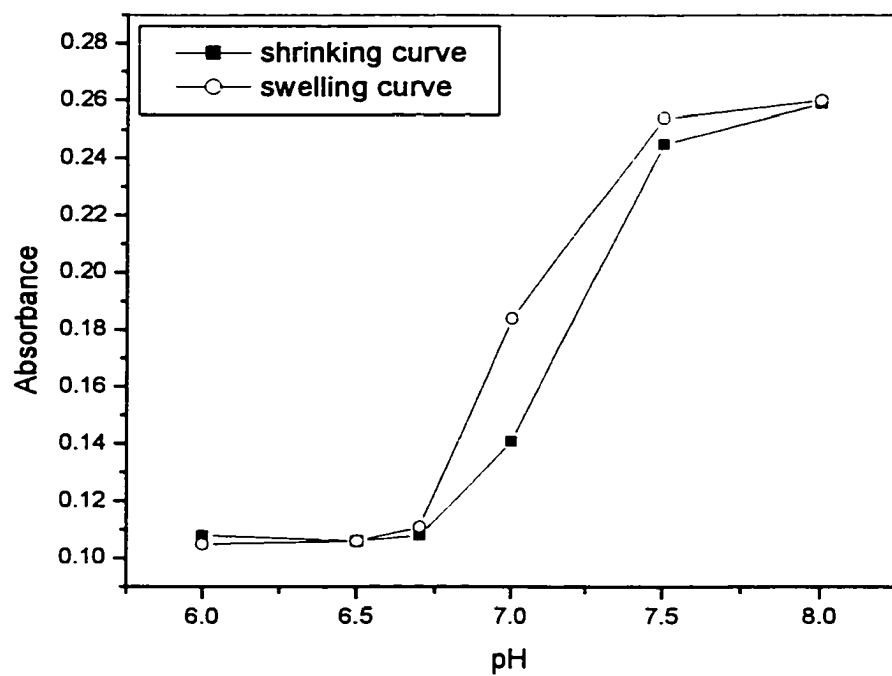
Figure 4-6 pH measurements using HYPAN HN 80 as the hydrogel membrane

69
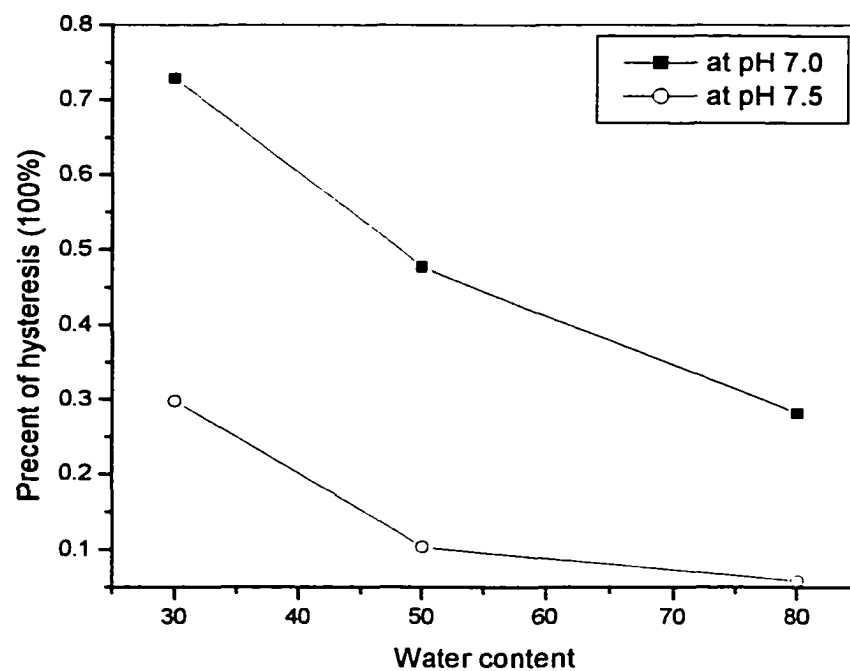
Figure 4-7 Relationship between the percentage of hysteresis and water content of the HYPAN membrane

70

4.3.3 Effects of HYPAN type on response time

HYPAN type also affects the rate of response to pH changes. The upper curve in

Figure 4-8 shows the response time when the pH sensitive membrane is transferred from

pH 6.0 to pH 8.0 buffer. This is a shrinking curve. The lower curve shows the response

time when the pH sensitive membrane is transferred from pH 8.0 to pH 6.0 buffer. This

is a swelling curve. HYPAN HN 30, HN50, and HN 80 are used in Figure 4-8, Figure 4-

9, and Figure 4-10, respectively. If we compare the three shrinking curves, we find that

the response becomes faster when the water content of the membrane increases. In

Figure 4-10, the turbidity changes immediately when the sensitive membrane is placed in

the pH 8.0 buffer. The same trend is observed in the swelling curves.
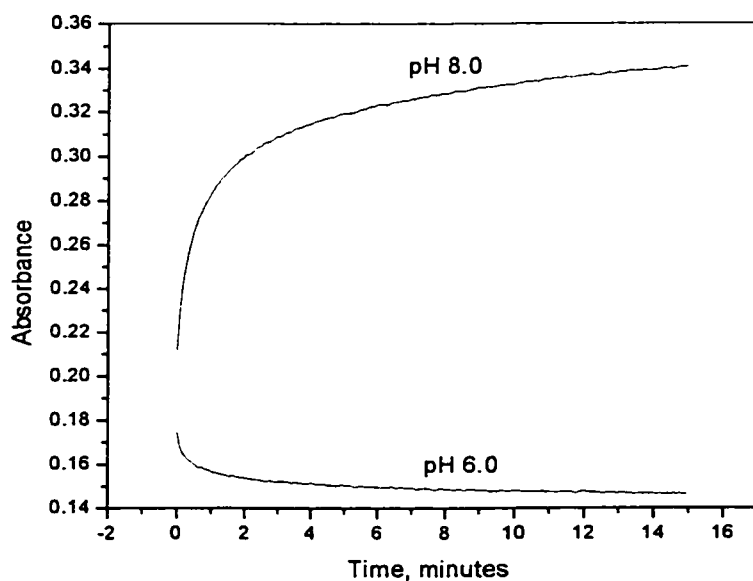
Figure 4-8 Response time when the pH sensitive membrane is placed in pH 6.0 and pH
8.0 buffers. HYPAN HN 30 is used as the hydrogel membrane.

71
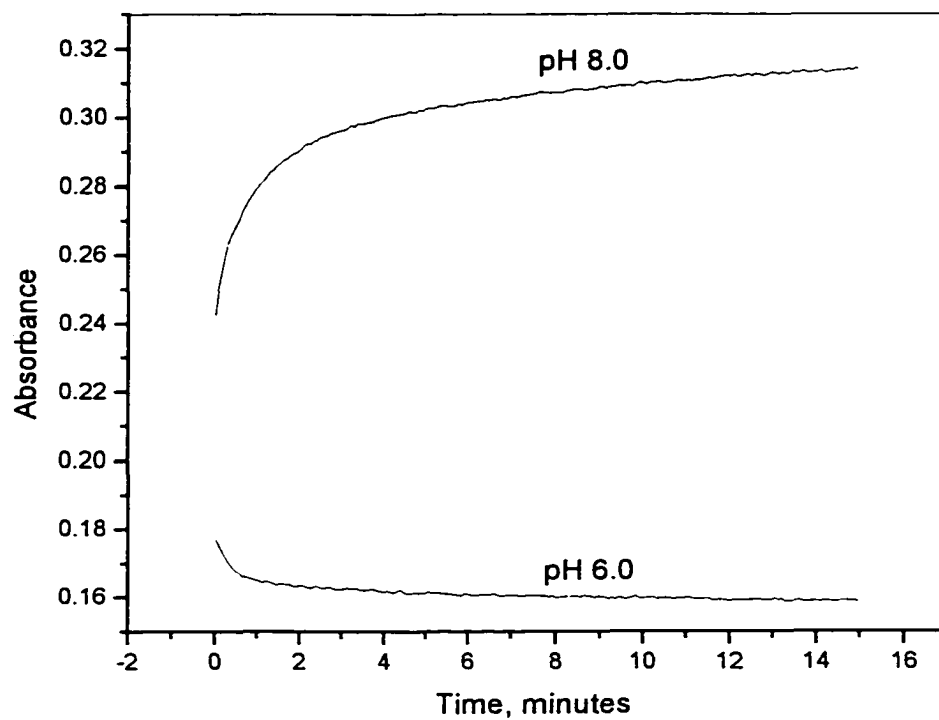
Figure 4-9 Response time when the pH sensitive membrane is placed in pH 6.0 and pH 8.0 buffers. HYPAN HN 50 is used as the hydrogel membrane.

72
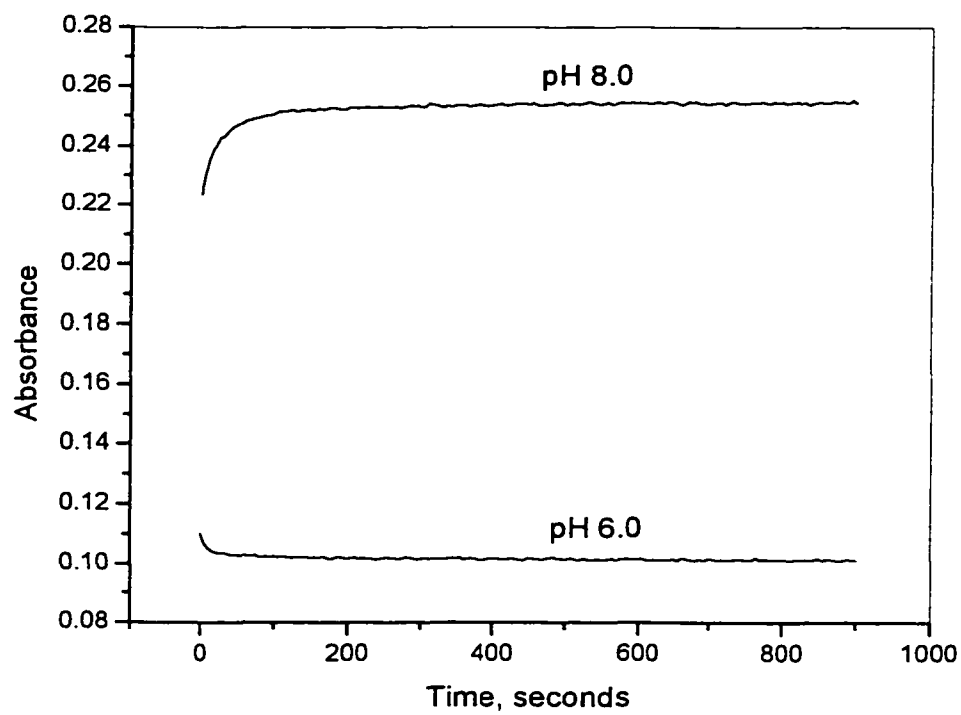
Figure 4-10 Response time when the pH sensitive membrane is placed in pH 6.0 and pH 8.0 buffers. HYPAN HN 80 is used as the hydrogel membrane.

73

4.3.4 Effects of PVA membrane on the turbidity measurements

PVA, a widely known hydrogel, has been used for a long time in our group.[72]

Although PVA is not suitable for magnetoacoustic sensors due to its poor adhesion to the

magnetic ribbons, it is good for turbidity measurements. Figure 4-11 shows the response

time when entrapping the pH sensitive particles in PVA membrane. It takes about 5

minutes for the shrinking curve to level off. The swelling curve levels off more quickly

when the membrane is placed in pH 6.0 buffer. Figure 4-12 compares the effects of the

PVA and HYPAN HN 50 on the response times. It shows that the response is faster

using PVA, especially for the swelling curve. The PVA membrane responds immediately

after it is placed in pH 6.0 buffer. This means the swelling process is completely

dominated by the swelling force of the particles. The PVA membrane, which contains

ca. 90% water, has less effect on particle swelling and shrinking.

Figure 4-13 and 4-14 show the hysteresis of turbidity measurements. In Figure 4-

13, the PVA membrane is equilibrated in buffer for 2 minutes before each measurement.

In Figure 4-14, the PVA membrane is equilibrated in buffer for 15 minutes before each

measurement. The hysteresis decreases as the equilibration time increases. As shown in

Figure 4-11, the sensitive membrane has reached shrinking equilibrium after it sits in pH

8.0 buffer for 15 minutes. Therefore, equilibration time is a factor affecting hysteresis.
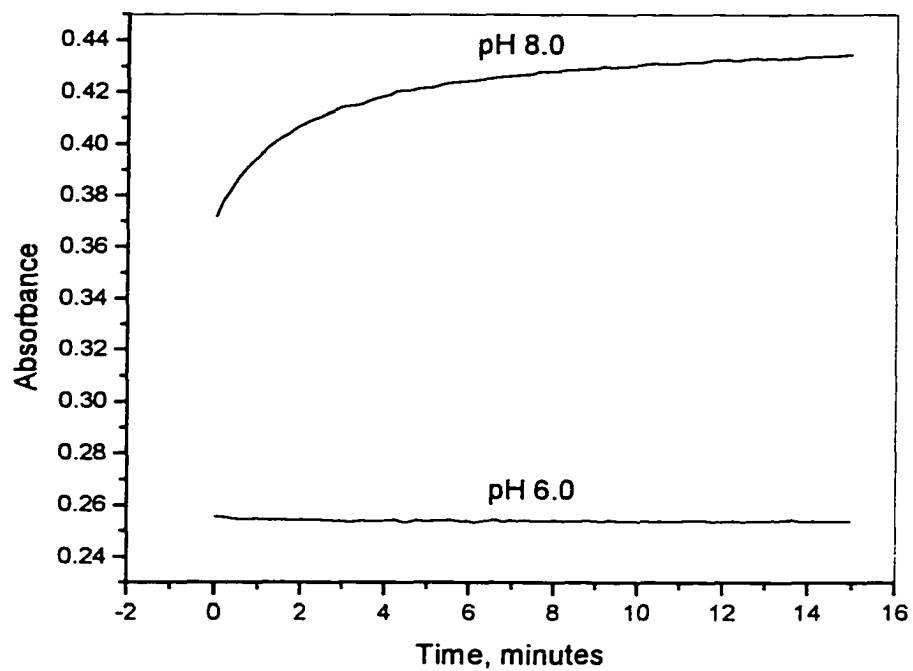
Figure 4-11 Response time when the membrane is placed in pH 6.0 and pH 8.0 buffers. PVA is used as the hydrogel membrane.
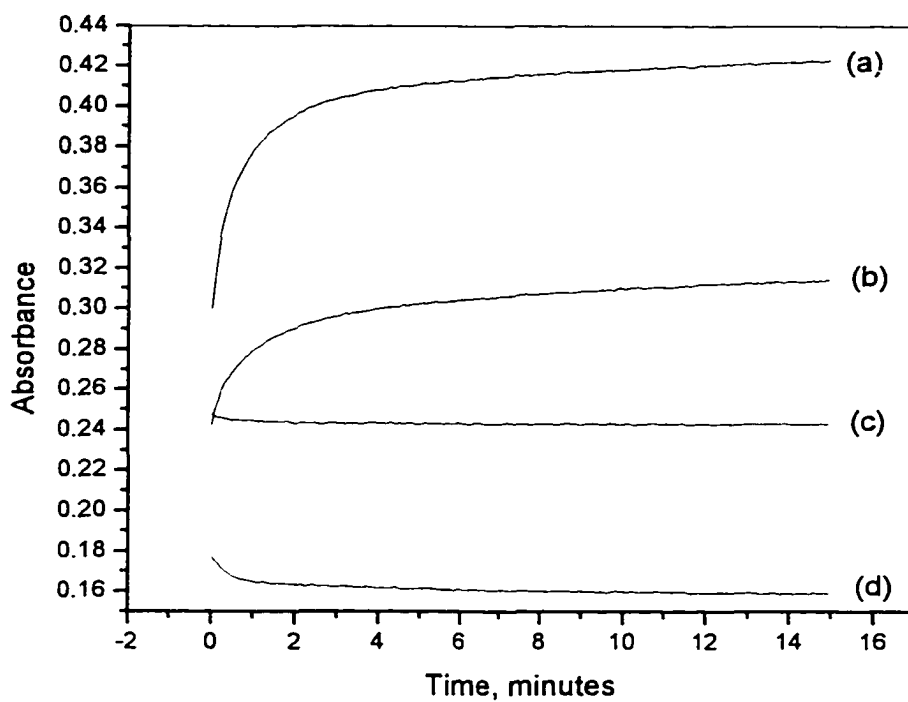
Figure 4-12 Response time when the membranes are placed in pH 6.0 and pH 8.0 buffers. (a) in pH 8.0 buffer using PVA (b) in pH 8.0 using HYPAN HN 50 (c) in pH 6.0 using PVA (d) in pH 6.0 using HYPAN HN 50

76
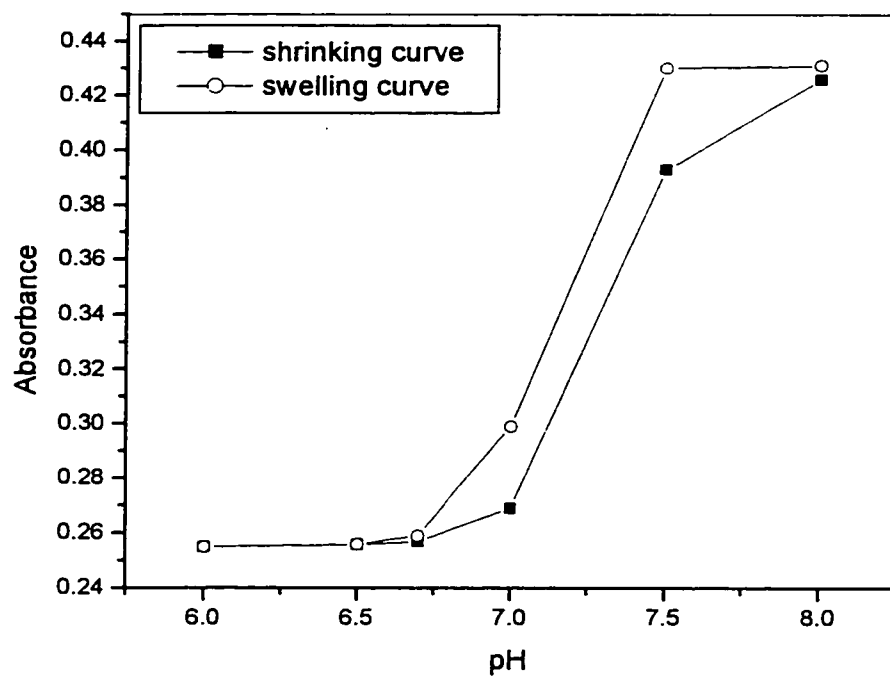
Figure 4-13 Turbidity vs. pH when the PVA membrane is equilibrated in buffer for 2 minutes before each measurement

77
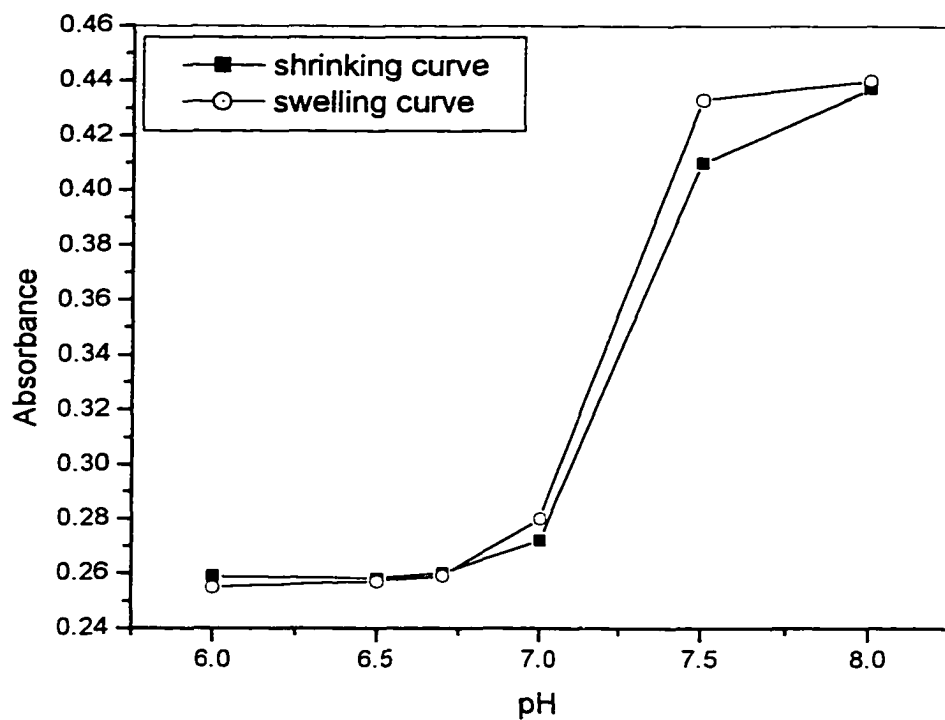
Figure 4-14 Turbidity vs. pH when the PVA membrane is equilibrated in buffer for 15 minutes before each measurement

78

4.4 Preparation and Derivatization of PolyVBC Microspheres

PolyVBC particles were prepared by suspension polymerization. However, we use the SPG technique to prepare the emulsion rather than the traditional method, which requires vigorous stirring and special reactors to suspend the monomer as droplets in the continuous phase. The principle and operation of the SPG emulsification technique have been described in Section 2.4 and Section 3.3.3, respectively. Usually large particles and a broad size distribution are obtained by traditional methods.

Figure 4-15 shows a SEM picture of polyVBC particles that were made by SPG technique. At that time, we didn't operate the SPG instrument very well. For example, the porous membrane was not completely cleaned and wetted, and the applied pressure was set too high. Therefore, we obtained large particles and a broad size distribution. These particles are very similar to those made by traditional suspension polymerization.

Figure 4-16 shows polyVBC particles with small sizes and narrow size distribution. These particles were obtained after we were experienced in operating the SPG instrument. It shows that SPG is a good technique to make emulsions with small droplet sizes. The pores inside the particles are due to the addition of porogenic solvent during polymerization. A typical formulation is shown in Section 3.3.5. The porogenic solvent is a mixture of xylene and dodecane with volume ratio of 2 to 1. The volume ratio of porogenic solvent to monomer and crosslinker is 4:10. The solvent is removed after polymerization leaving pore space. The affinity of the solvent for the polymer determines the pore size. If a solvent has low affinity to the polymer, it separates into a distinct phase as polymerization proceeds and forms large pores. In our cases, the poor solvent that has less affinity to the polymer is dodecane. The good solvent is xylene.

79

In this study polyVBC particles were derivatized with diethyl malonate in a non-aqueous system as described in Section 3.3.8. These particles were then hydrolyzed to obtain the final derivatized particles. We tried different methods to hydrolyze the diethyl malonate groups. One of them was to put the particles in 6 M NaOH in a flask and reflux at 100 °C for three days. Another one was to hydrolyze the particles in a mixture of DMSO and 3 M HCl with a volume ratio of 1:1. But the hydrolyzed particles obtained by the above two methods did not respond to pH changes. Finally we hydrolyzed diethyl malonate groups in a mixture of DMSO and 6M NaOH with a volume ration of 1:4. The mixture was refluxed at 50 °C for three days. The response of these particles to pH change is described in the next section.
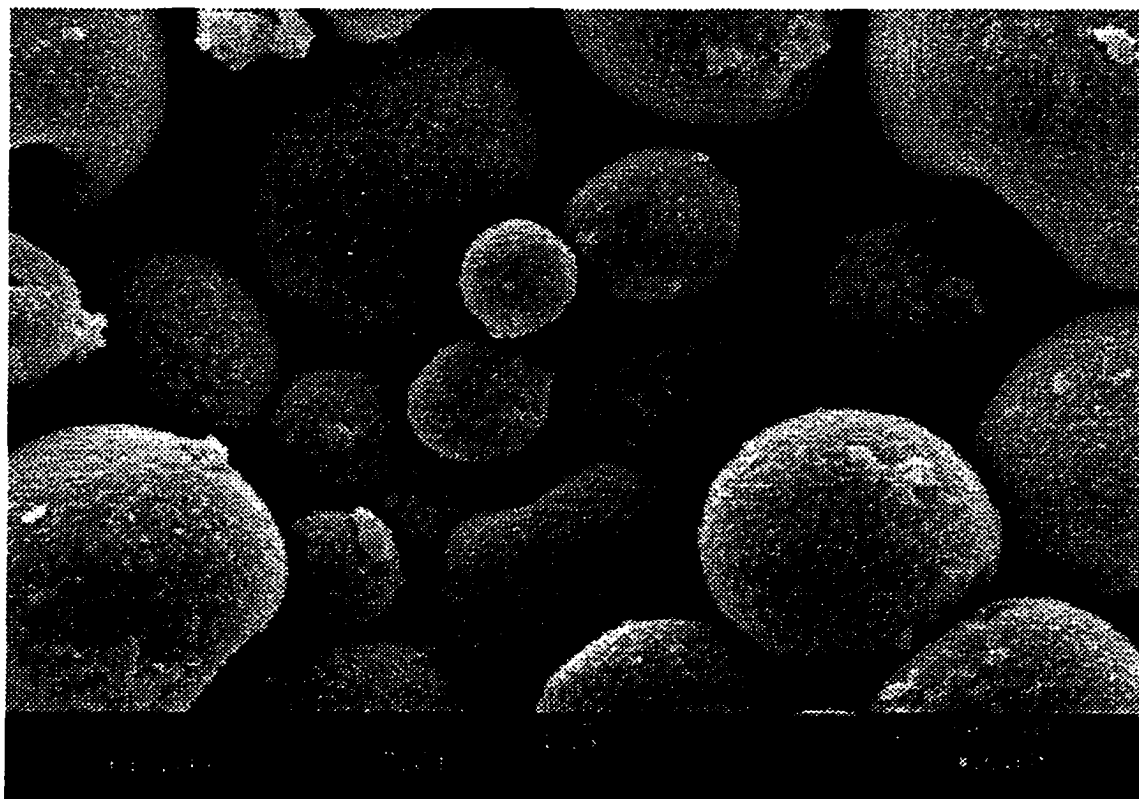
Figure 4-15 PolyVBC particles with large sizes and a broad size distribution prepared before we were experienced with SPG emulsification.
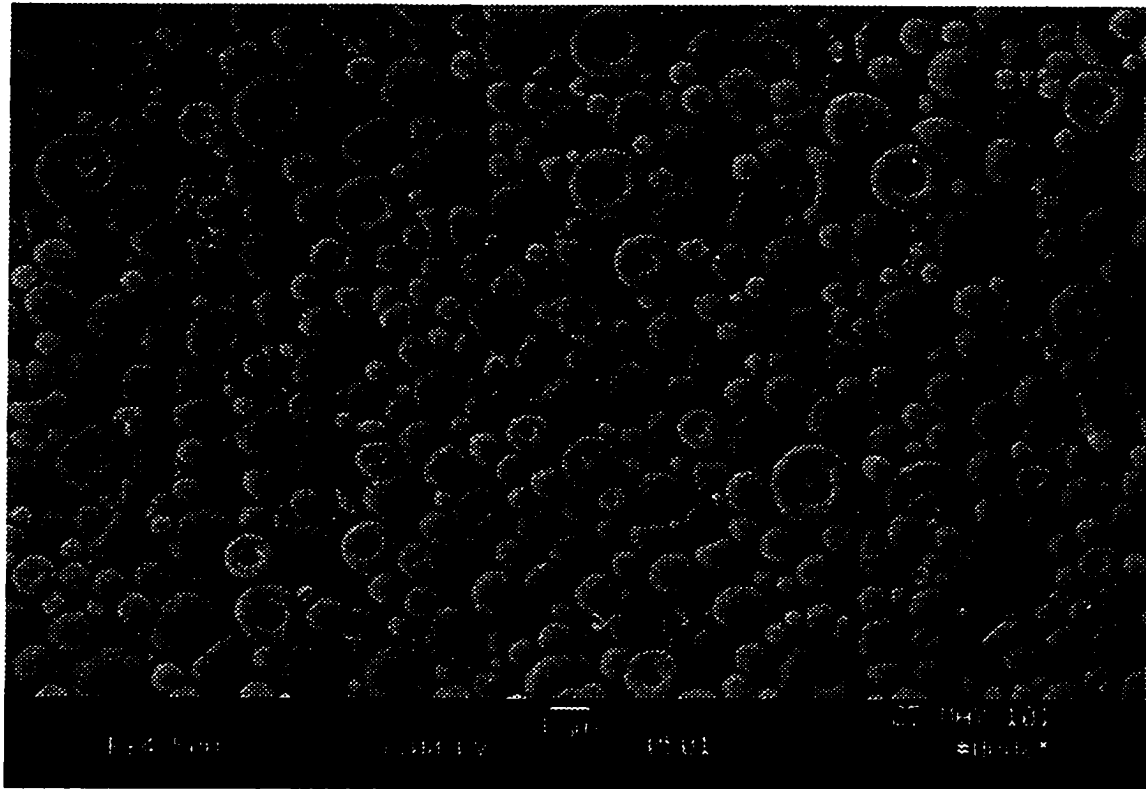
Figure 4-16 PolyVBC particles with small sizes and a narrow size distribution prepared after we were experienced with SPG emulsification.

81

4.5 Optical Properties of PolyVBC Microspheres Containing Carboxylate Groups

Figure 4-17 shows the turbidity spectra for derivatized polyVBC particles containing carboxylic groups. The turbidity of the membrane was different in pH 2.0 and pH 8.0 buffers. The membranes were prepared from a suspension of 1.0% derivatized particles in 8% HYPAN HN 50 solution in DMSO. The membrane thickness was 51 μm. The glitch at 800 nm is not the response of the membrane because the instrument changes detectors there. This figures shows that the membrane turbidity at pH 8.0 is smaller than that at pH 2.0. The reason is that protonation of the particles at low pH neutralizes the negative charge of the carboxylates, causing the particles to shrink. This trend is in contrary to the results obtained with diethylamine derivatized polyTCPA-VBC particles. Figure 4-18 shows the response time when the membrane is placed in pH 2.0 and pH 8.0 buffers. It takes less than 5 minutes for the derivatized particles to reach swelling and shrinking equilibrium. Figure 4-19 shows the membrane turbidity as a function of pH. Malonic acid has two pKa's, one at 2.847 and one at 5.696. But they are not resolved in Figure 4-19. Probably not all carboxylic groups are hydrolyzed, which results in a continuous turbidity change. Figure 4-19 also shows that the pH response of the carboxylated microspheres is subject to a high degree of hysteresis.
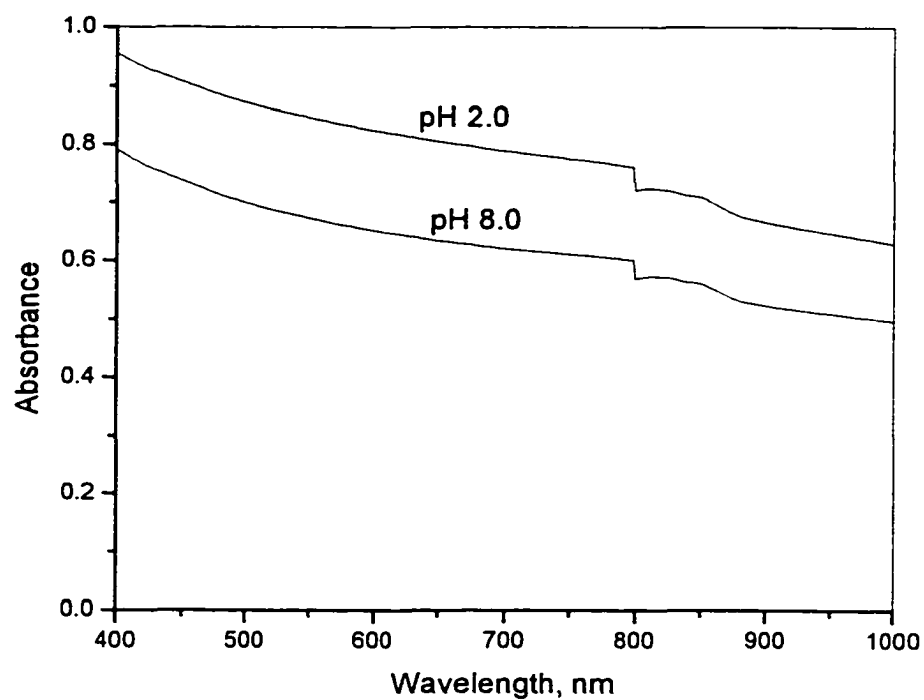
Figure 4-17 Turbidity spectra for derivatized polyVBC particles containing carboxylate groups. The hydrogel is HYPAN HN 50.

83
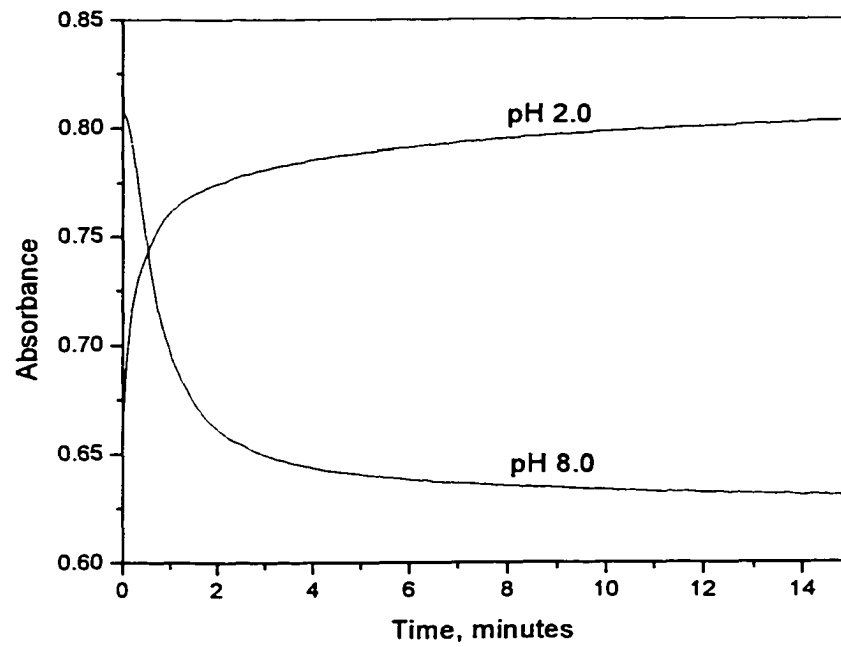
Figure 4-18 Response time when the membrane is placed in pH 2.0 and pH 8.0 buffers.

84
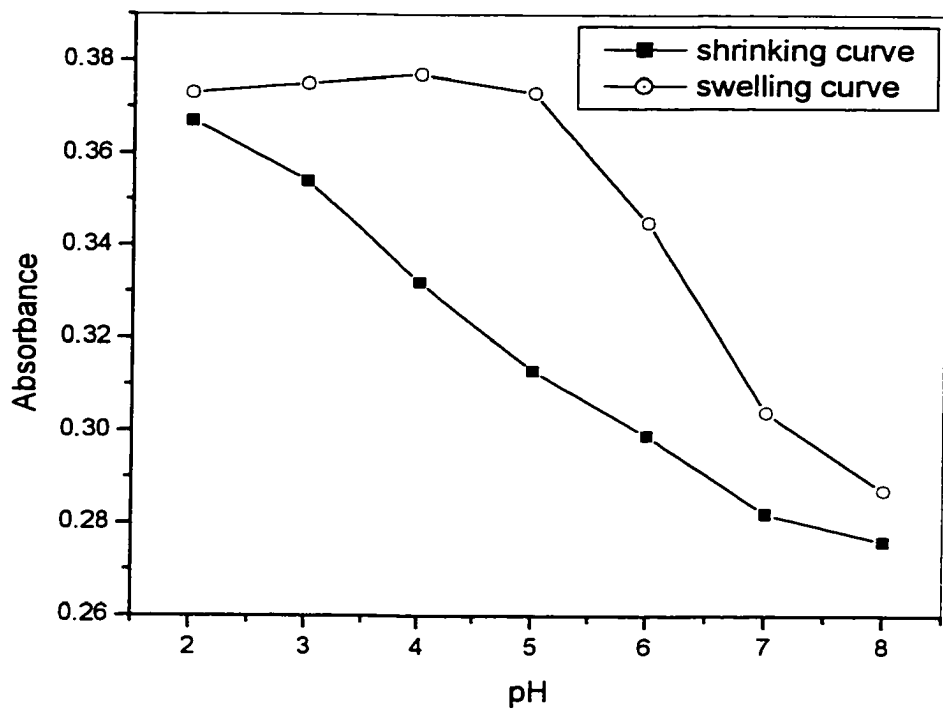
Figure 4-19 Hysteresis in turbidity vs. pH measurements using a HYPAN HN 50 membrane

4.6 Conclusions

The purpose of the research described in this chapter was to make microspheres that swell and shrink with changing pH. These were required to develop magnetoacoustic chemical sensors. These derivatized polymer microspheres were used to prepare pH sensitive ribbons for chemical sensors. Therefore, it was necessary to obtain such pH sensitive particles before we could move forward.

Basically this chapter was divided into two parts. The first part discussed the preparation, derivatization, and optical properties of diethylamine derivatized polyTCPA-VBC particles. These microspheres were prepared using dispersion polymerization. Usually we obtained small and uniform microspheres through this method. Here we used TCPA as a co-monomer. The big 2,4,5-trichlorophenol groups are displaced with small diethylamine groups. This forms micropores in the particles that greatly decrease the response time. Both PVA and HYPAN polymers were used to make hydrogel membranes for turbidity measurements. However, only HYPAN polymers can be used for magnetoacoustic chemical sensors because they adhere well to the magnetic ribbon. Hysteresis was observed during turbidity measurements. We use the percentage of hysteresis to describe the effects of different HYPAN types on the hysteresis. It shows that the percentage of hysteresis decreases as the water content in the hydrogel membrane increases. Of course, larger water content means higher analyte permeability. In addition, the material modulus may also affect the turbidity measurement. A thin layer of sensitive membrane was coated on the ribbon in order to decrease the membrane modulus effects. This is be discussed in Chapter 5.

86

The second part of this chapter discussed the preparation, derivatization, and optical properties of the derivatized polyVBC particles containing carboxylate groups. The polyVBC particles were prepared by suspension polymerization. However, a new technique called SPG was used to prepare the emulsion. It generates small and uniform emulsion droplets compared to those obtained from the traditional method. We used a mixture of xylene and dodecane as the porogenic solvent. Here xylene was used as a good solvent that has high affinity to the polymer. The space occupied by the porogenic solvent becomes small micropores after polymerization and the solvent is removed. Dodecane is used as a poor solvent that leaves large pores in the particles after it is removed. The pore size can be controlled by varying the ratio of xylene to dodecane. The purpose of forming pores in the particles is to decrease the response time. The derivatized particles were studied by turbidity measurements. As with diethylamine derivatized polyTCPA-VBC particles, the turbidity of the membrane decreases when the particles swell and increases when the particles shrink. In other words, the turbidity decreases when the particles take up water and increases when the particles lose water.

In summary, we have prepared two kinds of pH sensitive polymer microspheres. Their responses to pH have been studied through turbidity measurements. The results are positive. This means that a chemical response system has been built. We have accomplished the first step required to develop magnetoacoustic chemical sensors.

87

CHAPTER 5

STUDY OF MAGNETOACOUSTIC CHEMICAL SENSORS

5.1 Introduction

The next two chapters investigate magnetoacoustic sensors. The goal of this research was to develop a new kind of chemical sensor. Three main fields were involved in this study. First, we need to understand not only the operation of the resonance meter, but also its physical principle. Second, we need to build a chemical response system that can determine analytes in a chemical environment. In our group, this chemical response system is a hydrogel membrane with entrapped polymer particles that swell and shrink with changes in analyte concentration. Third, we need to solve the interface problem when we combine the resonance meter with the chemical response system. This step is critical since the chemical response system has to generate a magnetoacoustic signal.

In our first experiments, we monitored the viscosity of a starch solution, using a bare, untreated magnetoelastic ribbon. The purpose of these experiments was to study resonant frequency shifts when the sensor was used in a simple chemical environment. We found that resonance frequency varied with the square root of the product of viscosity and density of the starch solution. The resonance frequency shifts were proportional to the starch concentration. This result was useful in the development of a sensor to follow polymerization processes, because the monomer mixture becomes viscous during polymerization. However, as the working frequency range is from 35 to 75 kHz, our

88

instrument can only determine limited viscosity change. So, we can't monitor polymerization by directly putting a magnetic ribbon in the monomer mixture. This is a typical interface problem that is encountered when resonant meter is coupled to a chemical response system.

In this chapter, other factors that affect the resonance peak shifts were also studied, like bending the ribbon, positioning the membrane on different places on the ribbon, and the effect of membrane modulus changes. Usually we constructed a theoretical model first, and then tested the model with experiments. The purpose of these experiments was to help us understand the factors that affect the resonance peak shift.

5.2 Characteristics of the Magnetoelastic Ribbon

Magnetoelastic ribbons were METGLAS@ magnetic alloy 2826MB from Honeywell. The ribbon is 12.50 mm width, 0.035 mm thickness, and hundreds of meters long. In our research, we cut the ribbon to a length of 38.00 mm with a pair of scissors. The length was measured with a vernier caliper.

Table 5-1 shows the elemental analysis of the ribbon surface by X-ray photoelectron spectroscopy (XPS) measurement. The ribbon is an iron-nickel alloy. The bright side and the dull side have almost the same elemental composition.

Figure 5-1 (a) shows the frequency-dependent response of a 38.00 mm x 12.50 mm x 0.035 mm ribbon in the frequency range from 10 to 80 kHz. There are two peaks in this range, one around 30 kHz and the other around 57 kHz. The signal around 30 kHz is due to background of the magnetic field. Figure 5-1 (b) shows that the 30 kHz peak is observed when there is no ribbon inside the pick-up coil. All our measurements

89

monitored the resonance frequency shifts of the 57 kHz peak. Amplitude changes were not considered because they are affected by the outside magnetic field. Unless otherwise specified, the magnetic ribbon was placed in the Teflon cell shown in Figure 5-2 (a) and (b). Figure 5-2 (a) is a top-view of the cell, and Figure 5-2 (b) is a cross-section view. The dimensions of the cell are 10.0 mm high, 47.2 mm long, and 16.1 mm wide. There are two crossbeams 1.2 mm high, 16.1 mm long, and 1.5 mm wide at the bottom of the cell. They are 27.90 mm away from each other. The test ribbon was placed on the crossbeams, and the cell was filled with the test solution. Typically 2.5 ml of solution was added to the cell, just enough to cover the ribbon. Figure 5-3 shows the frequency shifts for a ribbon in contact with different media. The peak measured in air was at 58.525 kHz. When the ribbon was immersed in distilled water, the resonance frequency downshifted to 58.175 kHz, a very small shift. When a piece of Scotch tape was stuck on one side of the ribbon, the resonance frequency shifted to 52.129 kHz, a much larger shift. These experiments give us two kinds of information. First, the responses of the Resonance Meter are resonance frequency shifts. One resonance peak shows up in the frequency range from 35 to 75 kHz no matter whether the ribbon is free to vibrate in air or the ribbon is bonded to some material. The bonded material changes the frequency by changing the mass and modulus of the system. These results are consistent with the principle of magnetoacoustic sensors that was described in Section 2.1. This means that magnetoacoustic chemical sensors can be developed by coating a sensitive membrane on the ribbon. Second, it is better to bind the reacting reagents on the ribbon than to put them in the solution because larger signals or a larger frequency shifts will be obtained when the analytes interact with reagents bonded to the ribbon.

90

Table 5-1 Elemental analysis of a magnetic ribbon by XPS

Element	Bright side		Dull side	
	Atomic conc%	Mass conc %	Atomic conc %	Mass conc %
C	24.02	11.99	16.46	7.57
Mo	0.87	3.46	0.90	3.30
B	11.49	5.17	7.72	3.2
Ni	9.61	23.47	10.29	23.13
Fe	12.06	28.00	15.21	32.53
O	41.96	27.91	49.42	30.27

91
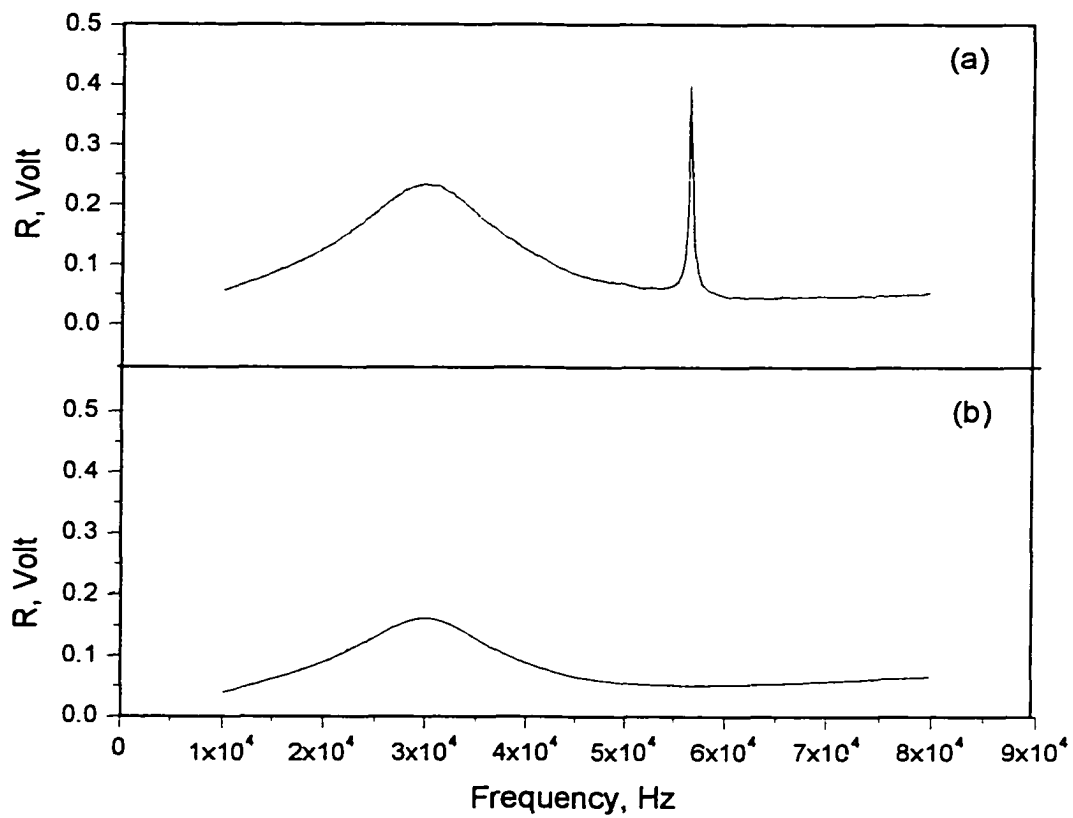
Figure 5-1 Frequency-dependent response of a magnetoelastic ribbon. (a) A ribbon inside the pick-up coil. (b) No ribbon inside the pick-coil.

92
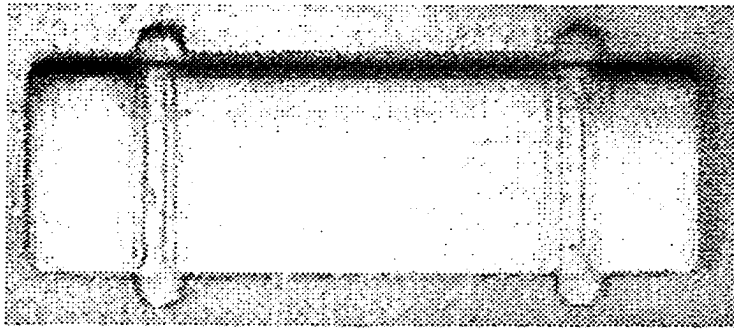
Figure 5-2 (a) Top-view of the Teflon measurement cell

Teflon cell

Magnetoelastic ribbon

Two crossbeams at the bottom of the cell
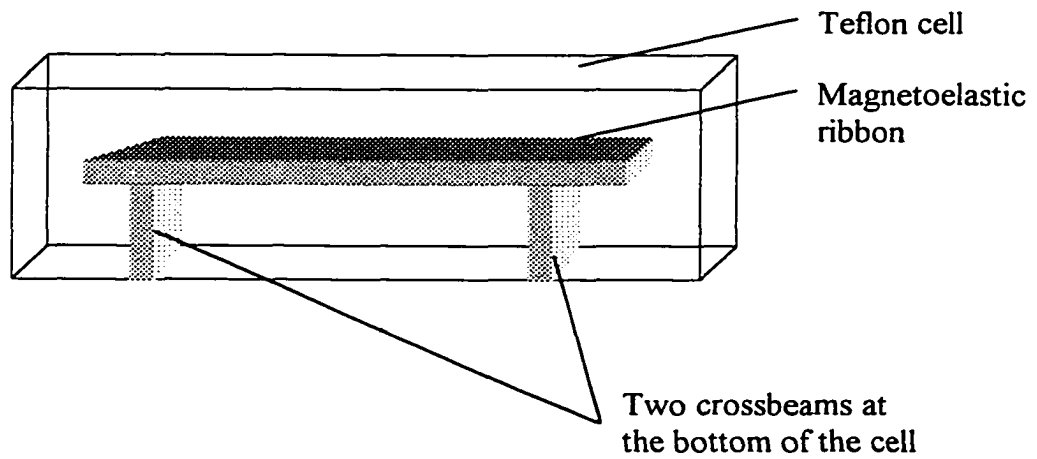
Figure 5-2 (b) The cross-section view of the Teflon cell

93
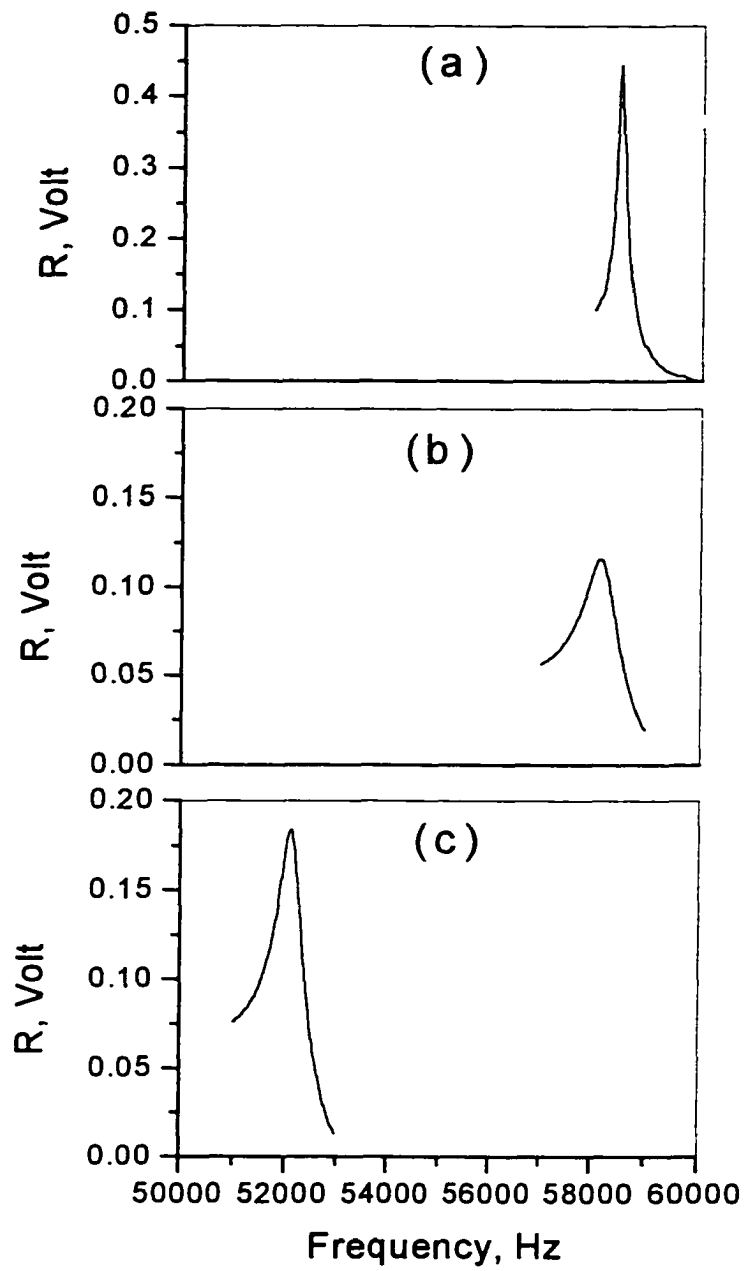
Figure 5-3 Resonance frequencies of a magnetoelastic ribbon in contact with different media. (a) air (b) water (c) in air with a piece of Scotch tape stuck to the ribbon

94

5.3 Viscosity Monitoring

The effect of viscosity on the resonant frequency of the magnetoelastic ribbon was evaluated by using starch powder that was soluble up to 10% (w/w) in cold water. The viscosity measurement was described in Section 3.4.8. Figure 5-4 shows how viscosity increases with starch concentration. The density changes are negligible compared to the viscosity changes when the starch concentration increases from 0% to 10%. Therefore, the viscosity change is equivalent to the change of the product of viscosity and density of starch solution. Figure 5-5 shows how the resonance frequency of the ribbon varies with the square root of the viscosity and density product of the starch solution. The frequency shift appears to depend on the interface between the ribbon and the starch solution. At high levels above 6.00 g/100ml, starch molecules deposit onto the magnetoelastic ribbon forming an adsorbed layer. This affects both the surface area and the interfacial tension between the ribbon and the external medium. Therefore, the slope at low starch concentration differs from the slope at high starch concentration.

Figure 5-6 shows the resonant frequency shifts as a function of starch concentration. The frequency shift Δf is the difference between the frequencies measured before and after the ribbon was immersed into the starch solution. The linear regression equation for the relationship between the frequency shift and the starch concentration is $\Delta f = 19.98C - 10.73$, where C is the concentration of the starch solution. The correlation coefficient is 0.997. This means the new sensor can directly monitor analytes that affect viscosity.
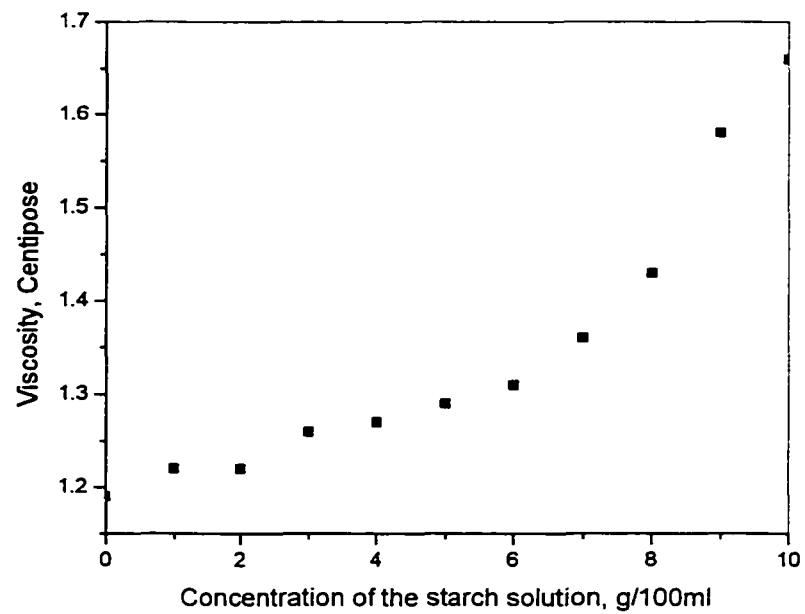
Figure 5-4 Viscosity vs. starch concentration

96
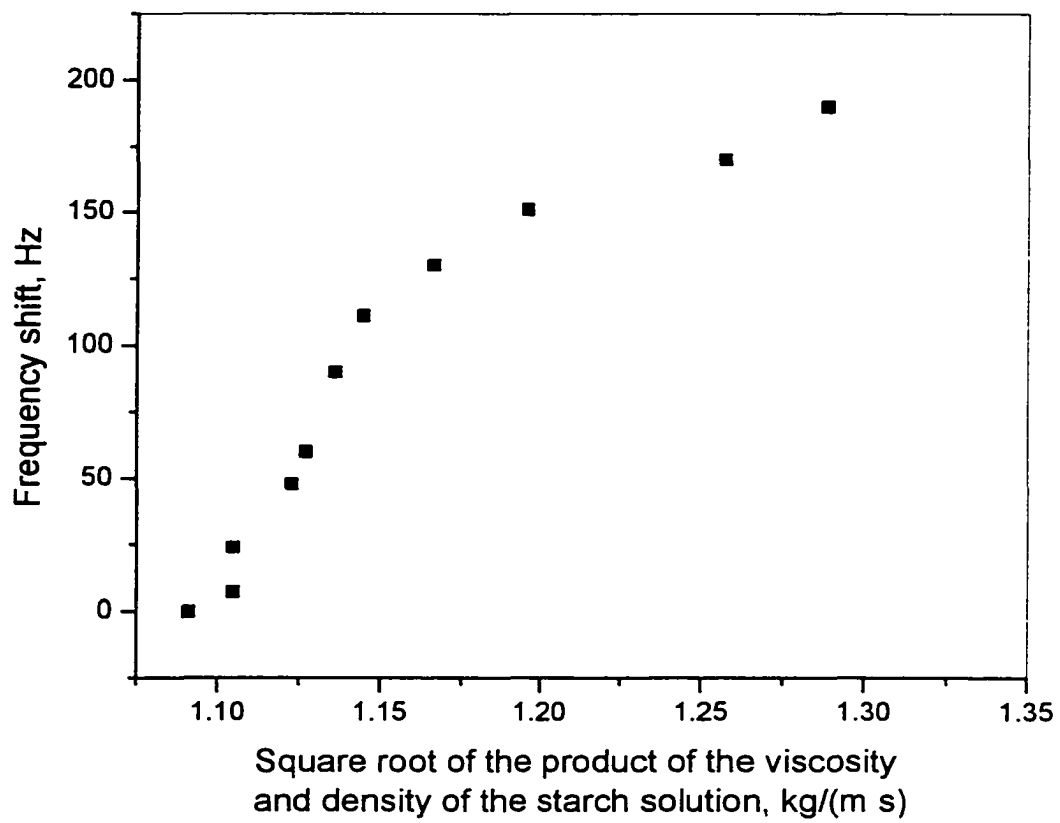
Figure 5-5 Frequency shift vs. square root of the product of the viscosity and density of the starch solutions

97
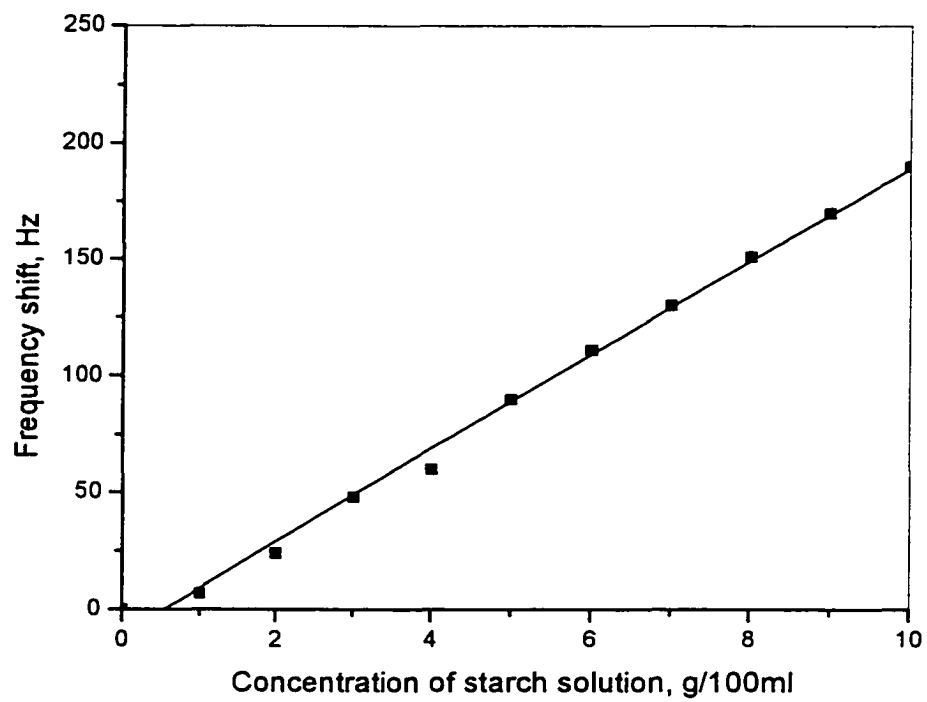
Figure 5-6 Frequency shift vs. starch concentration

98

5.4 Mass loading Monitoring

The effect of mass loading on resonant frequency was studied by adding water to free ribbon and ribbon coated with poly(hydroxyethyl acrylate) (polyHEA). This experiment was described in Section 3.4.9. Figure 5-7 shows the frequency response versus water loading on the free ribbon and ribbon coated with polyHEA membrane. When loaded water was under 1.5 mg, there was no response for the free ribbon. When mass loading was increased from 1.5 to 8.4 mg, the resonance frequency shifted slightly. Only when mass loading was larger than 8.4 mg did the free ribbon respond to water loading. However, after the ribbon was coated with polyHEA membrane, its sensitivity to water loading was greatly increased. The frequency shift was detectable when the mass loading was 0.5 mg. This may be caused by the modulus change of the polyHEA membrane when it takes up water. This implies that modulus is a more important factor than mass loading in causing the resonance frequency to shift.

5.5 Polymerization Monitoring

Bao[73] studied the hydrolysis of starch catalyzed by of α-amylase using a bulk acoustic wave viscosity sensor. Muramatsu[21] monitored viscosity changes in a liquid using a piezoelectric quartz crystal to determine endotoxin concentration by gelation of limulus amebocyte lysate. A piezoelectric quartz crystal was also used to study hemorheological phenomena.[74] Therefore, after we demonstrated that the resonance frequency shifts with viscosity and mass change, the possibility of following polymerization processes was investigated. The system used to investigate this involved the polymerization of 2-hydroxyethyl methacrylate (HEMA) as monomer, ethylene

99

glycol dimethacrylate (EGDMA) as crosslinker, and 2,2-dimethoxy-2-phenyl-

acetophenone (DMPAP) as photoinitiator. A typical formulation included 14.75 g of

HEMA, 0.222 g of EGDMA, and 0.225 g of DMPAP. These components were mixed

together and sonicated to dissolve DMPAP. The starting experiments were to put 25 µl

of monomer solution on a bare ribbon. Then the ribbon was placed under a 400 W

mercury lamp to polymerize for a period of time. The resonance frequencies were

measured at different time. Figure 5-8 shows how resonance frequency shifts during

polymerization. There was only one single peak in Figure 5-8 (a) to (d). A small peak at

58.880 kHz appeared besides the peak at 59.848 kHz in Figure 5-8 (e). The amplitude of

this peak became larger in Figure 5-8 (f). At the same time, the curve between 60 and 70

kHz became more irregular compared to Figure 5-8 (a) to (d). Several peaks appeared in

Figure 5-8 (g). The variation of amplitude with frequency became more complicated.

The resonance frequency is plotted vs. time in Figure 5-9 assuming that the highest peak

is the resonant peak.
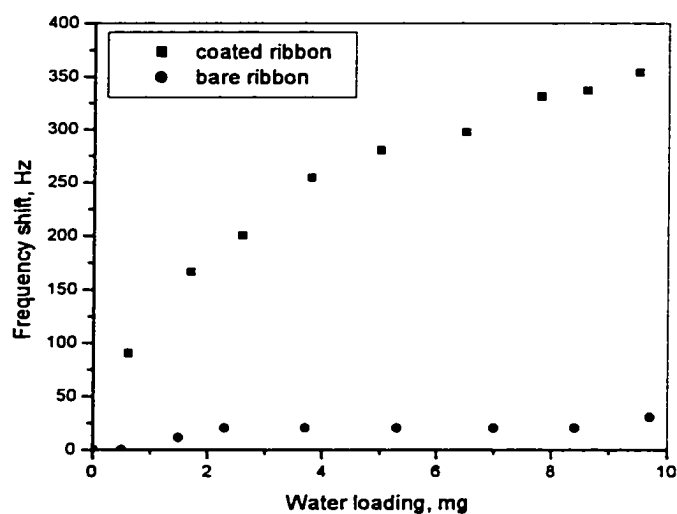
Figure 5-7 Frequency shifts of the coated and bare ribbons after water loading

100
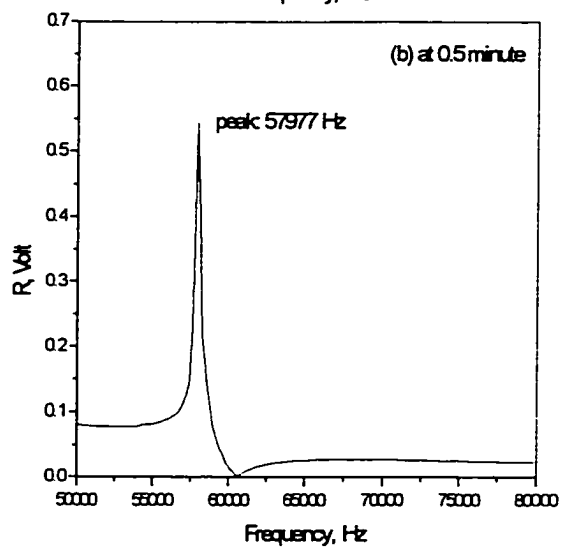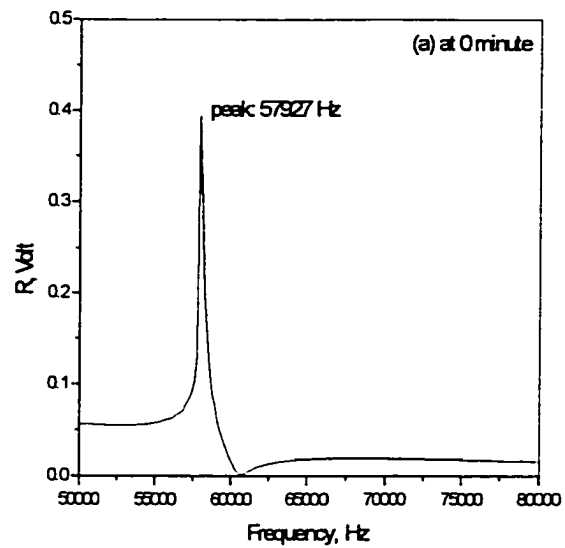
Figure 5-8 Polymerization of HEMA at (a) 0 minute, (b) 0.5 minutes
(Continued on next page)

101
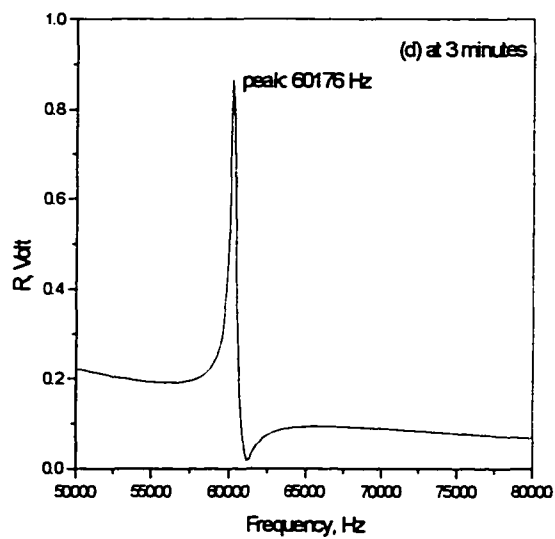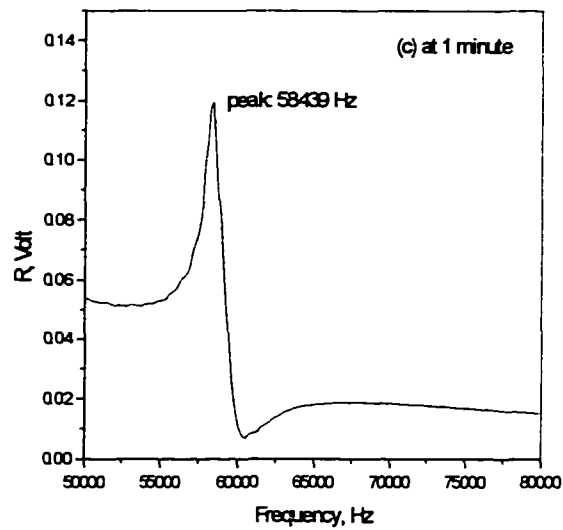
Figure 5-8 Polymerization of HEMA at (c) 1 minute, (d) 3 minutes
(Continued on next page)

102
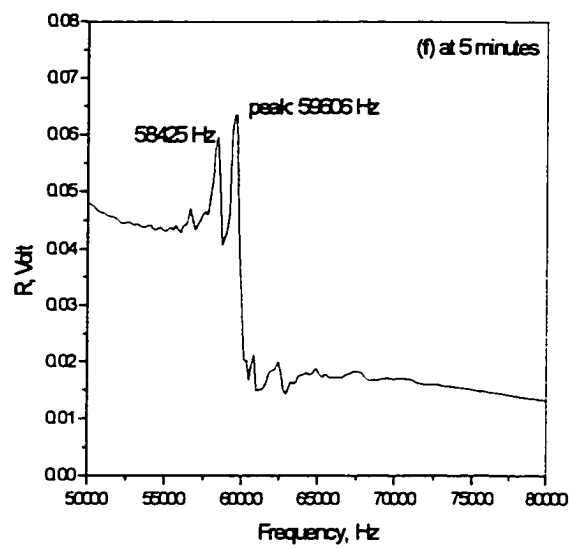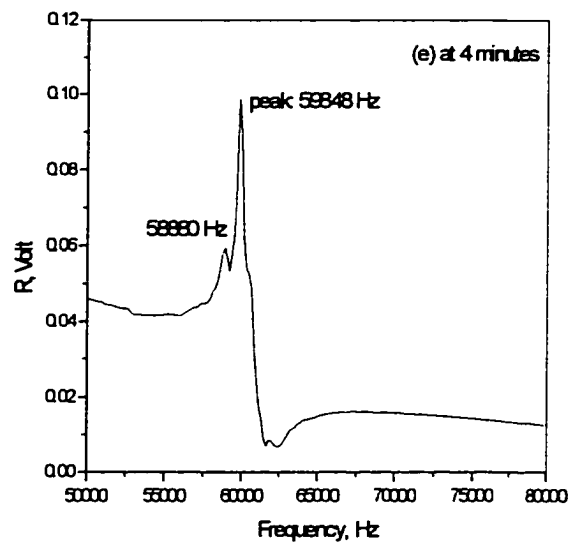
Figure 5-8 Polymerization of HEMA at (e) 4 minutes, (f) 5 minutes
(Continued on next page)

103
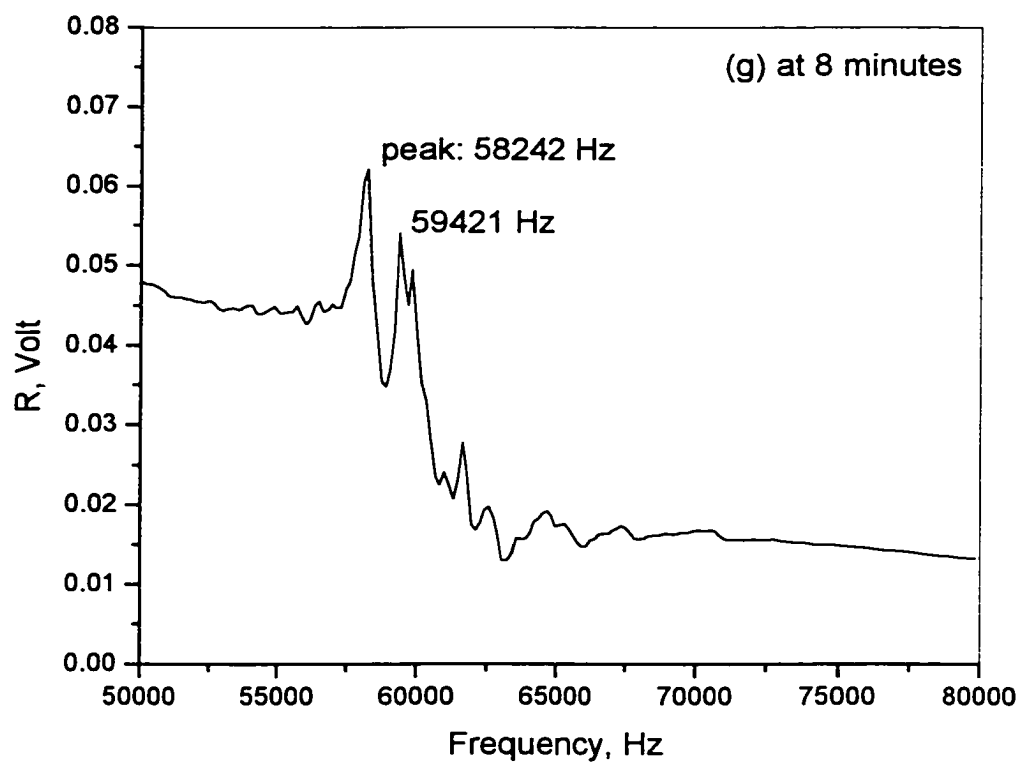
Figure 5-8 Polymerization of HEMA at (g) 8 minutes

104
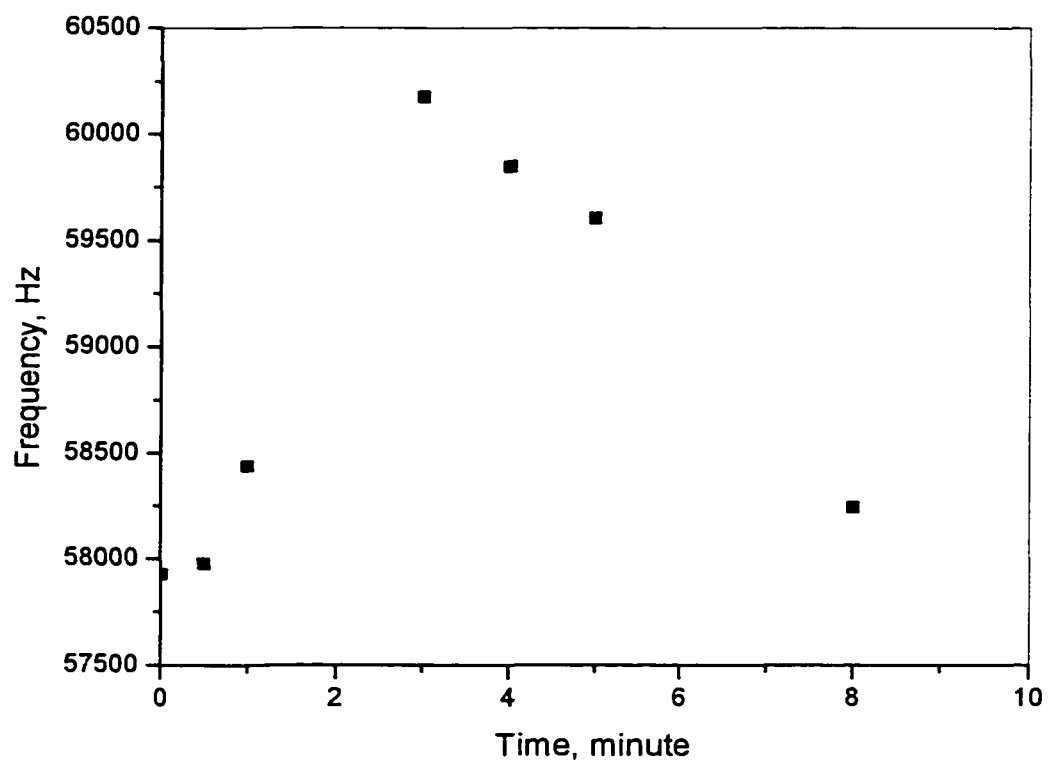
Figure 5-9 Frequency vs. time for HEMA polymerization

105

It is hard to explain the data point trend in Figure 5-9. It is known that many factors, not only mass, viscosity, and elasticity but also surface stress, and adhesion, can affect the resonance frequency shifts. Recently, some investigations have considered these factors. For example, Yang[23] explained the influence of surface stress on the resonance frequency. Most important, we found that the results reported by Shou-Zhuo[74] for hemorheological phenomena using a piezoelectric quartz crystal were very similar to our results shown in Figure 5-9. Even the experimental procedures were similar to ours. They added a drop of venous blood to the surface of a quartz crystal maintained at 37 °C and monitored the frequency. The results were divided into three regions. In the initial stage, the resonance frequency shifted slightly downward. In the second stage, the resonance frequency increased quickly. In the last stage, the resonance frequency gradually decreased again. To explain this, Shou-Zhuo[74] adopted the electrical equivalent circuit model[75] shown in Figure 5-10. In this model, the capacitance C represents the mechanical elasticity of the vibrating body. The inductance L corresponds to a measurement of the vibrating mass. The resistance R represents the loss in mechanical energy dissipated to the surrounding medium and the supporting structures. The parallel capacitance C_o comes from the electrodes on the quartz plate.

106
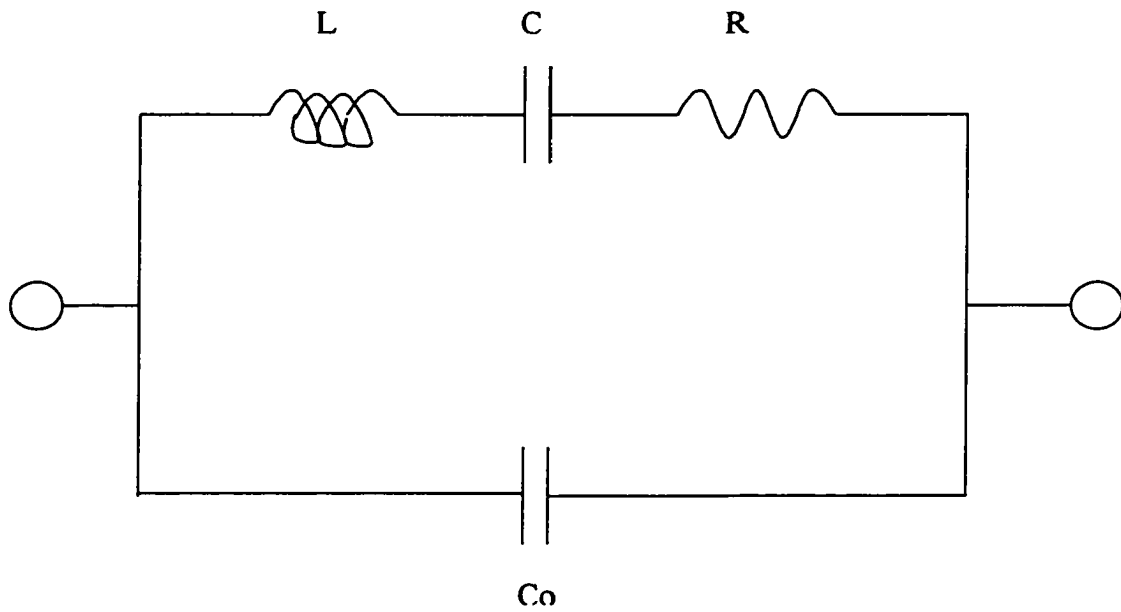
Figure 5-10 Electrical equivalent circuit for an AT-cut piezoelectric crystal oscillator

107

According to Shou-Zhuo's explanation, the increasing viscosity, which corresponds to the increasing resistance R in the equivalent electrical circuit, was the main factor causing the resonance frequency to decrease in the initial stage. The increase of the resistance R suggested that more energy was dissipated to the blood clot during the biochemical reaction forming fibrin at this period of time. In the second and third stage, the rheological character was controlled by the water amount inside the coagulated blood film after fibrin generation was complete. In other words, the mass effect dominated. In the equivalent electrical circuit, this corresponded to an increase of the inductance L in the second stage and a decrease of the inductance in the third stage. On the other hand, the water content dominated the adhesion of the coagulated blood film on the crystal. The water content was larger in the second stage than in the third stage because of evaporation. The adhesive force of blood film was larger in the second stage, too. This resulted in larger surface stress. Therefore, the resonance frequency increased rapidly during this period of time. The maximum resonance frequency was even larger than without coagulated blood film. In the third stage, the water content decreased because of evaporation. This decreased the adhesive force, and then the surface stress. During this period of time, the resonance frequency gradually decreased. This explanation was proved by experiments varying humidity inside the sensor chamber. It took a longer period of time to decrease the surface stress in higher humidity. Shou-Zhuo's explanation was adapted to describe the results shown in Figure 5-9. In Figure 5-9, the points can be divided into two regions. The region between 0 to 3 minutes corresponds to the second stage in Shou-Zhuo's results. The region between 3 to 8 minutes corresponds to the third stage. It is noticed that the initial stage where the resonance

108

frequency decreased disappeared in Figure 5-9. The reason is that the HEMA polymerization is faster than blood clotting. Therefore, resonance frequency was dominated by the mass effect. From 0 to 3 minutes, the resonance frequency rapidly increased. The liquid monomer solution became solid. It was found that the product strongly stuck on the ribbon surface. This caused large surface stress. As shown in Figure 5-8 (b) to (d), there was only one resonance frequency peak appearing. The shape of the peak was very sharp. This demonstrated that the ribbon together with the monomer solution or the product vibrated as an entirety. From 3 to 8 minutes, the resonance frequency began to decrease due to unreacted monomer and crosslinker evaporating from the polyHEMA membrane. The adhesive force decreased, which resulted in surface stress decreasing. As shown in Figure 5-8 (e) to (g), the frequency spectrum became complicated. Some small peaks showed up. This demonstrated that the ribbon didn't vibrate with the polyHEMA membrane as an entirety. This became worse at the end of the polymerization. The drying process may have generated some cracks at the interface of the ribbon and the polyHEMA membrane.

Although the above results demonstrate that HEMA polymerization can be monitored by the magnetoacoustic sensor, we were not very satisfied with it. First, it is not an in-line monitoring method. A sample has to be taken out from the monomer solution. Because the sample amount is very small, its components may change if evaporation occurs. Second, the surface stress depends on contact area. It is difficult to keep the same contact area every time when dropping the sample on the ribbon. Third, the sample's position on the ribbon affects the resonance frequency. This is discussed

109

later in this chapter. Therefore, we tried to find another sensing method to monitor polymerization.

Equation (2-1) in Section 2.1 describes the resonance frequencies of a ribbon that freely vibrates in its basal plane. When the integer n is 1, it gives the fundamental resonance frequency. The realistic boundary conditions include:[76]

1. a fixed, fixed ribbon when both ends of the ribbon are fixed.

2. a fixed, mass-loaded ribbon when one end is fixed, and the other end is terminated with some kind of inertance that behaves like a mass

3. a fixed, resistance-loaded ribbon when one end is fixed, and the other end is attached to a dashpot that constrains its motion.

In our Resonance Meter, the frequency spectrum can be obtained by sweeping the ac magnetic interrogation field over a pre-determined frequency range. So far in the system discussed in this chapter, the ribbon has uniformly contacted the surrounded media, air or liquid. There is no resonance frequency peak observed in the working frequency range from 30 to 70 kHz if the ribbon is entrapped in a solid or even in a very viscous liquid. This was observed in our previous experiments. Figure 5-11 shows two extreme cases. Figure 5-11 (a) is a ribbon vibrating freely in air. Figure 5-11 (b) is a frequency spectrum of a ribbon that is put in the middle of two microscopy slides. The two slides are tightly held together with a pair of clips so that the ribbon can't vibrate. There is no resonance frequency peak in the range between 20 and 70 kHz in Figure 5-11 (b). However, when we studied equation (2-1) and the boundary conditions, it posed a question. Is it possible to create a condition in which we can continuously keep the resonance frequency peak in the working frequency range when the medium changes

110

from a low viscosity liquid to a high viscosity liquid or a solid? If we can do so, we can monitor polymerization.

The initial step was to develop a physical model. Figure 5-12 is a schematic drawing of an experimental arrangement for determining the resonance frequency of a free, fixed ribbon inside the pick-up coil. One end of the ribbon is in air. The other end is placed in the middle of two microscopy slides, which clipped tightly together. The middle of the free end is positioned at the center of the pick-up coil. We assume that the free end can vibrate freely, and the other end doesn't vibrate. It is shown in Equation (2-1) that the resonance frequencies are inversely proportional to the ribbon length. Therefore, we can vary the fixed length to look for a suitable boundary condition in which the resonance frequency peak falls in the range from 30 to 70 kHz. Figure 5-13 (a) shows a ribbon of 37.58mm long vibrating freely in air. Its resonance frequency is 58893 Hz. Figure 5-13 (b) shows a frequency spectrum of the same ribbon when 0.64 mm is tightly held between two microscopy slides. A sharp peak appears at 29699 Hz. Physically, the boundary conditions in Figure 5-13 (a) and Figure 5-13 (b) are totally different, resulting in a large frequency shift. Figure 5-13 (c) shows a peak at 30000 Hz when 2.00 mm of the ribbon is fixed. Figure 5-13 (d) shows a peak at 30701 Hz when 4.02 mm of the ribbon is fixed. The shapes of these two peaks are similar to that in Figure 5-13 (a), but the resonance frequency shifts upward. There is a small bulge to the left of the peak at 33601 Hz in Figure 5-13 (e) in which 6.98 mm of the ribbon is fixed. This bulge became larger in Figure 5-13 (f) in which 9.00 mm of the ribbon is fixed, and in Figure 5-13 (g) in which 11.58 mm of the ribbon is fixed. It can be seen that two peaks clearly show up in the frequency spectrum between 20 and 70 kHz in Figures 5-13

111

(g), (h), and (i). One of the peaks is broader around 30 kHz and doesn't shift. The other peak is sharp and shifts upward from 40799 Hz in Figure 5-13 (g) to 51300 Hz in Figure 5-13 (i). The fixed length is 13.30 mm in Figure 5-13 (h) and 17.76 mm in Figure 5-13 (i). Now we can understand the data in Figure 5-13. First, Equation (2-1) is still suitable to explain the resonance frequency shift for a free, fixed ribbon. The background peak around 30 kHz appears no matter whether it is a free ribbon or a free, fixed ribbon. Second, the resonance frequency upward shifts when the fixed length increases and the free length decreases. This is summarized in Table 5-2 that lists the fixed length, 1/(free length) and the resulting resonance frequency. Figure 5-14 shows that the resonance frequency of a free, fixed ribbon increases as the fixed length increases. Figure 5-15 shows the relationship between the resonance frequency of a free, fixed ribbon and 1/(free length). The linear regression equation is:

$$f = 9.93856 \times 10^5 \times \frac{1}{L}$$

where f is the resonance frequency of a free, fixed ribbon, and L is the length of the free end. The unit is Hz for f, and millimeter for L. The correlation coefficient is 0.997. This result confirms that equation (2-1) can be used to describe the resonance frequency of a free, fixed ribbon.

112
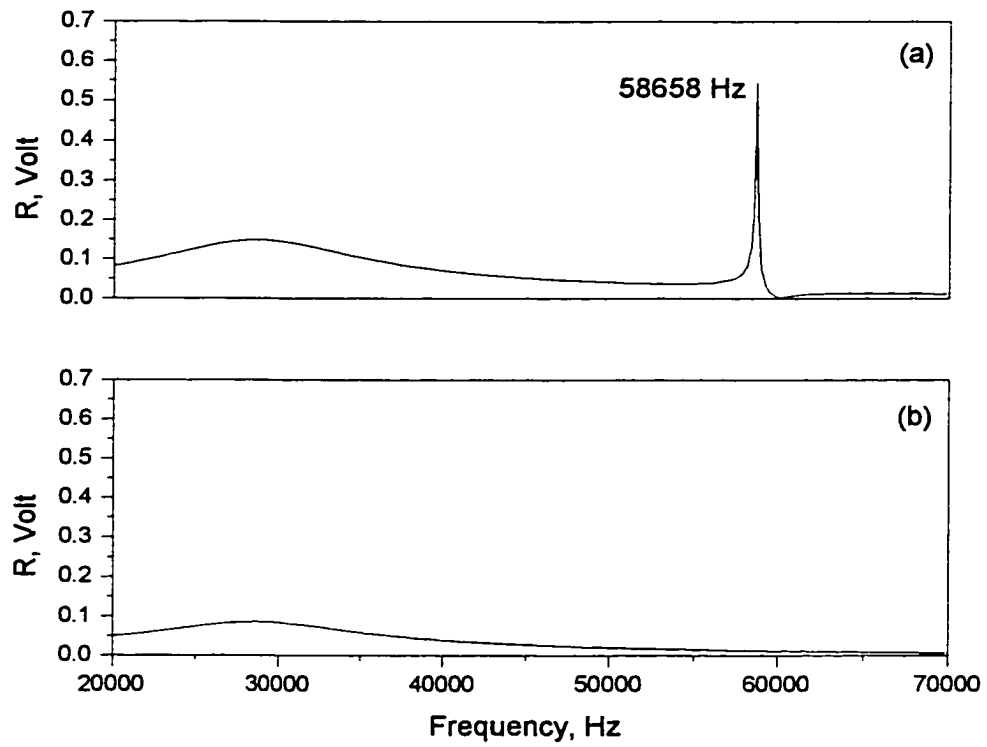
Figure 5-11 Frequency spectrum of a ribbon: (a) in air (b) in the middle of two microscopy slides.

113
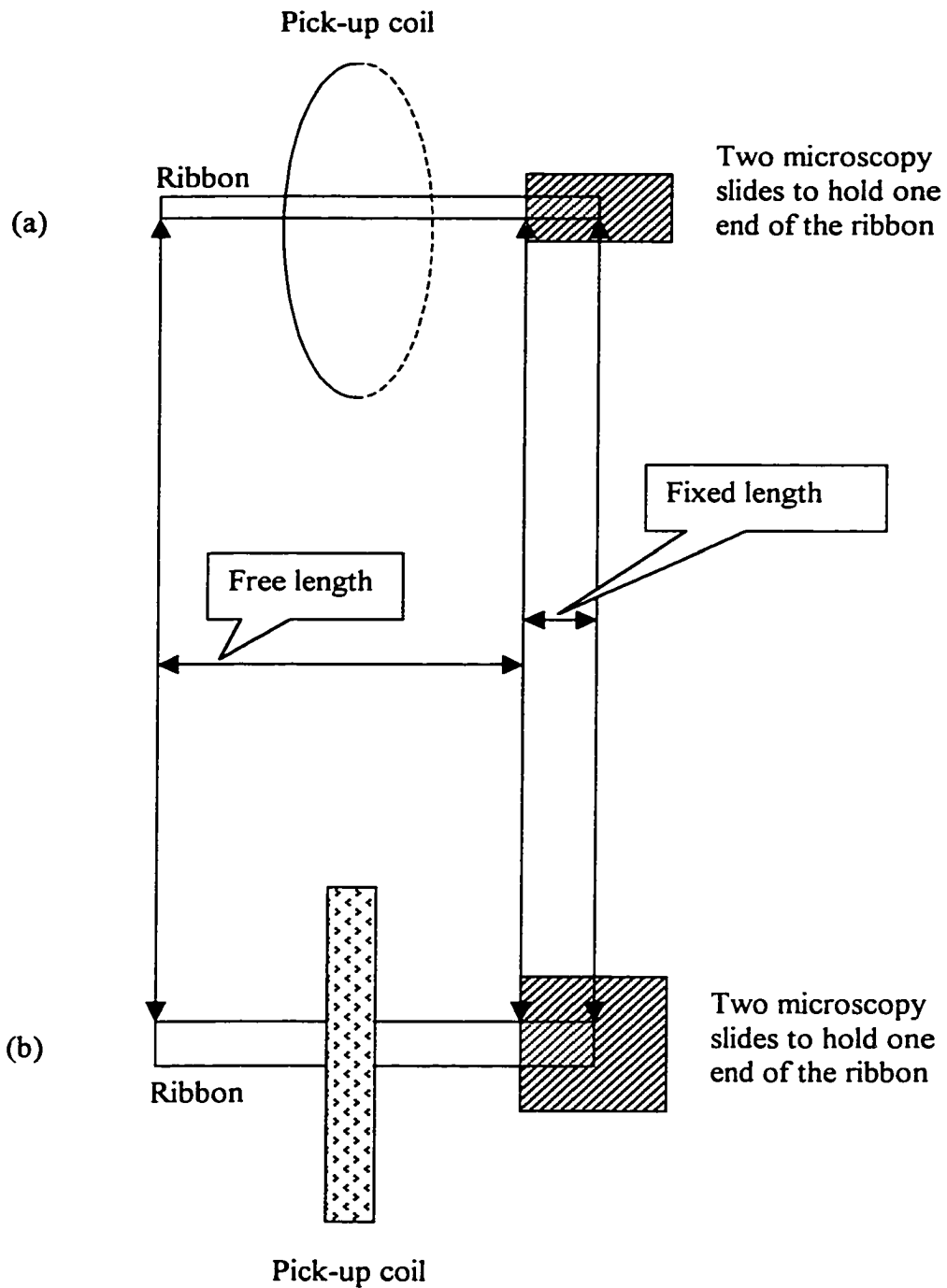
Figure 5-12 Schematic drawing of an experimental arrangement for determining the resonance frequency of a free, fixed ribbon inside the pick-up coil. (a) side view, (b) top view.
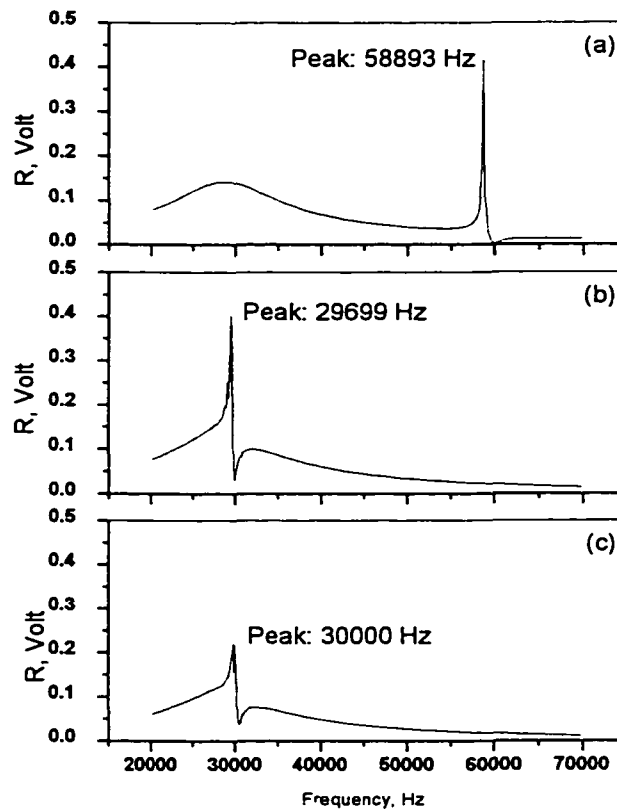
114

Figure 5-13 Resonance frequency of a 37.58 mm long ribbon with different fixed lengths. The fixed length is (a) 0 mm, (b) 0.64mm, (c) 2.00 mm
(Continued on next page)
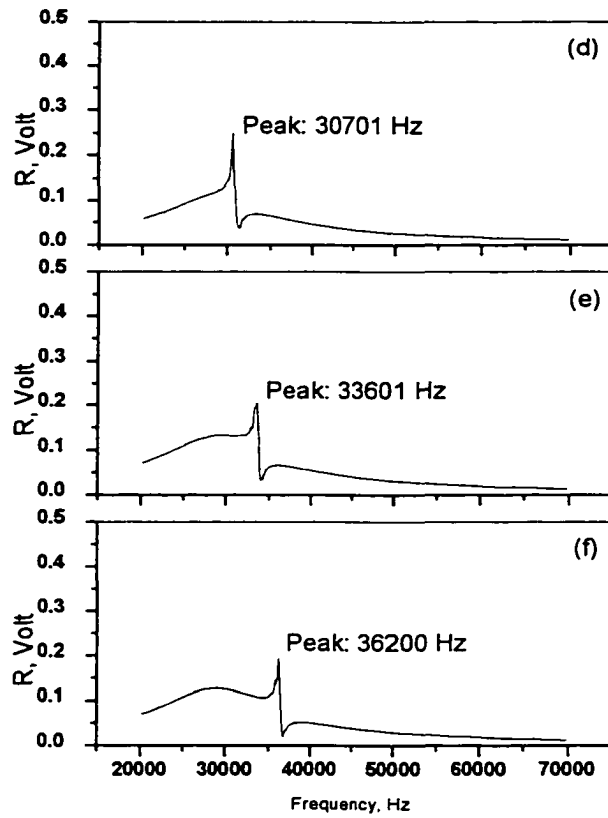
115

Figure 5-13 Resonance frequency of a 37.58 mm long ribbon with different fixed lengths. The fixed length is (d) 4.02 mm, (e) 6.98 mm, (f) 9.00 mm
(Continued on next page)
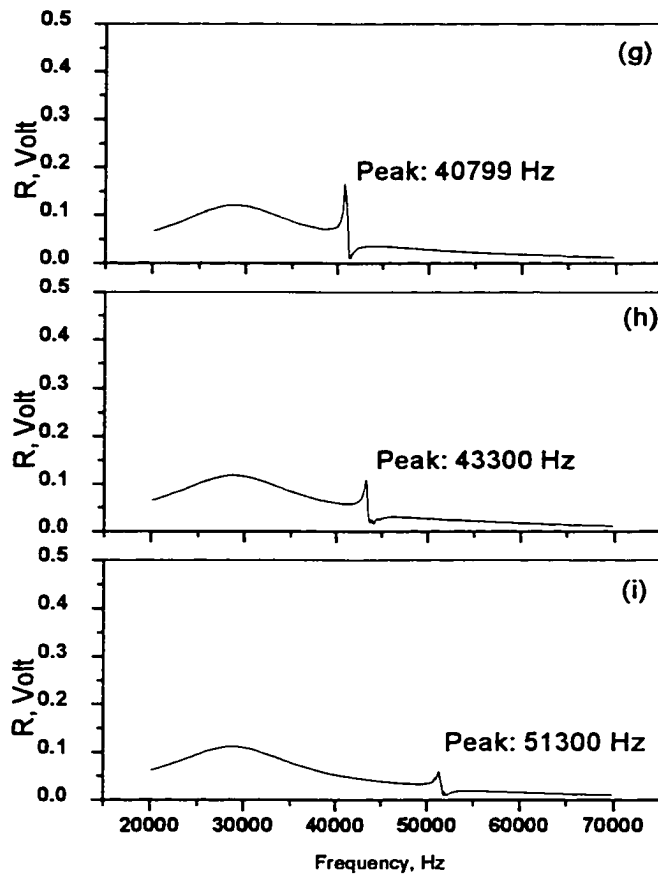
116

Figure 5-13 Resonance frequency of a 37.58 mm long ribbon with different fixed lengths. The fixed length is (g) 11.58 mm, (h) 13.30 mm, (i) 17.76 mm

117

Table 5-2 Calculation of 1/(free length) and related resonance frequency and amplitude

Fixed length, mm	Frequency, Hz	Amplitude, Volt	1/(free length), 1/mm
0.64	28699	0.14029	0.02707
2.00	30000	0.21631	0.02811
4.02	30701	0.24915	0.0298
6.98	33601	0.20691	0.03268
9.00	36200	0.19525	0.03499
11.58	40799	0.16724	0.03846
13.30	43300	0.10846	0.04119
17.76	51300	0.06116	0.05045

118
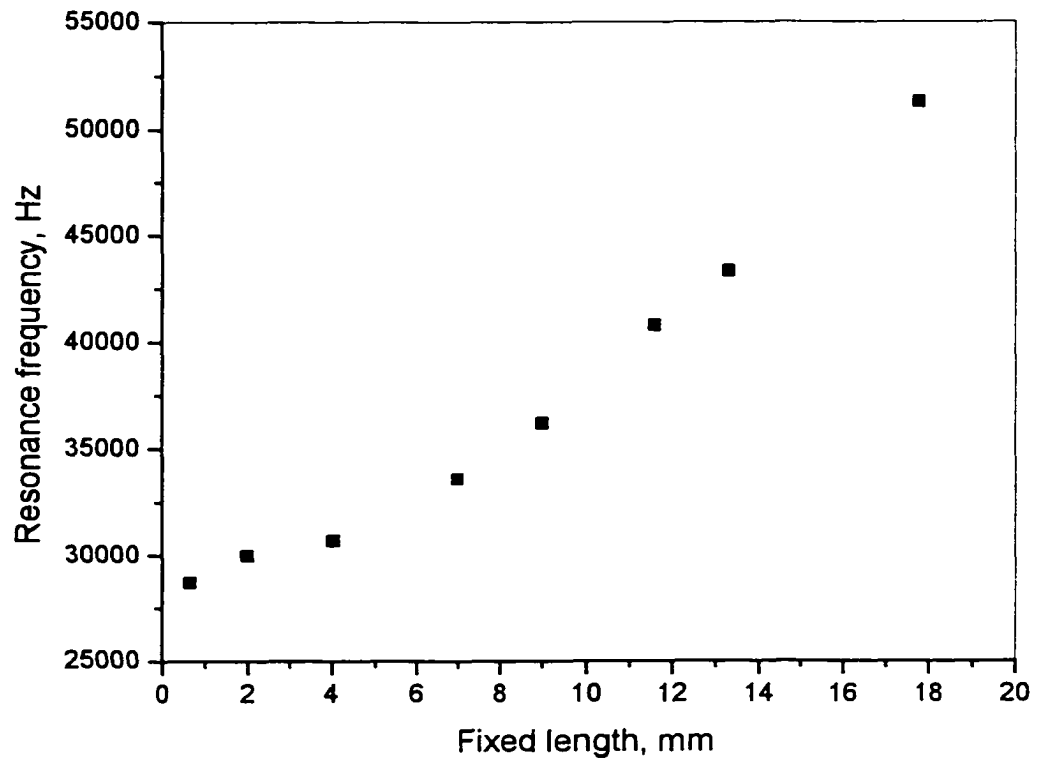
Figure 5-14 Resonant frequency of a free, fixed ribbon vs. its fixed length

119
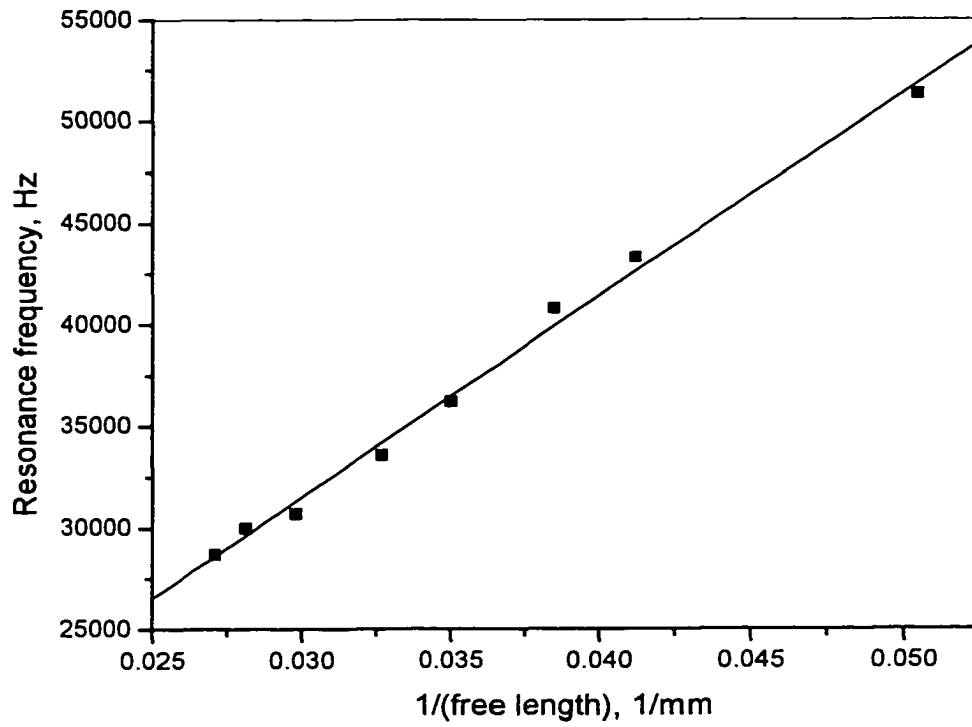
Figure 5-15 Resonance frequency of a free, fixed ribbon vs. 1/(free length)

120

The above experiments demonstrate that equation (2-1) can be used to describe the resonance frequency of a free, fixed ribbon. The most important result is that a resonance frequency peak falls in the working range between 20 and 70 kHz. To monitor polymerization, part of the ribbon was dipped in a monomer solution. Before the polymerization, the boundary condition is similar to a free, resistance-loaded ribbon. There should be a resonance frequency peak appearing in the working range because of the low viscosity of the monomer solution. During the polymerization, the viscosity increases, which implies that the resistance increases. The resonance peak probably will disappear if the viscosity or the resistance is too large because the mechanical energy dissipates to the surrounding medium. After polymerization, the boundary condition is equivalent to a free, fixed ribbon if the product becomes a solid. If this is true, the resonance frequency peak should show up again between 20 and 70 kHz based on the above results. That means we can monitor polymerization in situ by dipping the ribbon inside the monomer solution in the reactor.

Now let us choose the best boundary condition, that is, the optimum length dipped into the solution. In Figure 5-13 (b), (c), and (d), the resonance frequency peaks overlaps with the background peak. From Figure 5-13 (e) to (j), it is observed that the resonance frequency peak gradually separates from the background peak. Therefore, the optimum dipped length should be one of those shown from Figure 5-13 (e) to (i) because the resonance frequency peak differs from the background. In addition, we would like the amplitude at the resonance frequency to be high so that we can most accurately measure the resonance frequency. Figure 5-16 shows the relationship between the amplitude at the resonance frequency and the fixed length. The first three points belong to Figure 5-13

121

(b), (c), and (d), respectively. We don't consider them because the peak overlaps the background for these data. Figure 5-13 (e) is not so good because the resonance frequency peak is very close to the background peak. Figure 5-13 (j) is not so good either, because the amplitude at the resonance frequency is very small. Therefore, the optimum dipped length is between 9.00 mm and 13.30 mm.

Before carrying out the experiments to monitor polymerization, the apparatus was adjusted. Figure (2-3) shows the original set-up of the Resonance Meter. The axis of the driving and pick-up coils is parallel to the lab bench. A magnetoelastic ribbon is placed horizontally inside the Teflon cell at the center of the pick-up coil shown in Figure 5-2 (a) and (b). The entire ribbon is immersed in a solution in the Teflon cell. In order to create a boundary condition of a free, fixed ribbon, we re-arranged the driving coils and pick-up coils as shown in Figure 5-17. In this set-up, the axis of the driving and pick-up coils is vertical to the lab bench. This arrangement allows us to dip a ribbon into our sample. Figure 5-18 shows the sensor to monitor HEMA polymerization. It includes a front-view of a section of the pick-up coil. The mixture of HEMA, EGDMA, and DMPAP was added to a 15x45 mm round bottom glass bottle. The height of the solution was 10.90 mm. A magnetoelastic ribbon with a length of 37.00 mm was dipped into the solution. Because of surface tension, some of solution at the ribbon surface stayed the solution level. The real height of the solution at the ribbon surface was 12.50 mm. 24.50 mm of the ribbon vibrated freely in air. The two side edges of the ribbon slightly contacted the inner surface of the glass bottle. The arc shape of the glass bottle prevented the whole ribbon from contacting the bottle's inner surface. It is assumed that the slight contact of the side edges of the ribbon does not affect the boundary conditions. Some cardboard

122

was used to support the bottle. The height of the bottle was adjusted in order to keep the

middle of the free end of the ribbon at the center of the pick-up coil. The polymerization

was initiated under a 400 Watt mercury lamp. The resonance frequency was

automatically recorded with a programmed computer. Due to limitations of the current

program that controls the Resonance Meter, the resonance frequency was only recorded

every 3.5 minutes. Figure 5-19 (a) is for a 37.00 mm ribbon freely vibrating in air. Its

resonance frequency was 58.750 kHz. This resonance frequency decreased after 12.50

mm of the ribbon was immersed in solution. Figure 5-19 (b) shows the resonance

frequency is 58.155 kHz before the polymerization. At this time, the upper end of the

ribbon freely vibrated in air. The lower end of the ribbon was in the solution, which was

neither rigidly fixed nor completely free to vibrate. Its boundary condition was similar to

a free, resistance-loaded ribbon because the lower end of the ribbon was loaded with a

kind of mechanical impedance. Once polymerization started, the viscosity of the polymer

solution increased which caused the mechanical resistance to increase. As the viscosity

increased during the period between Figure 5-19 (b) and Figure 5-19 (c), much more

mechanical energy dissipated into the surrounding medium. This damped the vibration.

At 3.5 minutes shown in Figure 5-19 (c), the resonance frequency peak disappeared from

the range between 20 and 70 kHz. In the period between Figure 5-19 (c) and Figure 5-19

(d), the polymer chains were continuously propagating as chain radicals added to

monomer molecules. The polyHEMA began to solidify at 7 minutes. As shown in

Figure 5-19 (d), a resonance frequency peak appeared in the frequency range between 20

and 70 kHz. This confirms that our model successfully predicted the experimental

results. The boundary condition changed from a free, resistance-loaded ribbon to a free,

123

fixed ribbon between 0 and 7 minutes as shown in Figure 5-19 (b) to (d). The lower end

of the ribbon was gradually surrounded with the solidified polyHEMA product. Because

the polymer continued to solidify between 7 to 14 minutes as shown in Figure 5-19 (d) to

(f), the resonance frequency shifted upwards. Experimentally, polyHEMA became hard

and its modulus increased during this period of time. The loss of mechanical energy

through the lower end of the ribbon decreased when the ribbon is held more and more

firmly. According to equation (2-1), the resonance frequency increases when the

modulus of material increases. The HEMA polymerization was completed after 15

minutes. As shown in Figure 5-19 (f) to (l), the resonance frequency stayed at 37.262

kHz after 15 minutes. It was observed that a small peak appeared in Figure 5-19 (g).

This was probably caused by surface stress at the interface between the ribbon and the

poly-HEMA product. Figure 5-20 shows how the resonance frequency varies during

HEMA polymerization. The point of 0 Hz at 3.5 minutes was added artificially because

the resonance frequency peak disappeared at this time. The purpose of adding this point

is just to show how the resonance frequency changes. It was observed that the resonance

frequency levels off after 15 minutes, indicating that the polymerization was complete.

When we studied polymerization using optical methods, such as ultraviolet, we usually

monitor a specific chemical bond contained in the reactants. However, polymerization

often does not stop the monitored chemical bond has totally reacted, because the final

product may still undergo a phase transition. This phase transition is very important in

making polymer materials. With our new sensor, we can monitor polymerization

including a phase transition in-situ in a sealed reactor.

124

Figure 5-21 shows the relationship between the resonance frequency and the fixed

length of a ribbon inside the polyHEMA product. In these experiments, the ribbon was

dipped into the monomer solution with different dipping depth, i.e. fixed length. The

resonance frequency was measured after each polymerization when the ribbon was fixed

in the solid polyHEMA. It was observed that the resonance frequency peak overlapped

the background peak if the fixed length was less than 6.00 mm. The amplitude at the

resonance frequency became too small and the peak shape became broader when the

fixed length was larger than 15 mm, as shown in Figure 5-21 (e). Therefore, the

optimum fixed length was between 10 and 13 mm for our typical ribbon with a length

between 37 and 38 mm. This result is consistent with the physical model.
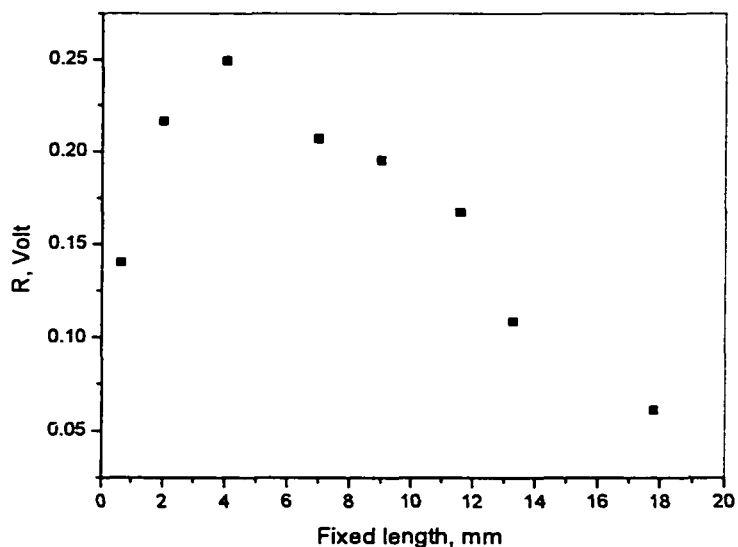
Figure 5-16 Resonance frequency amplitude vs. fixed length for a 37.58 mm ribbon

125
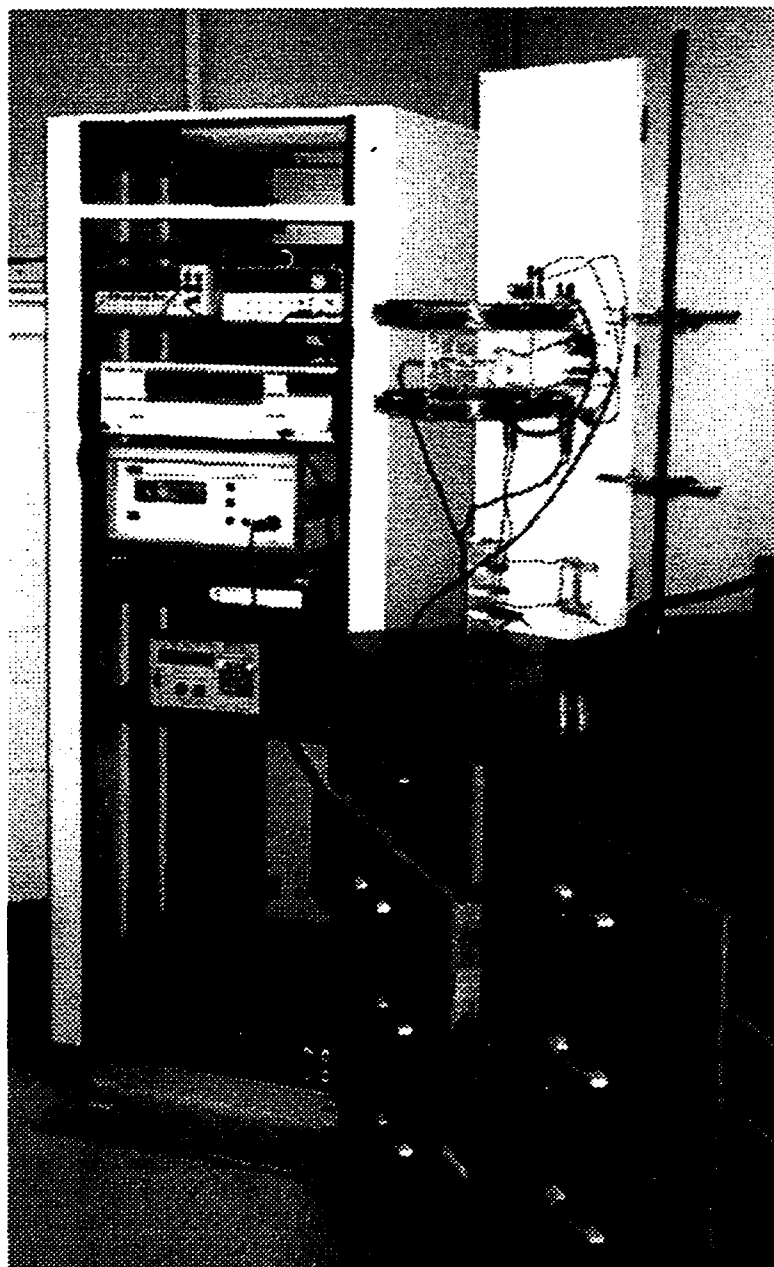
Figure 5-17 Experimental arrangement of driving and pick-up coils for monitoring HEMA polymerization

126
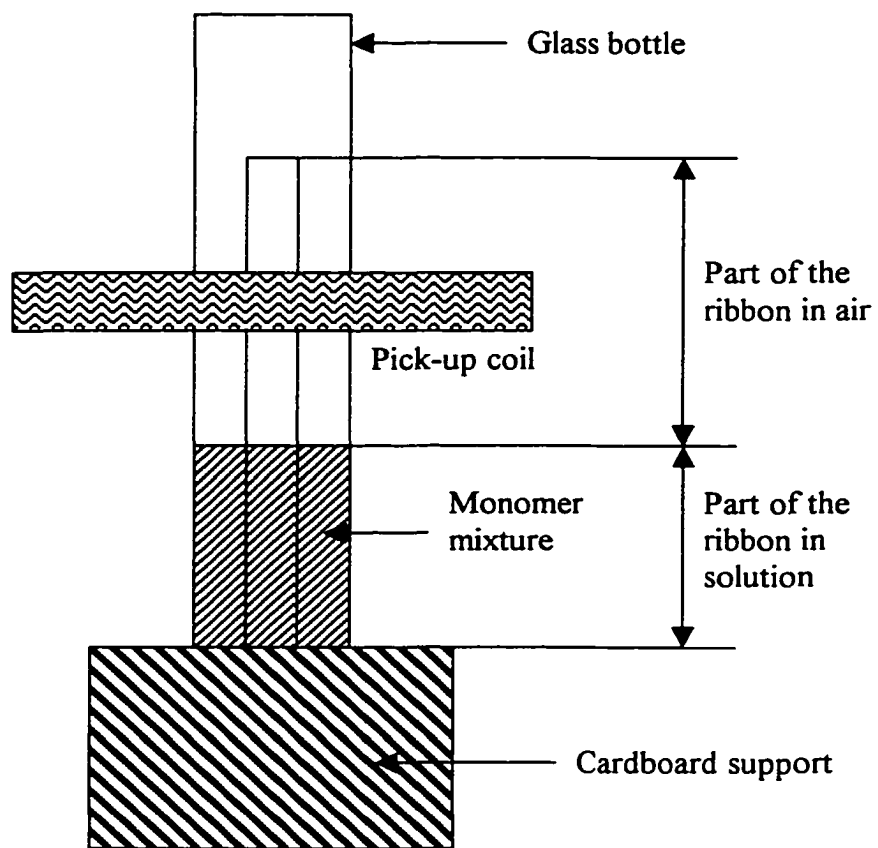
Figure 5-18 Front-view of the ribbon position for monitoring HEMA polymerization

127
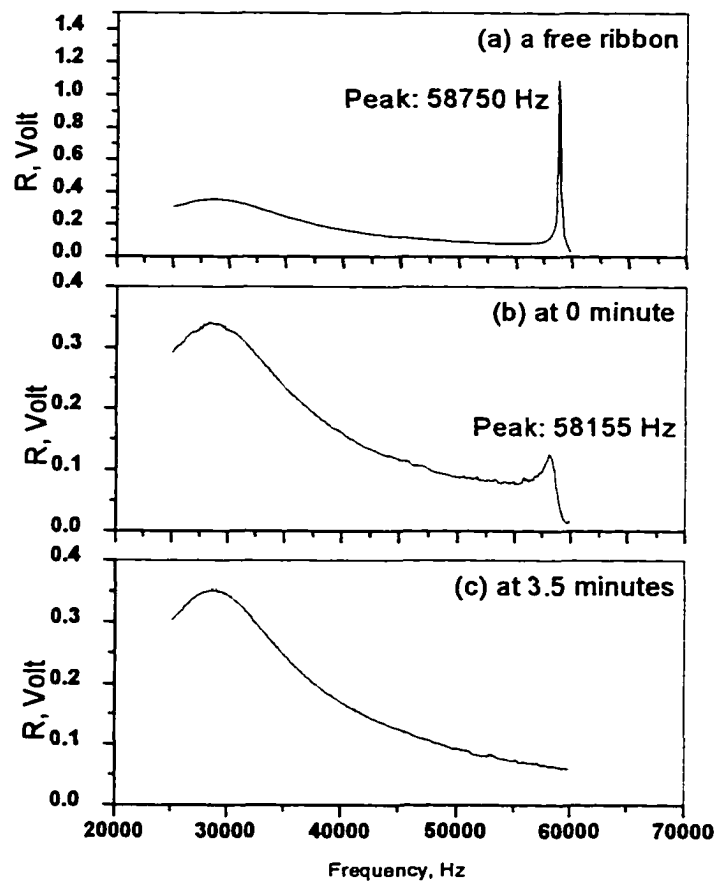
Figure 5-19 Monitoring HEMA polymerization (a) a free ribbon in air, (b) 12.50 mm of the ribbon sits in solution before polymerization, (c) after 3.5 minutes polymerization. (Continued on next page)

128
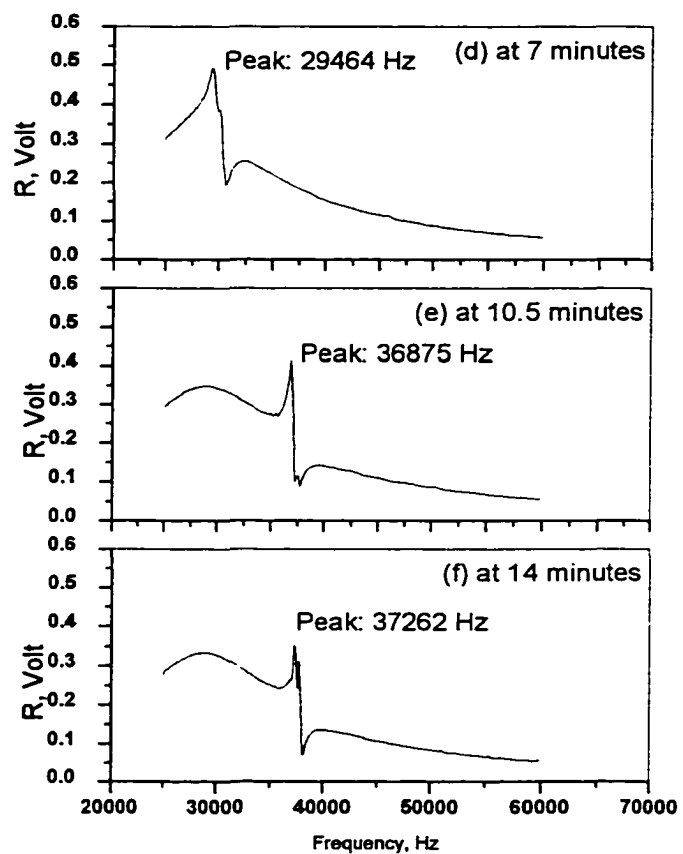
Figure 5-19 Monitoring HEMA polymerization (d) after 7 minutes, (e) after 10.5 minutes, (f) after 14 minutes.
(Continued on next page)

129
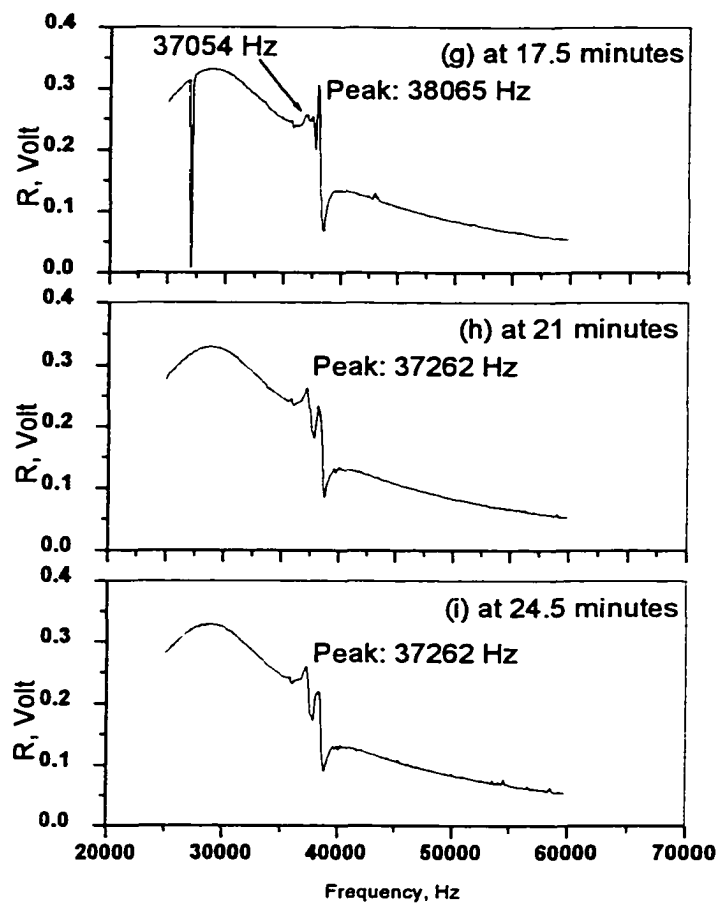
Figure 5-19 Monitoring HEMA polymerization (g) after 17.5 minutes, (h) after 21 minutes, (i) after 24.5 minutes
(Continued on next page)

130
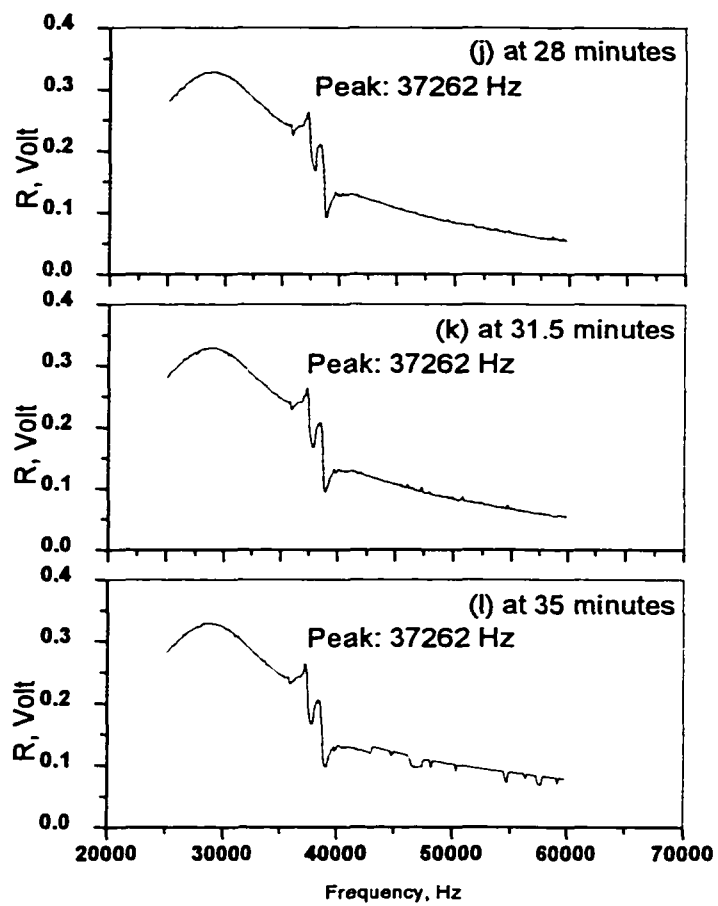
Figure 5-19 Monitoring HEMA polymerization (j) after 28 minutes, (k) after 31.5 minutes, (l) after 35 minutes.

131
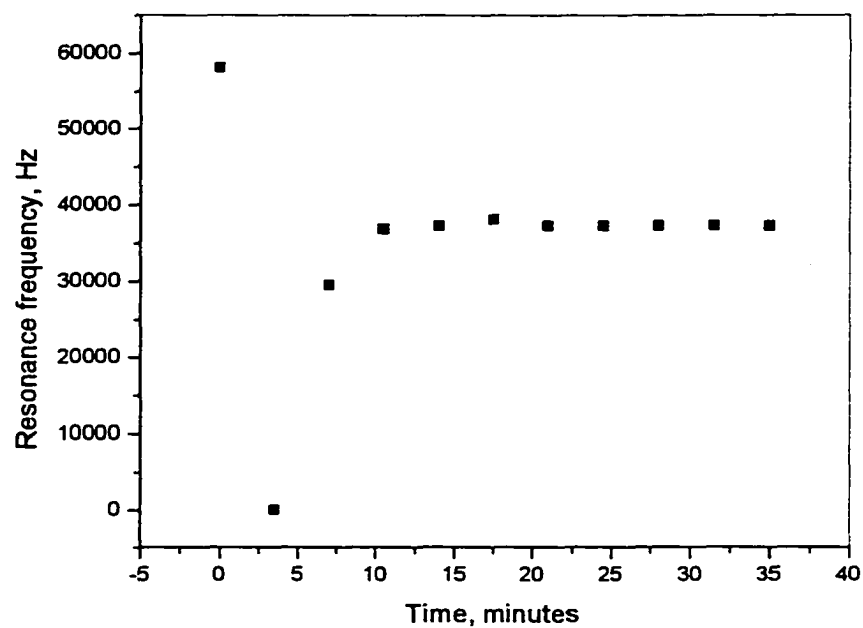
Figure 5-20 Monitoring HEMA polymerization with the Resonance Meter
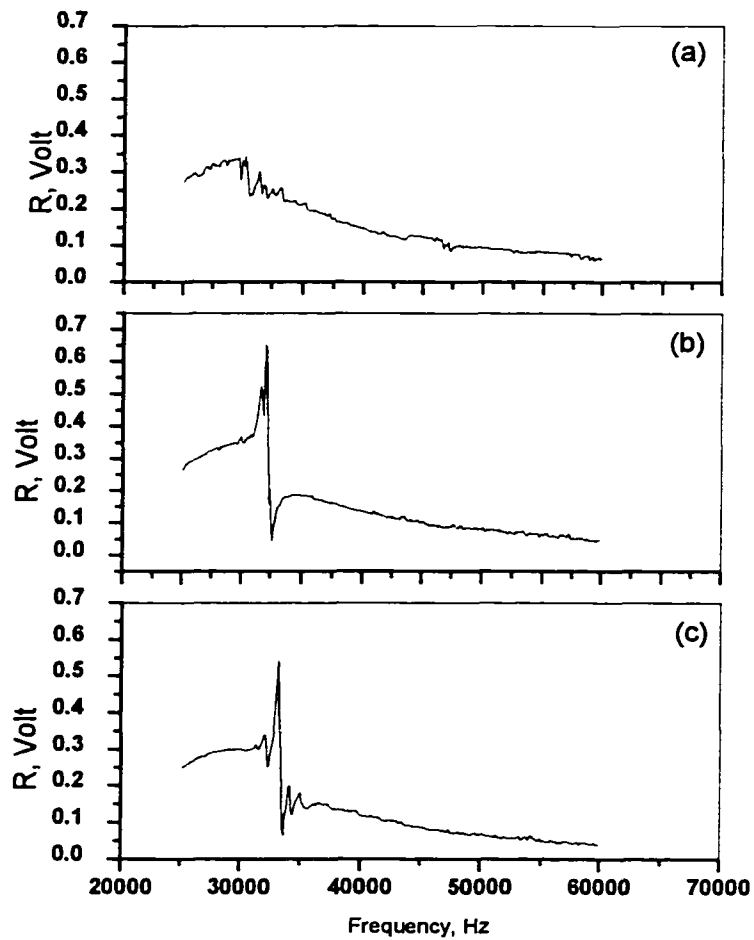
132

Figure 5-21 Resonance frequency vs. the ribbon fixed length in polyHEMA. The fixed length is (a) 3.98 mm, (b) 4.80 mm, (c) 6.42 mm
(Continued on next page)
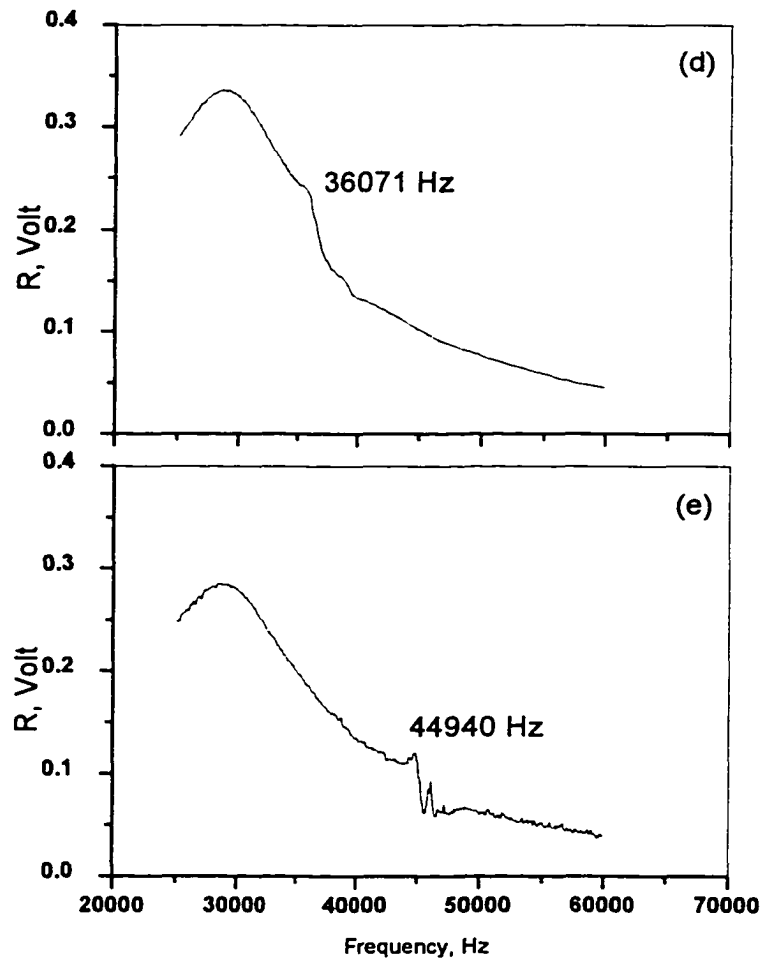
133

Figure 5-21 Resonance frequency vs. the ribbon fixed length in polyHEMA. The fixed length is (d) 11.08 mm, (e) 15.01 mm.

134

5.6 Other Factors that Affect Resonance Frequency

5.6.1 Potential ribbon bending caused by polymer swelling and shrinking

When we originally designed the sensor element configuration, we considered a sensing mechanism by which polymer membrane swelling would bend the ribbon. Later we found that swelling or shrinking caused the membrane to delaminate. This led to the application of entrapping sensitive polymer particles inside a hydrogel membrane, which we will discuss in next chapter. When we considered a sensor based on bending, we wanted to know how bending would affect the resonance frequency of the polymer coated ribbon so that we could understand the relationship between polymer swelling and resonance frequency.

The following experiments were designed to study the effect of bending. A piece of Scotch tape was placed on a straight flat ribbon, as shown in Figure 5-22 (a). The shadow part represented the ribbon, which was shorter than the tape length. The ends of the tape were stuck together, as shown in Figure 5-22 (b). By adjusting the stuck positions of the tape, we can adjust the bending of the ribbon. Figure 5-23 shows how to calculate the length change of the polymer membrane after it swells. The bowstring length L and the height of the bow H were measured with a vernier caliper. The corresponding resonance frequency was measured with the resonance meter. The ribbon length L_0 is 36.90 mm. Table 5-3 shows that there is a large change in frequency as the ribbon bends. Based on bowstring length L and the bow height H, we can calculate the radius R and the angle θ.

$$R = \frac{L^2 + 4H^2}{8H}$$

$$\theta = 4 arctg \frac{2H}{L}$$

(5-1)

135

We modeled a system in which a layer of swellable polymer coated on the ribbon external surface that was at the lower part of the bow. The original length of the polymer membrane was assumed to be the same as that of the ribbon. Its length was L_0 and its thickness was 0.035 mm. The ribbon was bent when the polymer swelled as shown in Figure 5-23. In order to make the calculation simple, we assume the thickness of the polymer membrane is 0.035mm and does not change after the membrane swells. This assumption is only for ease calculation. In practice, the membrane would become thicker as it swelled. But it does not affect the model itself because the swelling ratio is a constant for a hydrogel membrane. It only multiplies a constant in this model. In other words, we assume the swelling ratio is 1 in this model. If the external length of the swollen polymer membrane is represented using L', it is

$$L' = (R + 0.035mm) * \theta \qquad (5-2)$$

The inner length of the swollen polymer membrane L_0' is

$$L_0' = R * \theta \qquad (5-3)$$

The expected polymer length change would be (L'-L_0').

$$L' - L_0' = 0.035mm * \theta \qquad (5-4) \qquad \cdot$$

Here we see that the expected polymer length change is related to the membrane thickness. Angle θ is related to the properties of the polymer. For example, the membrane with high elastic modulus can easily bend the ribbon. Table 5-4 shows the calculation results. Figure 5-24 shows the linear regression line of the resonance frequency and the expected polymer length change. The regression equation is

$$f = 52147 + 231.25 * (\text{exp} ected \quad polymer \quad length \quad change) \qquad (5-5)$$

136

The expected resonant frequency shift is more than 200 Hz even if the polymer

membrane swells 1 μm when the membrane thickness is 35 μm.

The above model was tested with a polyHEA coated ribbon. The coating method

was described in Section 3.4.9. The thickness of the polyHEA membrane was 51 μm.

Figure 5-25 (a) shows that the resonance frequency of a dry polyHEA coated ribbon in

air is 54.685 kHz. Figure 5-25 (b) shows that the resonance frequency is 58.432 kHz

after the polyHEA coated ribbon was immersed in water. It was observed visually that

the ribbon was bent after the membrane had swollen. We found that the resonance

frequency in Figure 5-25 (b) is larger than that in Figure 5-25 (a). This result is in

contrary to that shown in Figure 5-3 (a) and (b), in which the resonance frequency

decreased after the ribbon was immersed in water. However, this result is consistent with

the above model. Although water content of the polyHEA membrane increases, the

swollen membrane bends the ribbon and dominates the resonance frequency shift. Here

the bending becomes the dominating factor. Figure 5-25 (c) shows that the resonance

frequency was 58.432 kHz after the membrane coated ribbon was taken out from water

and dried in air for 50 minutes. Figure 5-28 (d) shows the result when the coated ribbon

was put back in water again for 20 minutes.

The above experimental results show that there is a large change in frequency as

the ribbon bends. The effect of ribbon bending is opposite to that of water content and

modulus. It is known that increasing water content and lower modulus accompanying

swelling cause the resonance frequency to decrease. However, the ribbon bending that

also accompanies swelling causes the resonance frequency to increase. In the above

experiment, ribbon bending became the dominant factor affecting frequency. Therefore,

137

we should coat a very thin film on the ribbon to minimize bending as the membrane

swells. A thin membrane also minimizes frequency damping due to the mass loading.
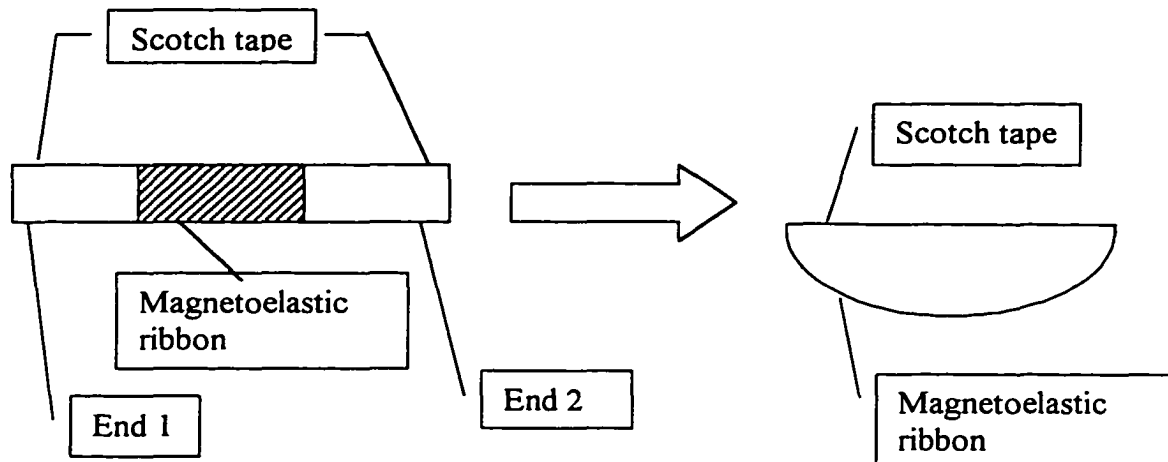
Figure 5-22 (a) Top-view of a piece of magnetoelastic ribbon stuck to a longer piece of Scotch tape.

(b) Side-view of the bent ribbon after the ends of the Scotch tape are put together.

138
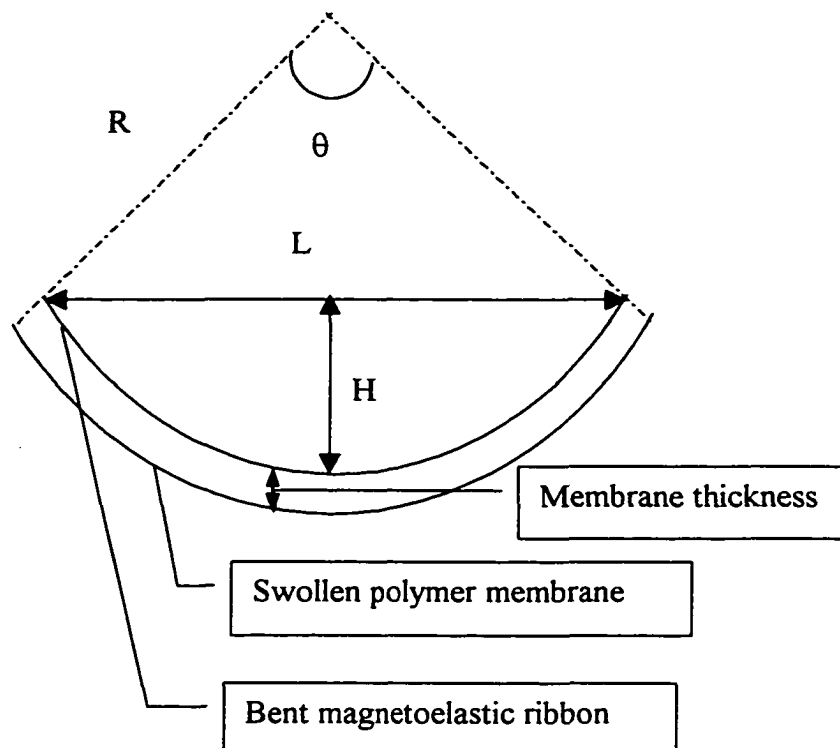
Figure 5-23. Schematic drawing showing model used to calculate the length change of the coated polymer membrane caused by swelling.

139

Table 5-3 Experimental resonance frequency vs. the bowstring length L and the bow height H

Original membrane length L_0, mm	Bowstring length L, mm	Bow height H, mm	Resonance frequency f, Hz
36.90	36.84	0.80	55100
	36.22	2.96	56722
	35.92	3.40	57927
	35.4	4.26	59293
	34.72	5.30	61173
	33.94	6.46	63053
	33.34	7.06	64054
	32.68	7.22	66318
	31.68	7.90	68314
	30.76	9.46	70504

Table 5-4. The expected polymer length change of a bent ribbon

R, mm	θ, radian	L_0', mm	L', mm	Expected polymer length change, um
212.460	0.174	36.886	36.892	6
56.881	0.648	36.862	36.884	22
49.136	0.748	36.772	36.798	26
38.901	0.945	36.751	36.784	33
31.081	1.185	36.839	36.880	41
25.520	1.455	37.129	37.180	51
23.211	1.602	37.194	37.250	56
22.100	1.664	36.780	36.838	58
19.830	1.851	36.697	36.762	65
17.232	2.206	38.010	38.087	77

141
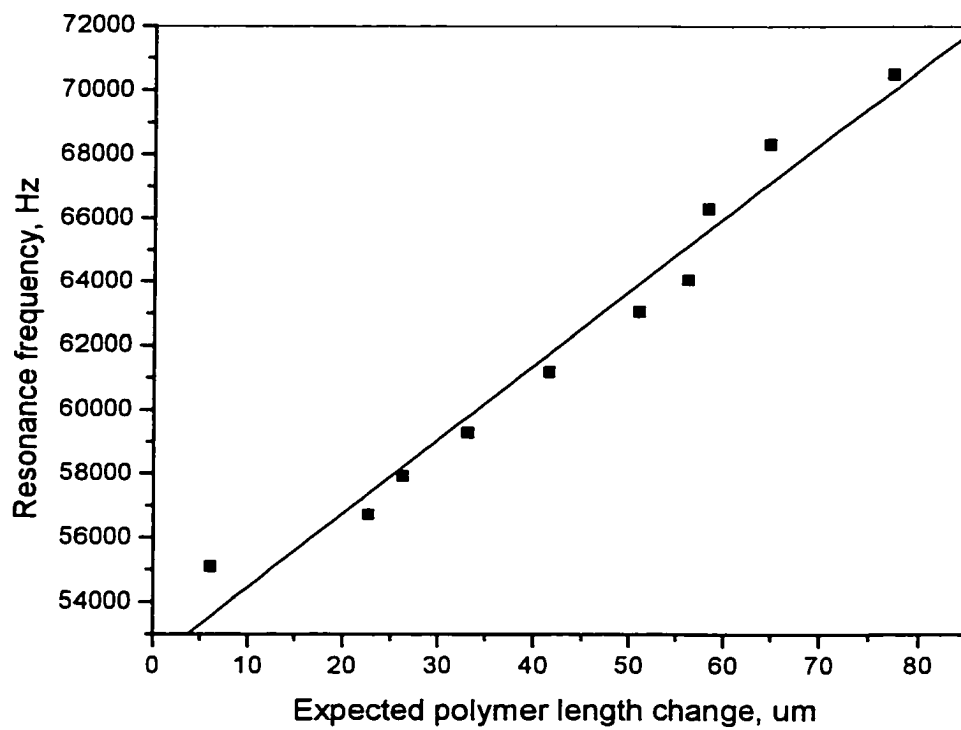
Figure 5-24 Resonance frequency vs. the expected polymer length change

142
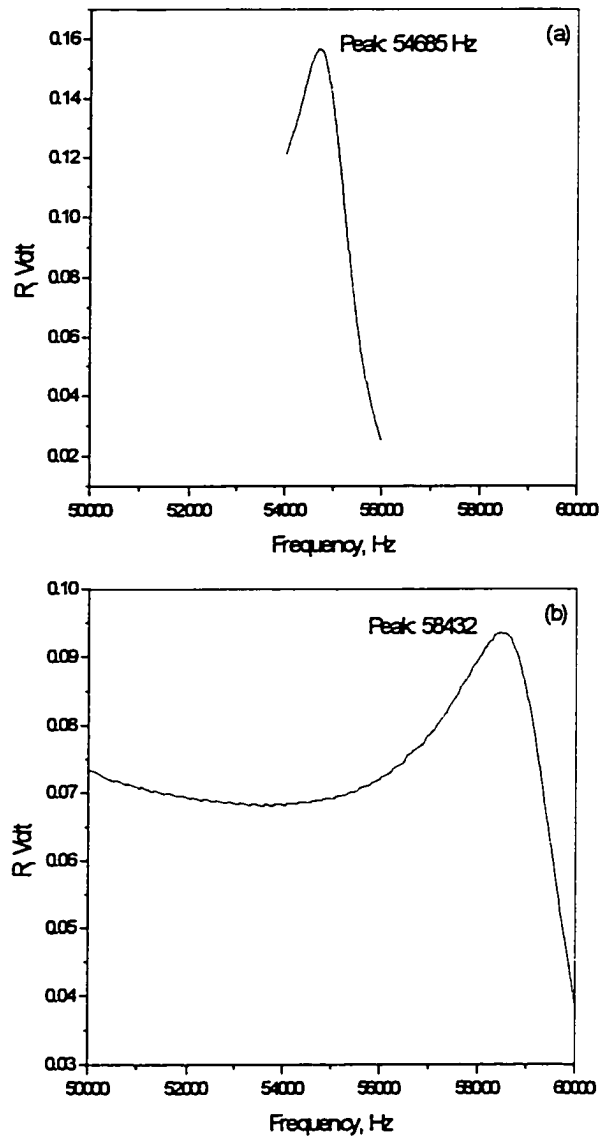
Figure 5-25 Effect of polyHEA membrane swelling on the resonance frequency (a) dry polyHEA coated ribbon, (b) polyHEA swollen in water to bend the ribbon. (Continued on next page)

143
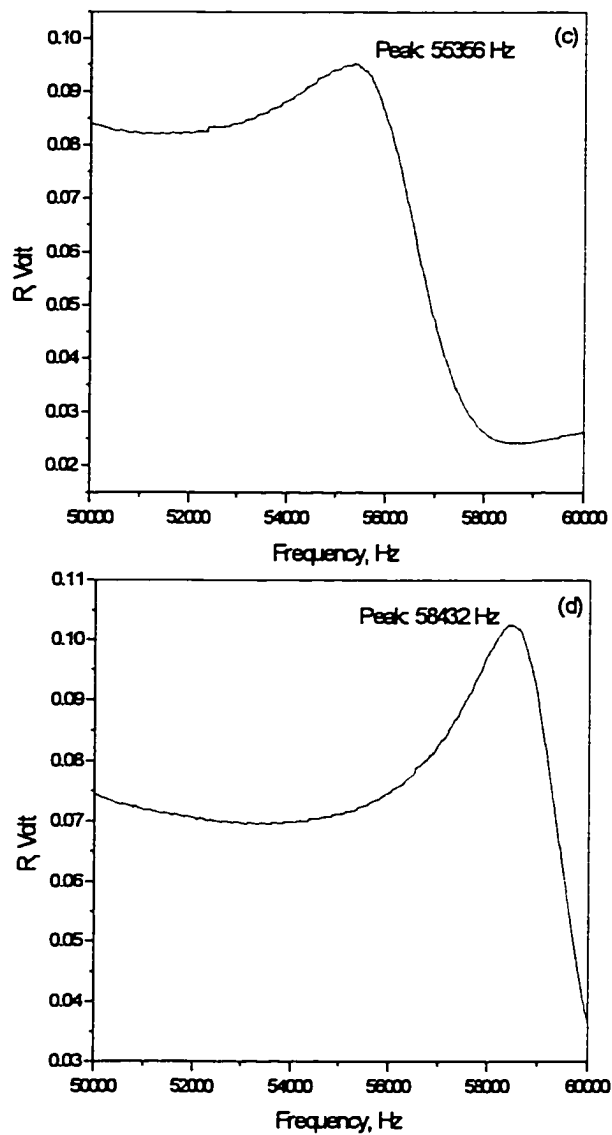
Figure 5-25 Effect of polyHEA membrane swelling on the resonance frequency (c) The polyHEA membrane is dried in air for 50 minutes. (d) The polyHEA membrane is put in water for 20 minutes.

5.6.2 Effect of membrane position on response

In some experiments we coated the polymer membrane on only part of the ribbon to minimize damping of the resonance frequency. Therefore, we were interested in whether position of the membrane affects the resonance frequency. A magnetoelastic ribbon of 37.60 mm length was evenly divided into 7 parts as shown in Figure 5-26. A piece of Scotch tape was cut into the same size as one division. This piece of tape was placed on position from 1 to 7 in turn. The resonance frequency was recorded when the tape was put on each position. The middle of the ribbon at position 4 was always placed at the center of the pick-up coil. Table 5-5 shows the measurement results. Figure 5-27 shows the resonance frequency as a function of tape position. It is observed that sensing position does affect the resonance frequency. The resonance frequency is at maximum when the membrane is coated at the middle of the ribbon at position 4. The resonance frequency decreases when the membrane is coated at positions away from the center of the ribbon. Figure 5-28 shows the amplitude at the resonance frequency when the tape was put on each position. The trend is same as that of the resonance frequency. From Figures 5-27 and 5-28, we see that the resonance frequencies vary with sensing position. This result gives us two pieces of information. First, we should put the sensing polymer at the center of the ribbon in order to increase the sensitivity if we only coat part of the ribbon with membrane. Second, we should keep the ribbon at the same place in the pick-up coil center during the measurement. In all our experiments, we place the middle of the ribbon at the center of the pick-up coil, and we always position it in the same direction.

| 1 | 2 | 3 | 4 | 5 | 6 | 7 |
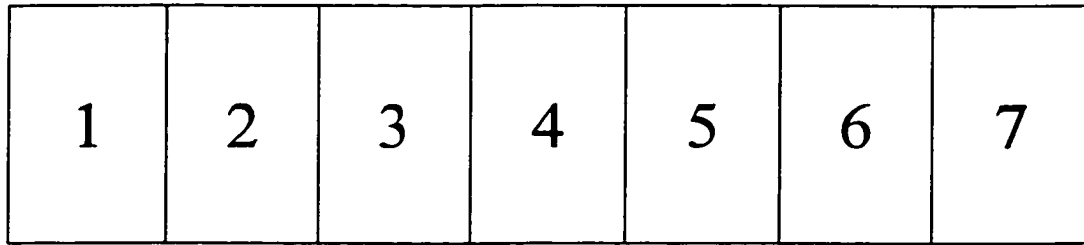
Figure 5-26. Top-view of a magnetoelastic ribbon evenly divided into seven parts.

Table 5-5 Resonance frequency vs. membrane position

Membrane position	Frequency, Hz	Amplitude, volt
No coating	58420	0.64934
1	56280	0.25305
2	57070	0.29185
3	58050	0.31265
4	58539	0.34414
5	58111	0.32701
6	57119	0.29869
7	56271	0.27234

146
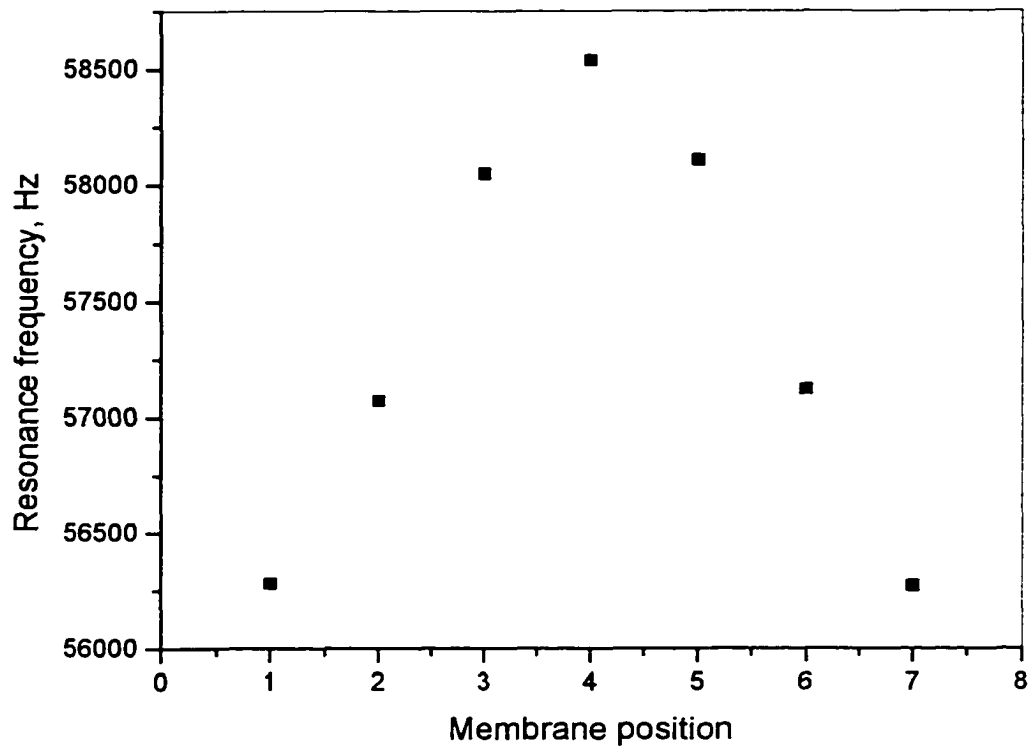
Figure 5-27 Resonance frequency vs. membrane position

147
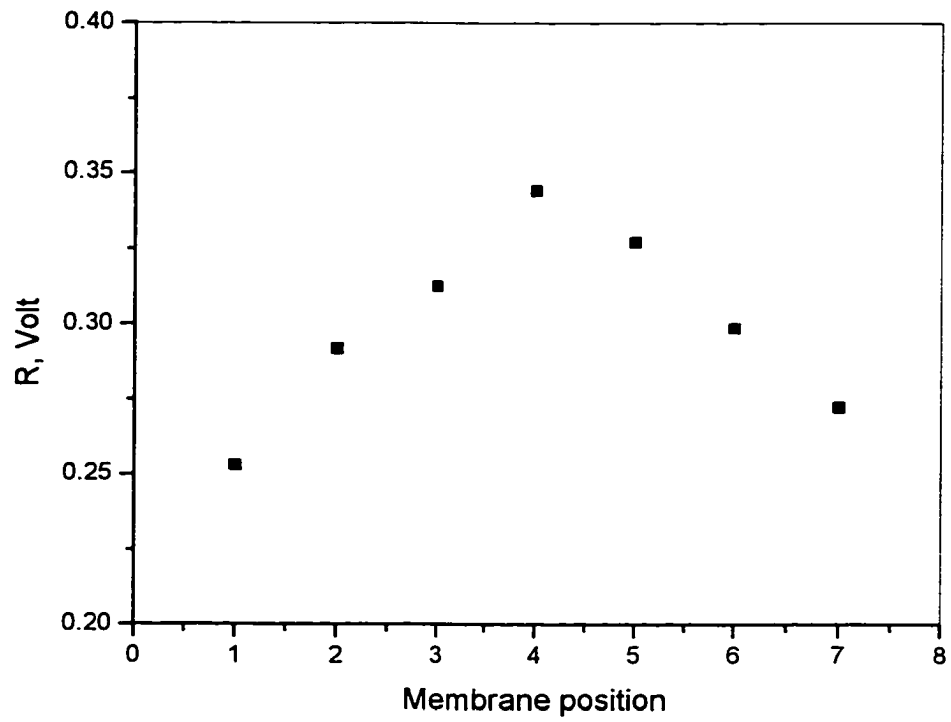
Figure 5-28 Amplitude at the resonance frequency vs. membrane position

148

5.6.3 Modulus change of the sensing membrane

Equation (2-1) shows that the material modulus is one of the main factors that affect resonance frequency. To make a sensor, we coat a layer of sensing polymer membrane on the ribbon. Usually the sensing membrane is a hydrogel membrane with swellable polymer particles. These particles swell or shrink with changing solution pH. We wondered whether the swelling and shrinking would affect the material modulus.

The particles that were used in this experiment were aminated polyTCPA-VBC. 4% particles suspended in 4% HYPAN HN 50 in DMSO solution. The mixture was put in a mold similar to that shown in Figure 3-8 except that the depth was 254 μm. After this mold was uniformly filled with the mixture, it was quickly immersed into water. The sensing membrane was easily peeled out from the mold. First, this membrane was put in pH 8.0 buffer to shrink the particles. The membrane modulus was measurement using a Dynamic Mechanical Analyzer (DMA 7e) equipped with a stainless-steel parallel plate measuring system. As shown in Figure 5-29, the shrunken membrane was placed on the base. A static force of 5 mN was applied on the parallel plate, which just barely contacted the polymer membrane. The measuring system was zeroed at this time. Once the pH 3.0 buffer was added into the testing cell, the measuring system recorded the displacement of the parallel plate caused by polymer membrane swelling. The test temperature was set at 23 °C. Figure 5-30 schematically shows the membrane displacement measurement. Figure 5-31 shows the relationship of the static modulus and the static strain during swelling. It is observed that the modulus decreases as the membrane swells. This is consistent with resonance frequency shifts described in the next chapter.

149
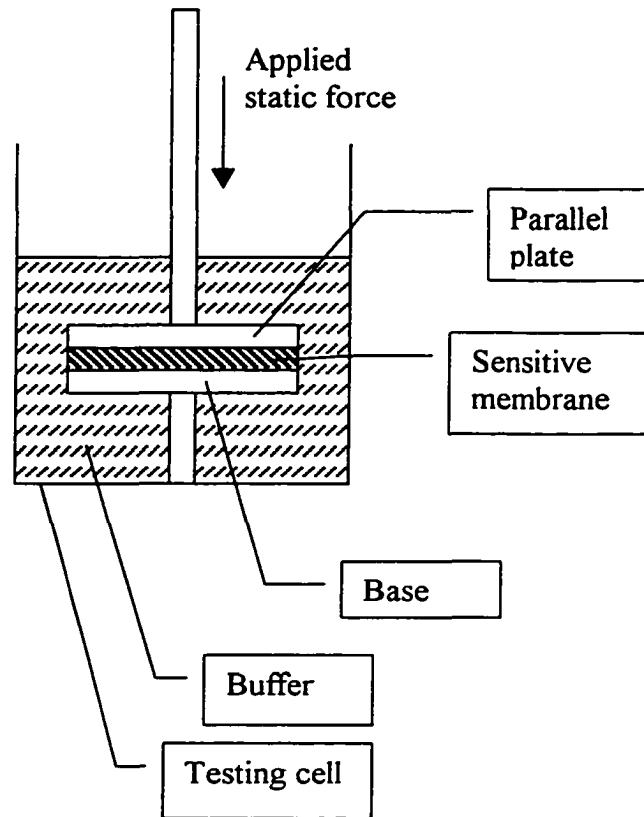
Figure 5-29 Schematic drawing of the static DMA with a parallel plate

150
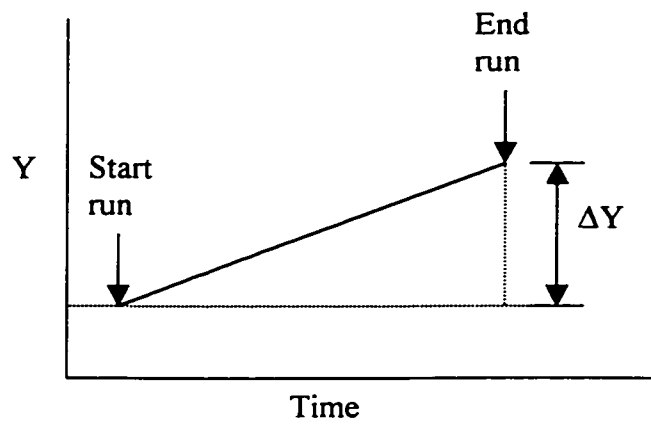
Figure 5-30 Displacement measurement of the parallel plate during the polymer membrane swelling

151
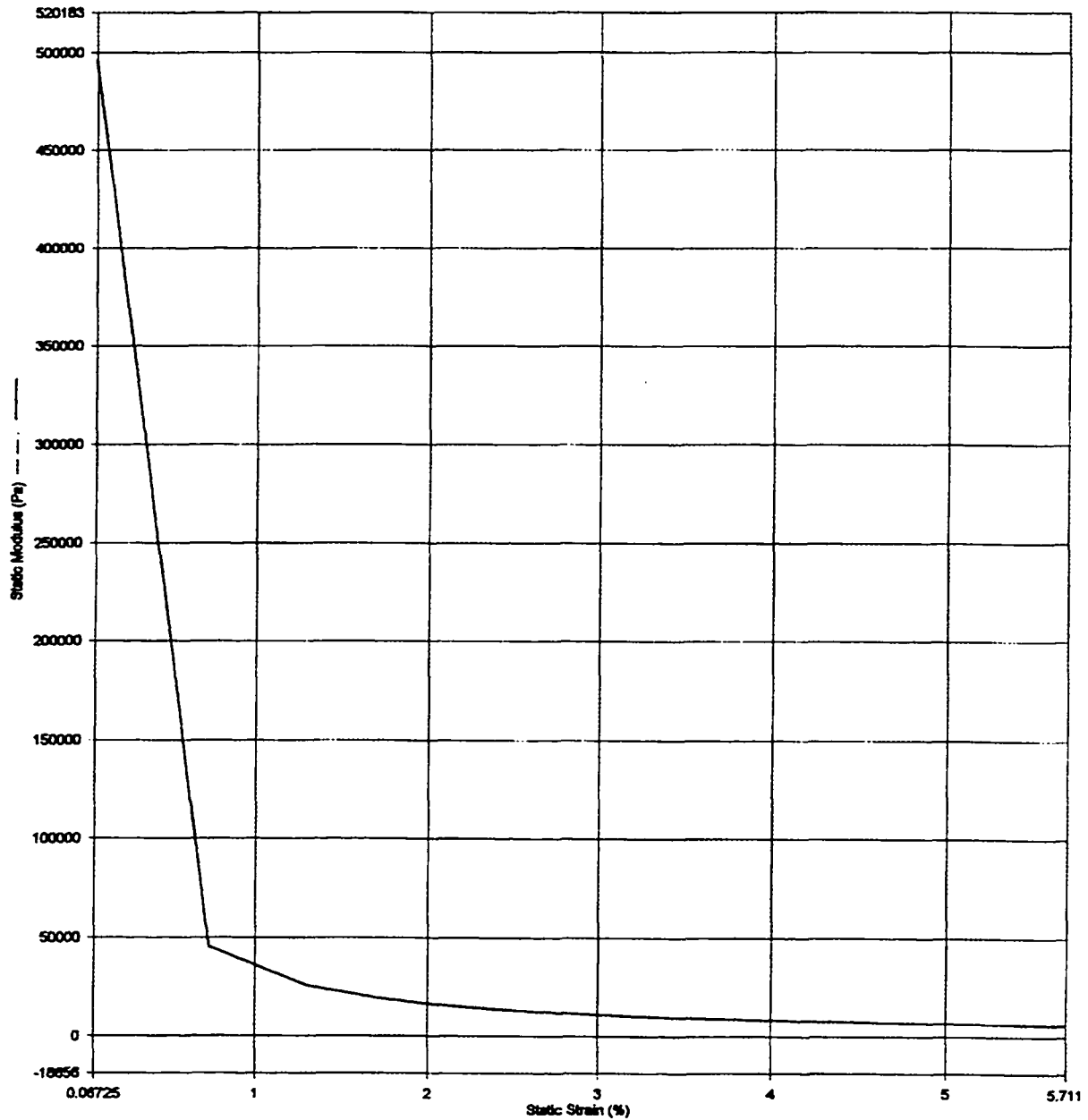
Figure 5-31 Static modulus decreases as the static strain increases during the sensitive membrane swelling.

5.7 Conclusion

The goal of this research is to develop a new type of continuously operating, remotely monitored sensor that does not require an electrical connection. The new sensor

152

is based on a magnetoelastic metallic glass ribbon. An externally applied alternating current (ac) magnetic field is used to excite magnetoelastic waves inside the magnetoelastic thin ribbon. Frequency responses are monitored with a pick-up coil located outside the test area.

We used several physical models to study the factors that affect the resonance frequency of the magnetoelastic ribbon. This chapter summarized this part of work. We studied the effects of liquid viscosity and mass loading on the resonance frequency of a magnetoelastic ribbon using models that have been widely accepted in the field of acoustic sensors. It was found that the working principle of magnetoacoustic sensors is similar to that of acoustic sensors. The new sensor responds to mass loading as a microbalance by decreasing its resonance frequency. When immersed in liquid, its resonance frequency is correlated with the square root of the product of liquid viscosity and density. We studied the relationship between the frequency shift and the square root of the product of viscosity and density of a starch solution. We found that the frequency shift is linearly proportional to starch concentration. After bonding a poly-hydroxyethyl acrylate (poly-HEA) membrane on the magnetoelastic ribbon, the sensitivity of the sensor to water loading is greatly increased.

One of the advantages of the new sensor is that it does not need an electrical connection to the ribbon. Therefore, it can monitor processes in situ such as polymerization and polymer curing. We built a physical model to monitor HEMA polymerization by immersing the end of a ribbon in the polymerizing solution. Another physical model was used to understand the effect of ribbon bending on the resonance frequency.

153

CHAPTER 6

MAGNETOACOUSTIC CHEMICAL SENSORS FOR MONITORING

SOLUTION pH

6.1 Introduction

Swellable polymer microspheres were first used in fiber optic sensors by Seitz.[46,47] The basic idea is to entrap swellable polymer microspheres in a hydrogel membrane. The polymer microspheres swell and shrink as a function of analyte concentrations. Any of the physical signals accompanying swelling, such as refractive index, physical displacement, electrical properties, mass change, and modulus change, can be monitored. Many different kinds of swellable microspheres have been developed in our group in the last few years.

In this chapter, we discuss pH monitoring using the Resonance Meter based on the swellable polymer microspheres. First, the pH sensitive microspheres are suspended in a hydrogel solution. Then this solution is spin-coated onto the surface of a magnetoelastic ribbon to form a hydrogel membrane with entrapped pH sensitive microspheres. These microspheres swell or shrink with changing liquid pH. When they swell, they take up water and become softer. This increases the water loading on the magnetoelastic ribbon and decreases the membrane modulus. Therefore, the resonance frequency for the swollen state is smaller than for the shrunken state

154

Making the chemically sensitive ribbon is the most important step in developing these sensors. Polyurethane is first coated on both sides of the ribbon to prevent it from corrosion. The coated strip is placed in an oven at 150 °C for 15 minutes to form a uniform polyurethane layer. Then a layer of sensitive polymer membrane is coated on one side of the ribbon. This membrane is left in air for 24 hours to evaporate the solvent. During this period of time, the hydrogel penetrates into the polyurethane layer and glues itself on the substrate. Currently the optimum hydrogel is HYPAN Structural Hydrogel from HYMEDIX International, Inc. The pH sensitive microspheres include amine derivatized polyTCPA-VBC and carboxylate derivatized polyVBC. Their responses in the Resonance Meter to pH are similar to those using optical methods described in Chapter 4. The resonance frequency of the sensitive ribbon increases as the solution pH increases from pH 6 to 8 for the amine derived polyTCPA-VBC microspheres. This is due to microsphere shrinking, which results in lower water content and increasing membrane modulus. In contrast, polyVBC microspheres that contains carboxylate groups gradually swell with pH from 2 to 8. This results in increasing water content and decreasing membrane modulus. Therefore, the resonance frequency of the sensitive ribbon made with this kind of microspheres decreases as the solution pH increases from pH 2 to 8.

As discussed in Chapter 4, all HYPAN polymers used in this study showed hysteresis during repeated swelling and shrinking. Therefore, it was not surprising to observe this phenomenon when monitoring solution pH magnetoacoustically. However, we found that hysteresis of the resonance frequency is related to the HYPAN types. The HYPAN hydrogel with high water content shows low hysteresis. This gives us a hint of

155

how to look for new hydrogel that is suitable for the magnetoacoustic sensors in the future. The size of the frequency shift is larger at high bead concentration. Bead concentration is limited by the ratio of the bead amount to the HYPAN polymer amount. This ratio dominates the properties of the membrane. Usually 4% beads are suspended in 4% HYPAN DMSO solution in our experiments.

6.2 Monitoring Solution pH

6.2.1 Polyurethane coatings on magnetoelastic ribbons

Corrosion and adhesion were serious problems when we started to develop pH sensors. Because the ribbons are made of an alloy of iron, nickel, molybdenum, and boron, they get rusty in humid environments. Typically, they get rusty when exposed to humid air for a week or to water for a day or two. We tried depositing a layer of inert metal, for example gold, on the ribbon surface. But this requires special approaches and introduces an adhesion problem between the inert metal and its substrate. It is also expensive compared to the cheap ribbons and the Resonance Meter itself. Therefore, we decided to focus on polymer coatings on ribbons to prevent them from corroding. Chemicals, such as Superglue and vinyltrimethoxysilane, failed as coatings because they formed rigid films that completely damped the resonance frequency. Finally, we tried polyurethane coatings, which are successfully used for a wide variety of applications.[77,78] Figure 6-1 shows the polyurethane chemistry.[79,80] Its focal point is the isocyanate group that can undergo many different reactions. Conventional solventborne polyurethane coatings include an isocyanate component and a polyol component. After mixing, the reaction begins immediately, which limits the amount of time for the system to be cleanly

156

applied. In this work we used Bayhydrol 110 from Bayer Corporation. Bayhydrol 110 is

an anionic dispersion of an aliphatic polyester urethane resin in water/1-methyl-2-

pyrrolidinone. It is a water compatible polyurethane coating. The typical water

compatible polyurethane is actually a polyurethane-polyurea that contains both the

urethane (-NH-CO-O-) and urea (-NH-CO-NH-) groups in a macromolecular chain.

Figure 6-2 shows one example of the formation of a polyurethane dispersion.[79] There are

many advantages to the polyurethane coatings, such as excellent adhesion, excellent

hardness and elasticity, and abrasion resistance.

First, the polyurethane dispersion is spin-coated on one side of a ribbon. The

spin-coater is set at 2500 rpm with quick start and stop for 20 seconds. Then the ribbon

is put in an oven at 150 °C for 15 minutes to from a polyurethane layer. After it is taken

out and cooled to room temperature, the other side is also coated with a layer of

polyurethane. The thickness of the polyurethane layer was measured with an Alpha-Step

100. As shown in Figure 6-3, it is 3.8 μm. After the polyurethane coatings are applied,

the ribbon can stay in water for more than one month without getting rusty. Figure 6-4

shows the effects of the polyurethane coatings on the resonance frequency of a

magnetoelastic ribbon. It is observed that the resonance frequency decreases after

applying polyurethane coatings. However, the resonance frequency peaks are very sharp

in all three cases: a bare ribbon, coating on one side, and coating on both sides of the

ribbon. Although the resonance frequency shifts downward a little, it is still in a good

working range. The sharp peak indicates a good balance between hardness and elasticity

of the polyurethane coatings.

$$R_1\text{—}N\text{==}C\text{==}O \ + \ R_2\text{—}OH \ \longrightarrow \ R_1\text{—}NH\text{—}\underset{\underset{O}{\|}}{C}\text{—}O\text{—}R_2 \quad \text{Urethane}$$

$$R_1\text{—}N\text{==}C\text{==}O \ + \ R_2\text{—}NH_2 \ \longrightarrow \ R_1\text{—}NH\text{—}\underset{\underset{O}{\|}}{C}\text{—}NH\text{—}R_2 \quad \text{Urea}$$

$$R\text{—}N\text{==}C\text{==}O \ + \ H_2O \ \longrightarrow \ \left[\,RNHCOOH\,\right] \quad \text{Carbamic Acid}$$

$$\downarrow$$

$$RNH_2 \ + \ CO_2$$

$$\downarrow \ + \ RNCO$$

$$R\text{—}NH\text{—}\underset{\underset{O}{\|}}{C}\text{—}NH\text{—}R$$
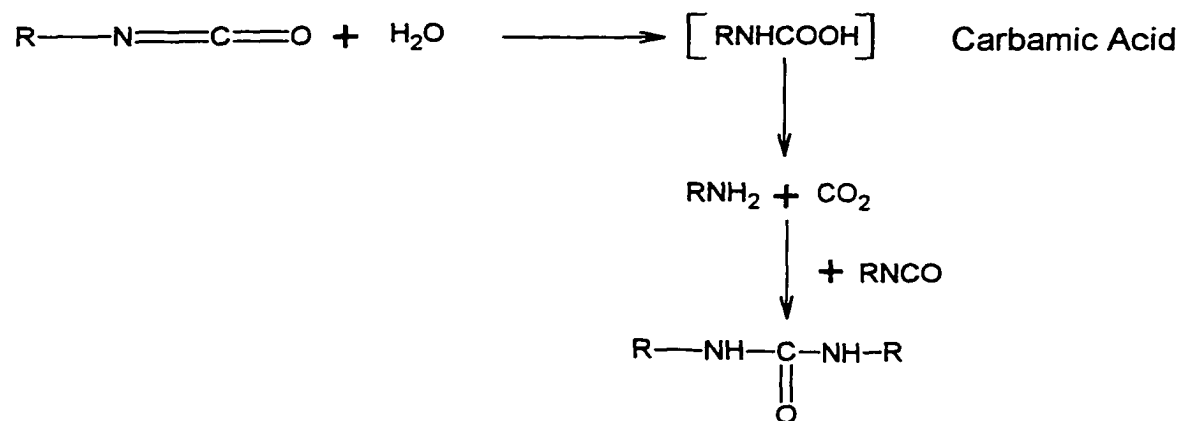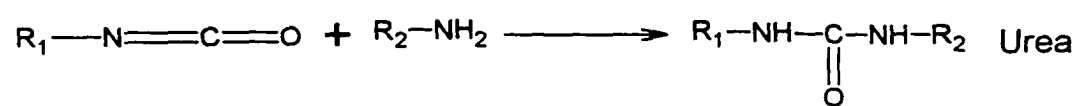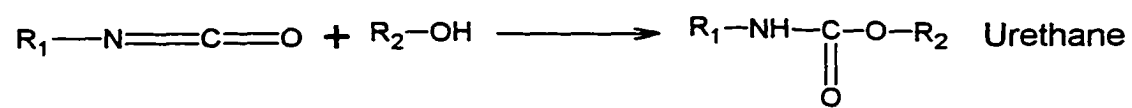
Figure 6-1 Addition reactions of isocyannates

158

$$\text{2n HO}\sim\sim\text{OH} + \text{n HOCH}_2\overset{\overset{\displaystyle CH_3}{\displaystyle |}}{\underset{\underset{\displaystyle CO_2H}{\displaystyle |}}{C}}\text{CH}_2\text{OH} + \text{4n OCN-R-NCO}$$

$$\text{OCN-R-NHCO}\sim\sim\text{OCNH-R-NHCOCH}_2\overset{\overset{\displaystyle CH_3}{\displaystyle |}}{\underset{\underset{\displaystyle CO_2H}{\displaystyle |}}{C}}\text{CH}_2\text{OCNH-R-NHCO}\sim\sim\text{OCNH-R-NCO}$$

NR_3

$$\text{OCN-R-NHCO}\sim\sim\text{OCNH-R-NHCOCH}_2\overset{\overset{\displaystyle CH_3}{\displaystyle |}}{\underset{\underset{\displaystyle CO_2\text{-}HNR_3}{\displaystyle |_{\ominus\ \oplus}}}{C}}\text{CH}_2\text{OCNH-R-NHCO}\sim\sim\text{OCNH-R-NCO}$$

Hydrophilic Isocyanate Terminated Prepolymer

1. Water

2. $\text{H}_2\text{N-R'-NH}_2$

$$\sim\sim\text{OCNH-R-NHCOCH}_2\overset{\overset{\displaystyle CH_3}{\displaystyle |}}{\underset{\underset{\displaystyle CO_2\text{-}HNR_3}{\displaystyle |_{\ominus\ \oplus}}}{C}}\text{CH}_2\text{OCNH-R-NHCNH-R'-NHCNH-R-NHCO}\sim\sim$$

Aqueous Dispersion of Polyurethane-Urea
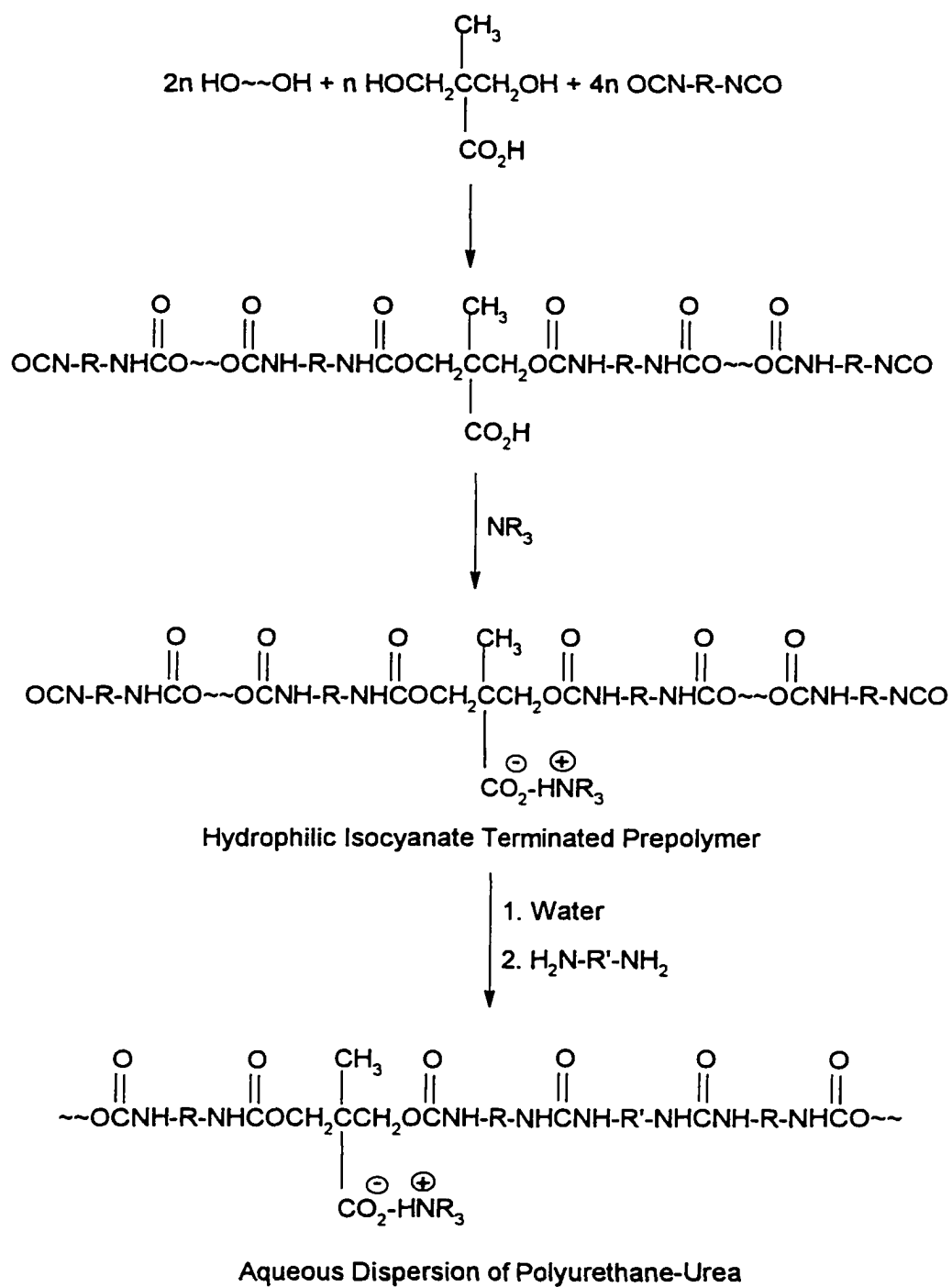
Figure 6-2 Preparation process for the polyurethane dispersion

159
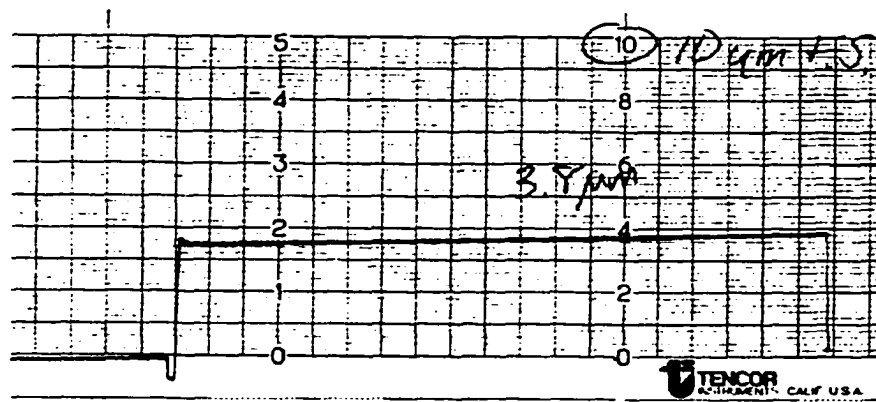
Figure 6-3 Thickness measurement of polyurethane layer
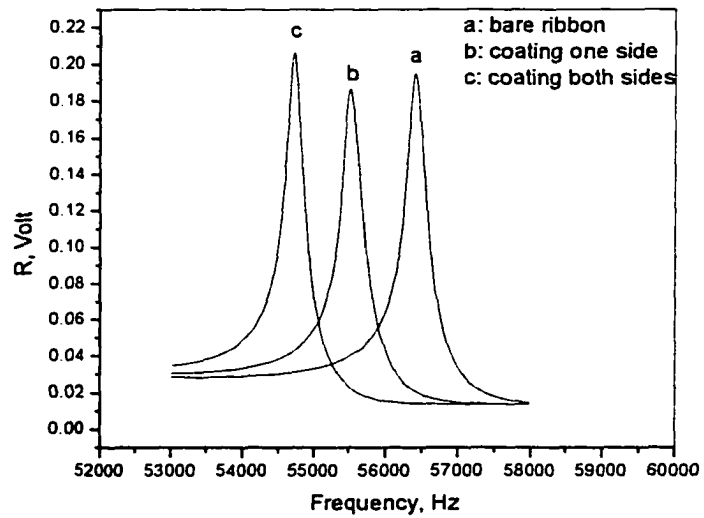
Figure 6-4 Effect of the polyurethane coatings on the resonance frequency of a magnetoelastic ribbon

160

6.2.2 Preparing polymer coated ribbons

Chemical sensors are prepared by coating ribbons with a layer of polymer on the polyurethane coated ribbons. The membrane is typically coated on only one side of the ribbon. It is a hydrogel containing pH sensitive polymer microspheres. Although there are a variety of hydrogels, such as PVA and polyHEMA, most of them have poor adhesion to the ribbons and polyurethane coated ribbons. The hydrogels used in this study were HYPAN Structural Hydrogels from HYMEDIX International, Inc. HYPAN polymers are hydrophilic acrylate derivatives with a copolymer structure that contains hard blocks and soft blocks in each polymer chain.[81,82] The hard blocks contain nitrile groups, which form organized, crystalline regions that are responsible for the mechanical strength of the hydrogel. The soft blocks contain hydrophilic groups derived from acrylic acid. They constitute the amorphous regions and are responsible for swelling, flexibility and other properties. Figure 6-5 shows the HYPAN copolymer structure and typical soft block groups.[81] The properties of HYPAN polymers are dependent on the relative lengths of the hard and soft blocks, and the functional groups on the soft blocks. There are many advantages to HYPAN structural hydrogels, such as controllable water content, high mechanical strength, and solvent resistance. In our experiments, we used HYPAN HN30, HN50, and HN80. The HN number represents the water content of that type of hydrogel. The water content is defined as a ratio of the amount of water in the swollen polymer to the total weight as shown in the following equation:

$$\text{water content (\%)} = \frac{\text{wet weight} - \text{dry weight}}{\text{wet weight}} \times 100$$

HYPAN HN30, HN50, and HN80 are neutral grades of HYPAN structural polymers. Their swelling is independent of solution pH. The only solvents that dissolve HYPAN

161

polymers are dimethylsulfoxide (DMSO), dimethylformamide, and a 55% solution of sodium thiocyanate in water. In our research, we evaluated 10% HYPAN polymer in both DMSO and a 55% solution of sodium thiocyanate (NaSCN) in water. A physical three-dimensional network is formed after solvent exchange or solvent removal. The former occurs when the HYPAN polymer in DMSO is placed in water. The latter involves drying.

The pH sensitive polymer microspheres are polyTCPA-VBC particles containing amine groups and polyVBC particles containing dicarboxylate groups. The bead concentration is 4% (w/w) if not otherwise mentioned. A typical formula is to add 0.0400 g of beads to 0.6000 g of DMSO. After completely suspending the beads by sonicating and stirring, 0.4000 g of 10% HYPAN polymer in DMSO is added into the mixture. Therefore, the final suspension contains 0.0400 g beads, 0.0400 g of HYPAN polymer, and 0.9600 g of DMSO. The above procedures and the amounts of beads, HYPAN polymer and DMSO are all critical to the sensor formulation. First, the solution of HYPAN polymer in DMSO is very viscous. At the same time, it has to be free of water to prevent coagulation. That means the microspheres must be dry when added to the HYPAN polymer solution. It is impossible to obtain a good suspension if the dry microspheres are directly added into the HYPAN polymer solution because the microspheres coagulate together in the viscous solution. Therefore, we first suspend the dry microspheres in DMSO and then add 10% HYPAN polymer solution to obtain a good suspension. Second, the HYPAN polymer concentration in the suspension is 4% (wt/wt) in DMSO. This concentration has low viscosity and good flow for spin coating. Figure 6-6 shows that the total thickness of the polyurethane and 4% HYPAN HN50 is about 8.0

162

μm. The HYPAN solution is also spin-coated at 2500 rpm with quick start and stop for 20 seconds. Therefore, the thickness of the HYPAN membrane is probably about 4.0 μm, the same as the polyurethane membrane shown in Figure 6-3. Third, DMSO can pre-swell the polyurethane layer, which promotes a good adhesion of the coating. The coating is dried at ambient temperature for 24 hours. Finally, the amount ratio of the microspheres to the HYPAN polymer in the sensitive membrane is 1:1. This ratio has suitable mechanical properties for monitoring solution pH.

6.2.3 pH measurements

The pH measurement was described in Section 3.4.7. Two kinds of microspheres were used for pH measurements. One was diethylamine derivatized polyTCPA-VBC. In our first experiment, the suspension was spin-coated on a bare ribbon without a polyurethane adhesion layer. Figure 6-7 shows that its resonance frequency varies with pH. We see that the resonance frequency increases as the pH increases. This result is probably caused by changes in both the water content and the material modulus. From Chapter 4 we know that the amine derived polyTCPA-VBC particles are protonated as the pH changes from 8.0 to 6.0. Due to the static electric force caused by introduction of a charge onto the polymer backbone, the particles swell when pH decreases. This results in increased water content and lower material modulus. Luckily, both these two factors affect the resonance frequency positively, and cause the resonance frequency to decrease. The particles deprotonated with increasing pH. At this time, the particles shrink. This causes the water content to decrease and material modulus to increase. It is observed that

163

the resonance frequency increase as the pH increasing. Usually the ribbon without a polyurethane layer gets rusty after one measurement cycle.

Figure 6-8 shows two measurement cycles for the resonance frequency of a pH sensitive ribbon with a polyurethane layer. It is observed that the polyurethane layer does not affect the solution pH measurement. Furthermore, this ribbon can withstand the pH changes for many cycles without rusting. It is observed that the pKa is around 6.8. Therefore, this sensitive ribbon responds to pH from 6.0 to 8.0.

The other pH sensitive microspheres that were used were polyVBC containing carboxylate groups. Figure 6-9 shows the resonance frequency of a pH sensitive ribbon. The ribbon is coated with polyurethane and HYPAN membranes. PolyVBC particles containing carboxylate groups are entrapped in the HYPAN membrane. It is known that malonic acid has two pKa's, one at 2.847 and one at 5.696. However, Figure 6-9 shows that the resonance frequency continuously decreases as the pH changes from 2.0 to 8.0. We can't see separate regions corresponding to different pKa's. This result agrees with that measured optically in Chapter 4 and is probably caused by partial hydrolysis of diethyl malonate. As mentioned in Chapter 4, we know that the sizes of polyVBC particles are larger than that of polyTCPA-VBC particles. Moreover, the thickness of the HYPAN membrane is about 4.0 μm. This results in poor adhesion of the HYPAN membrane containing large polyVBC particles on the polyurethane substrate. Therefore, we can't run multiple measurement cycles for the membrane used for the data in Figure 6-9. The variation in resonance frequency with pH in Figure 6-9 differs from that in Figure 6-8 because the polyVBC particles containing carboxylate groups are neutral when protonated at low pH and charged when deprotonated at high pH. However, the

effects of the water content and material modulus are same as for amine derivatized

polyTCPA-VBC particles.

Polyacrylonitrile Multi-Block Copolymer

Hard block   Soft block
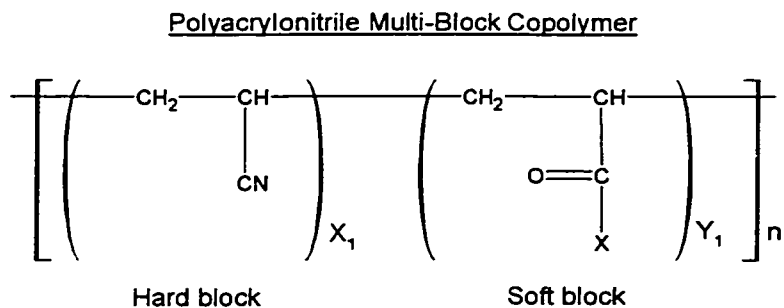
Soft Block Compositions
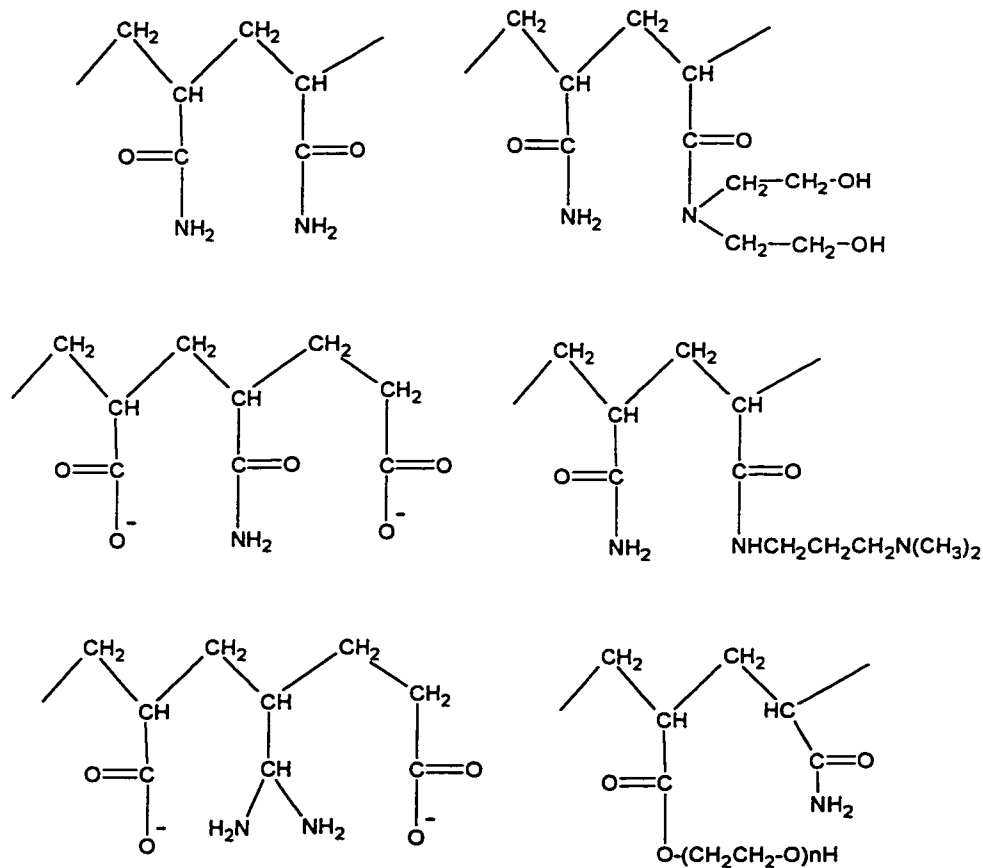
Figure 6-5 HYPAN copolymer structure and typical groups of the soft blocks

165
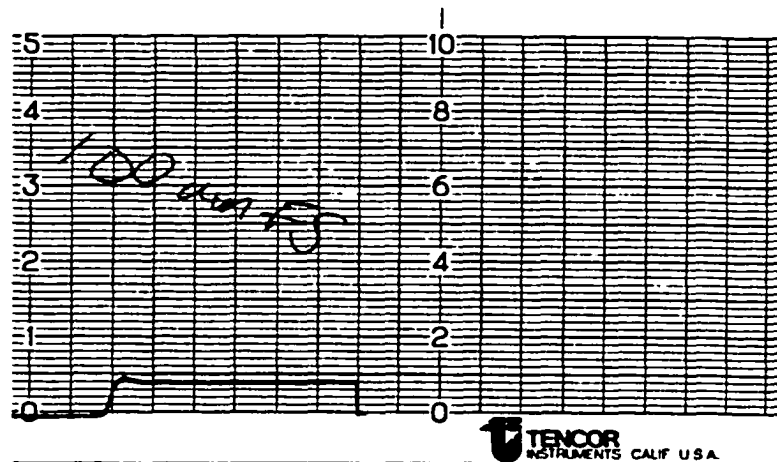
Figure 6-6 Total thickness of polyurethane membrane and 4% HYPAN HN50 membrane
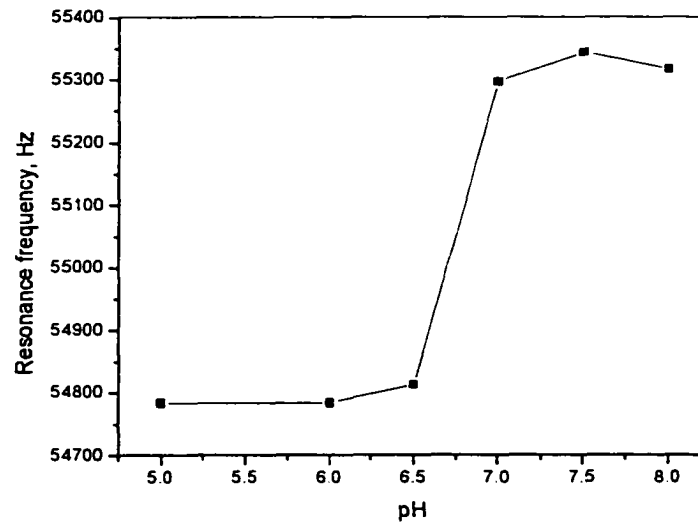
Figure 6-7 Resonance frequency vs. pH for a ribbon coated with HYPAN HN 50 membrane containing amine derivatized polyTCPA-VBC microspheres

166
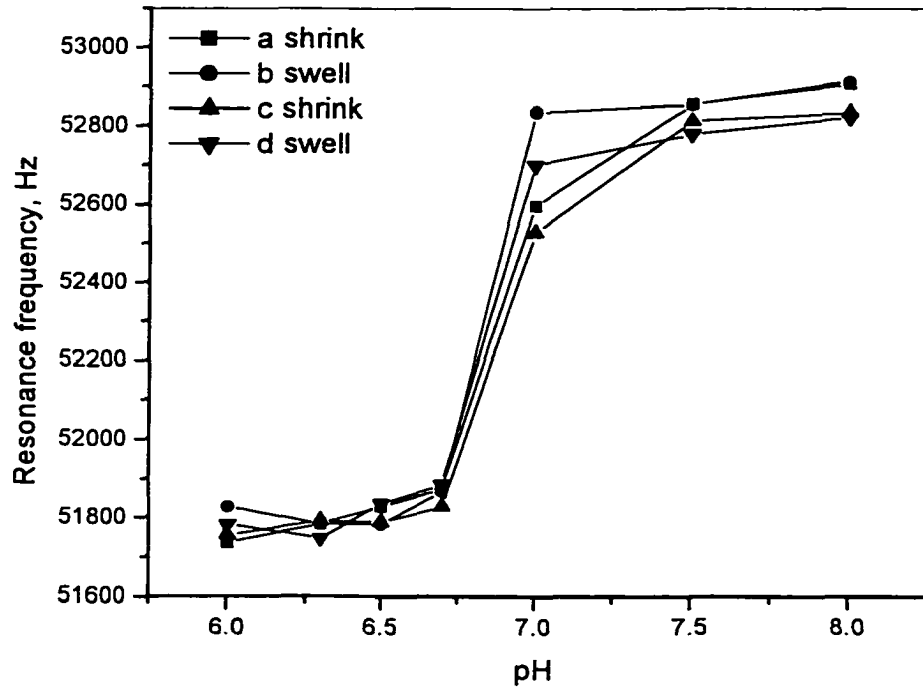
Figure 6-8 Resonance frequency vs. pH for aminated polyTCPA-VBC particles in HYPAN HN50 coated on the polyurethane layer

167
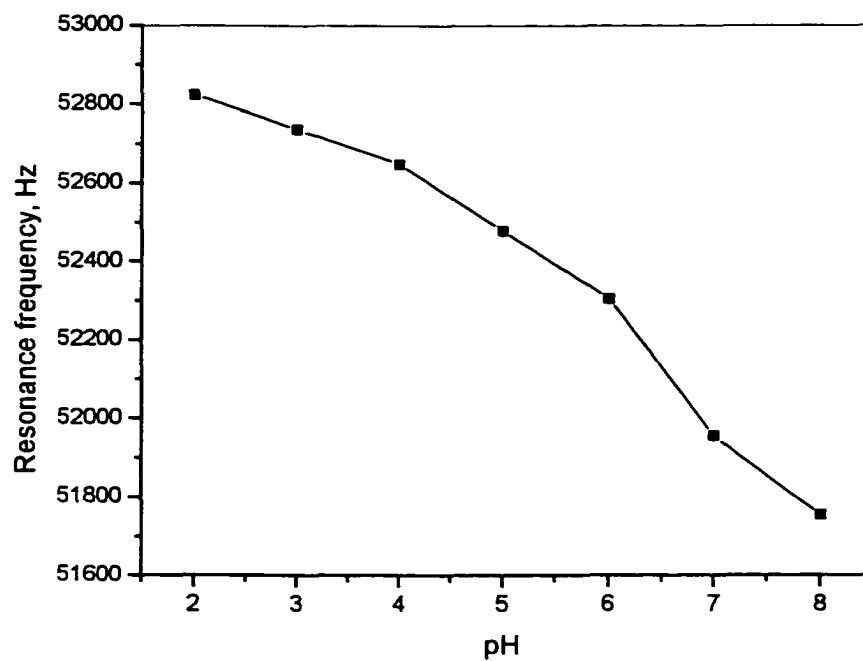
Figure 6-9 Resonance frequency vs. pH for a ribbon coated with polyurethane layer and HYPAN HN50 membrane entrapped with carboxylated polyVBC particles.

168

6.2.4 Response time

The current Resonance Meter in our group can only scan a pre-determined frequency range to obtain a resonance frequency peak. Then the resonance frequency is determined from this peak. Usually it takes 1 to 4 minutes to obtain one peak, depending on the pre-determined frequency range and scan rate. For example, it takes 3 minutes to scan from 56 to 58 kHz if 200 data points are taken. It is difficult to study the response time with this slow rate of recording the resonance frequency. Therefore, the Resonance Meter has been updated since it was developed in Grimes' research group. At present, the Resonance Meter in Grimes' group can directly record the resonance frequency without scanning the whole frequency range. It only takes 500 milliseconds to record a resonance frequency. Figure 6-10 shows the response time when a pH sensitive ribbon is immersed in different buffers. The ribbon was made in our research group. It was first coated with polyurethane and then coated with 4% HYPAN HN 50 with 4% amine derived polyTCPA-VBC microspheres. The response time was measured by the Grimes' research group with the updated Resonance Meter. The sensitive ribbon was alternately placed in pH 4.5 and pH 8.1 buffers. The buffers were made from a mixture of 0.015 M acetic acid and 0.015 M K_2HPO_4. The pH values were adjusted using 1 M HCl or 1 M NaOH. All measurements were performed at a temperature of 23 ± 1^0C. It is observed from Figure 6-10 that the pH sensitive ribbon is immersed in each buffer for 10 minutes. There are three measurement cycles. The response is so fast that the resonance frequency shifts immediately after changing the pH buffer. This agrees with the results measured with optical methods.

169
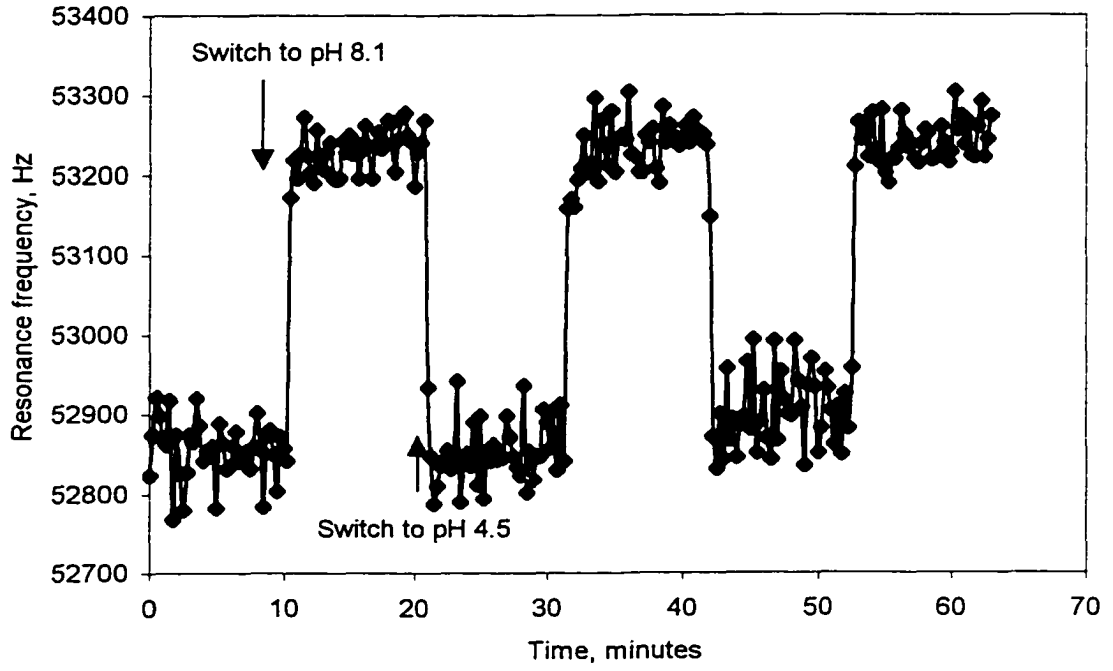
Figure 6-10 Response time of a ribbon coated with HYPAN HN 50 membrane containing amine derived polyTCPA-VBC particles

170

6.2.5 Hysteresis of the resonance frequency in different HYPAN membranes

HYPAN polymers have special swelling properties when they swell in water. The final water content depends not only on the type of HYPAN, but also on the polymer concentration before the coagulation step. Table 6-1 shows the water content of HYPAN HN68 at different polymer concentrations.[82] The swelling degree decreases as the polymer concentration increases. The reason is that intra-chain clustering dominates at low polymer concentration and inter-chain clustering dominates at high polymer concentration. The polymer swells more in the former case than in the latter. This means that the water content of the membrane can be controlled without changing chemical composition of the polymer. It is known that the modulus of HYPAN polymers decreases as the water content increases. Therefore, the material modulus is closely related to both the HYPAN type and its concentration. Table 6-2 shows the mechanical properties and permeability of HYPAN HN50 and HN70.[81] The strength E_0 of the material is defined as the stress at fracture. The elongation-to-break is defined as the strain at fracture. The larger the elongation-to-break is, the more ductile the material. The elastic modulus is the slope of the stress-strain curve evaluated at the origin. It is calculated using equation (2-2) where the elastic modulus is the ratio of the stress over the strain.

The above information is very important for developing sensitive ribbons and analyzing their frequency responses. First, the purpose of coating the hydrogel membrane is to hold pH sensitive microspheres on the ribbon. There are three main requirements for the hydrogel membrane. One is to adhere to the polyurethane substrate. Second is to have large shifts in the resonance frequency when the microspheres swell or

171

shrink. Another is to be highly permeable to the analytes. Considering all of these factors, we suspended 4% microspheres in 4% HYPAN polymer solution in DMSO. The dried sensitive membrane contains 1:1 (w/w) microspheres:HYPAN. We want to make the ratio as large as possible while maintaining good adhesion. Mechanical effects that depend on the hydrogel membrane were observed when using different HYPAN types. Figures 6-11, 6-12, and 6-13 show the resonance frequency vs. pH for sensors prepared with HN30, HN50, and HN80. The pH sensitive microspheres are amine derivatized polyTCPA-VBC. It is observed that the resonance frequency measured for increasing pH differs form that for decreasing pH, i.e. two curves measured during increasing and decreasing pH do not completely overlap. This phenomenon is known as hysteresis. The hysteresis differs for different HYPAN types. We find that the hysteresis decreases when the water content in the hydrogel increases. The hysteresis is smallest in Figure 6-13 using HYPAN HN80 to make the hydrogel membrane. From Table 6-2, we know that HN80 has the smallest elastic modulus and largest permeability coefficient among HN30, HN50, and HN80. The microspheres easily overcome the mechanical resistance of the hydrogel membrane to swell with decreasing pH. When they shrink, they do not collapse suddenly due to the small recovery force of the hydrogel membrane. In this case, the response of the sensitive ribbon is basically controlled by the properties of the microspheres.

172

Table 6-1. Water content of HYPAN HN68 at different polymer concentrations[82]

Polymer Concentration	Water Content at Swelling Equilibrium (%)
25%	71.0
35%	66.0
50%	60.7

Table 6-2 Mechanical properties and permeability of HYPAN HN50 and HN70[81]

Property	HN50	HN70
Water Content (%)	55.0	73.0
Tensile Strength (kg/cm^2)	65.0	15.0
Elongation at Break (%)	400	1180
E_0 (kg/cm^2)	70.0	16.0
Elastic Modulus (kg/cm^2)	16.3	1.3
Permeability Coefficient of water P x 10^7 (cm^2/sec)	7.0	50
Permeability Coefficient of NaCl P x 10^7 (cm^2/sec)	1.8	45
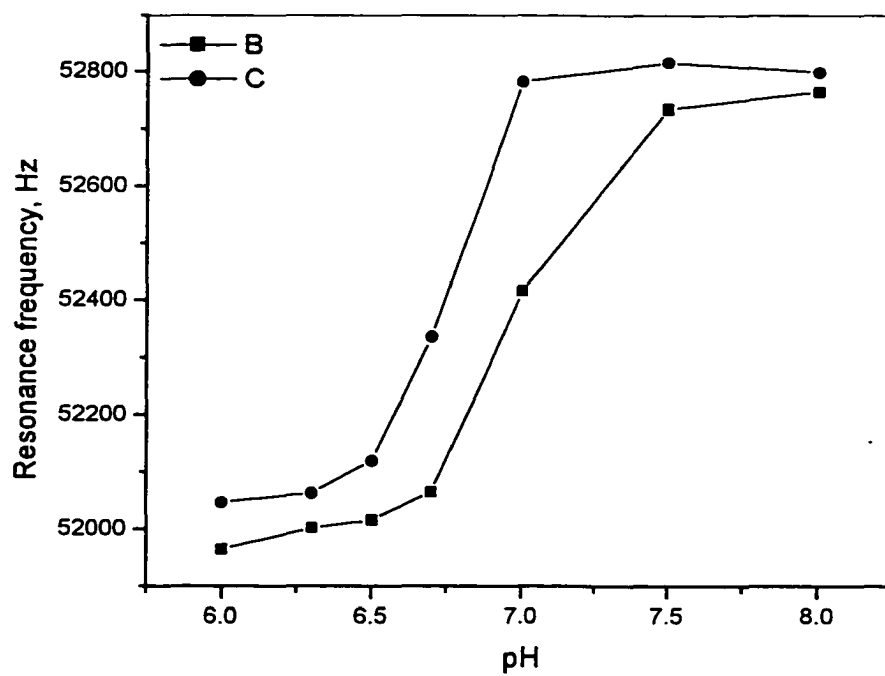
Figure 6-11 Resonance frequency vs. pH for HYPAN HN30 containing entrapped amine derivatized polyTCPA-VBC microspheres.

174
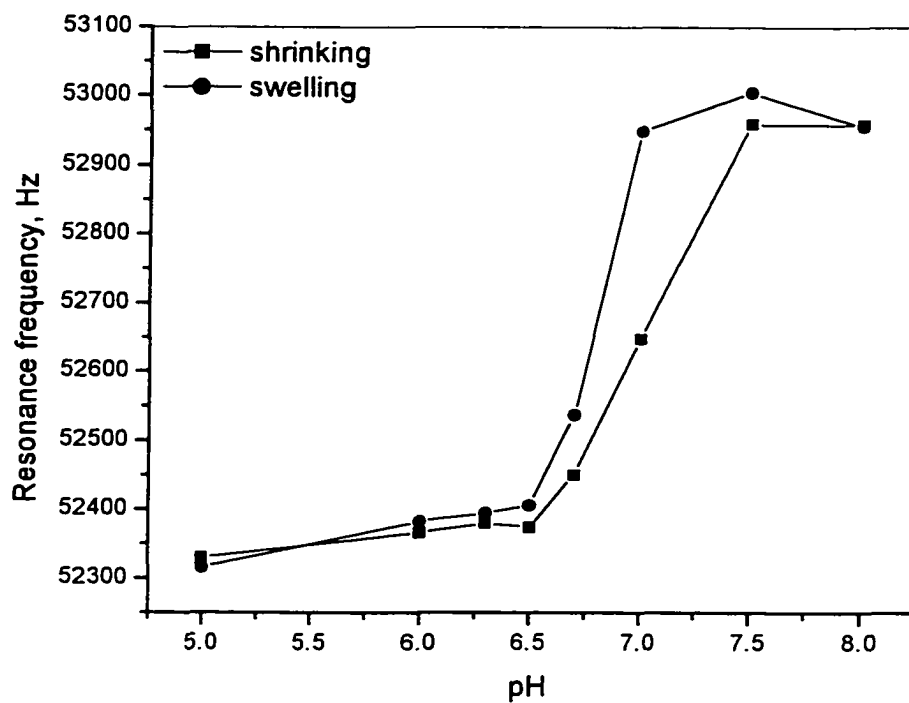
Figure 6-12 Resonance frequency vs. pH for HYPAN HN50 containing entrapped amine derivatized polyTCPA-VBC microspheres.
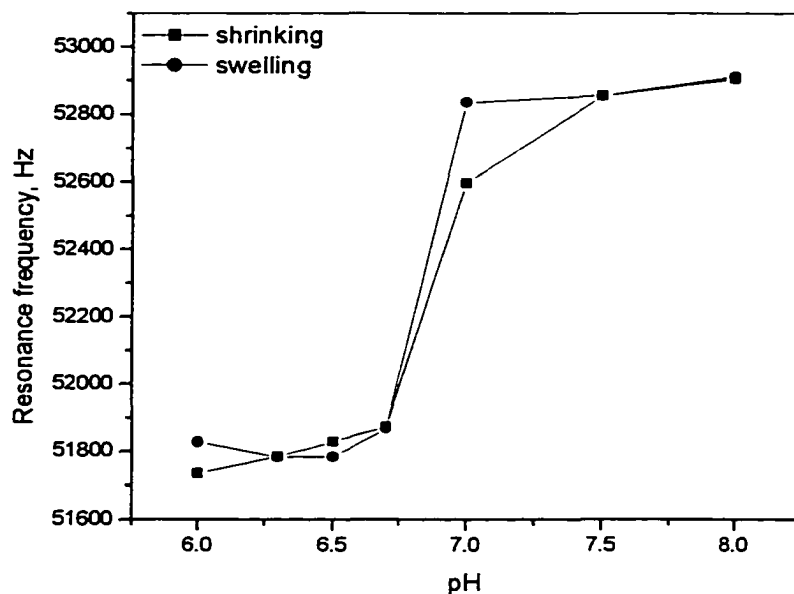
Figure 6-13 Resonance frequency vs. pH for HYPAN HN80 containing entrapped amine derivatized polyTCPA-VBC microspheres.

6.2.6 Stability

A ribbon coated with polyurethane and HYPAN HN 50 membrane containing amine derivatized polyTCPA-VBC microspheres was immersed in water for 10 hours, pH5 buffer for 10 hours, and pH8 buffer for 10 hours. Figure 6-14 shows that the resonance frequency fluctuated only slightly. First, it indicates that the polyurethane layer is a good protection from corrosion. As mentioned early, a bare ribbon would rust after 30 hours in water. Second, no sudden changes in resonance frequency were observed, which confirms that the HYPAN membrane adheres to the polyurethane layer very well. Curves a, b, and c in Figure 6-15 show the resonance frequency peaks for the

176

coated ribbon sitting in water for 10 hours, pH5 buffer for 10 hours, and pH8 buffer for

10 hours, respectively. It is observed that all three peaks remain sharp. This further

indicates that the membrane adheres to the substrate because the resonance frequency

peak would be damped if the HYPAN membrane partly delaminated from the

polyurethane layer. Finally, the pH sensitive microspheres continue to respond after

staying in the swollen and shrunken states for a long time. Usually, it takes only several

minutes to finish one measurement if we make disposable sensitive ribbons in the future.
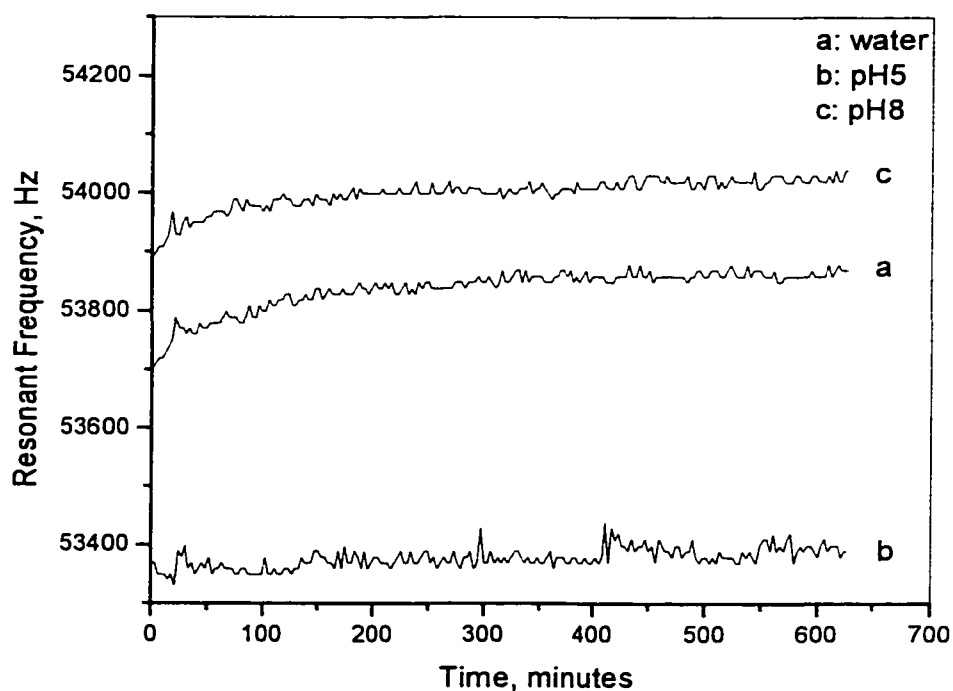
Figure 6-14 Resonant frequency vs. time for a coated ribbon containing amine
derivatized polyTCPA-VBC microspheres immersed in water for 10 hours, pH 5.0 buffer
for 10 hours, and pH 8.0 buffer for 10 hours.
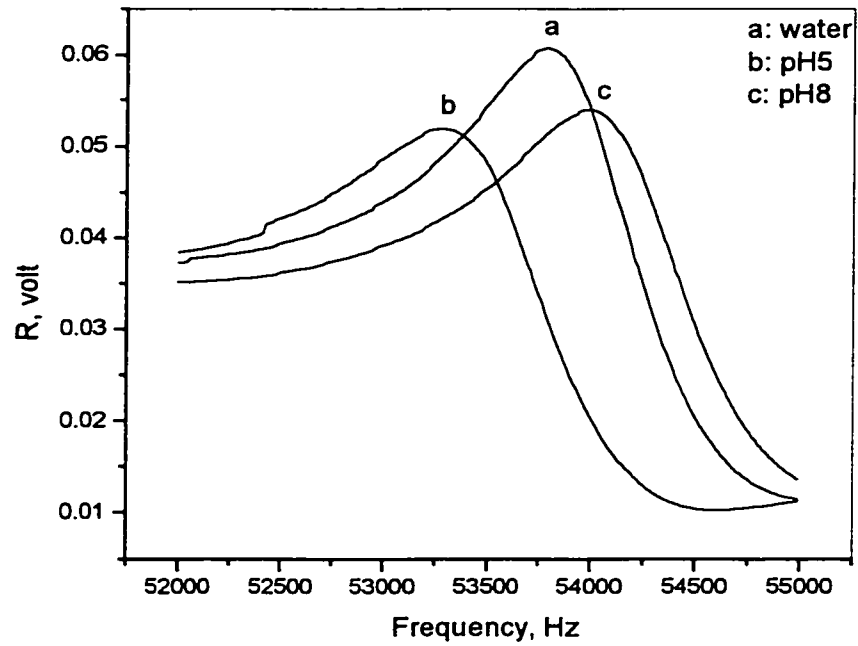
Figure 6-15 The resonance frequency peaks after the ribbon was immersed in water for 10 hours, pH 5.0 buffer for 10 hours, and pH 8.0 buffer for 10 hours.

178

6.2.7 Effect of bead concentration on the resonance frequency of a sensitive ribbon

Five ribbons were initially spin coated with polyurethane layers. Five suspensions were made of 4% HYPAN HN50 containing amine derivatized polyTCPA-VBC microspheres. Their concentrations were 0, 1.0%, 2.0%, 3.0%, and 4.0%, respectively. These suspensions were spin-coated onto the ribbons to make five coated ribbons containing different bead concentration. Table 6-3 shows the resonance frequency of each ribbon in different buffers. The resonance frequency of each ribbon was first measured in pH 3.0 buffer, and then in pH 8.0 buffer. The resonance frequency shift is defined as the difference between the resonance frequencies measured in pH 3.0 and pH 8.0. Figure 6-16 shows that the resonance frequency shift increases as the bead concentration increases. The linear regression equation is:

$$\text{Resonance frequency shift} = 26 + 249 \times (\text{beads concentration})$$

Obviously, a simple method to increase the signal is to increase the beads concentration. However, there is a maximum practical bead concentration. First, the HYPAN polymer solution in DMSO is very viscous. It is difficult to suspend the pH sensitive microspheres in the HYPAN solution without coagulation. Second, we notice that DMSO is removed through evaporation after the HYPAN membrane forms. Therefore, DMSO should not be included when calculating the true bead concentration in the HYPAN membrane. For example, the suspension of 4% beads in 4% HYPAN HN50 polymer in DMSO contains equal amount of beads and HYPAN HN50. There are only beads and HYPAN HN50 polymer left in the sensitive membrane after DMSO is removed. The bead concentration is actually 50% in the membrane. We know that the mechanical properties of both the beads and the hydrogel membrane affect the resonance

179

frequency of the coated ribbon. The mechanical properties are controlled not only by the

HYPAN types, but also by the ratio of beads to the HYPAN polymer. Therefore, we

should consider this ratio when we vary the beads or the HYPAN polymer concentration.

Table 6-3 Measurements of the resonance frequency at different beads concentrations

Beads concentration in the sensitive membrane, %(wt/wt)	Resonance frequency in pH3.0 buffer, Hz	Resonance frequency in pH8.0 buffer, Hz	Resonance frequency shift, Hz
0	54651	54657	6
1.0	54417	54805	388
2.0	54315	54723	408
3.0	54200	54940	740
4.0	53774	54847	1073

180
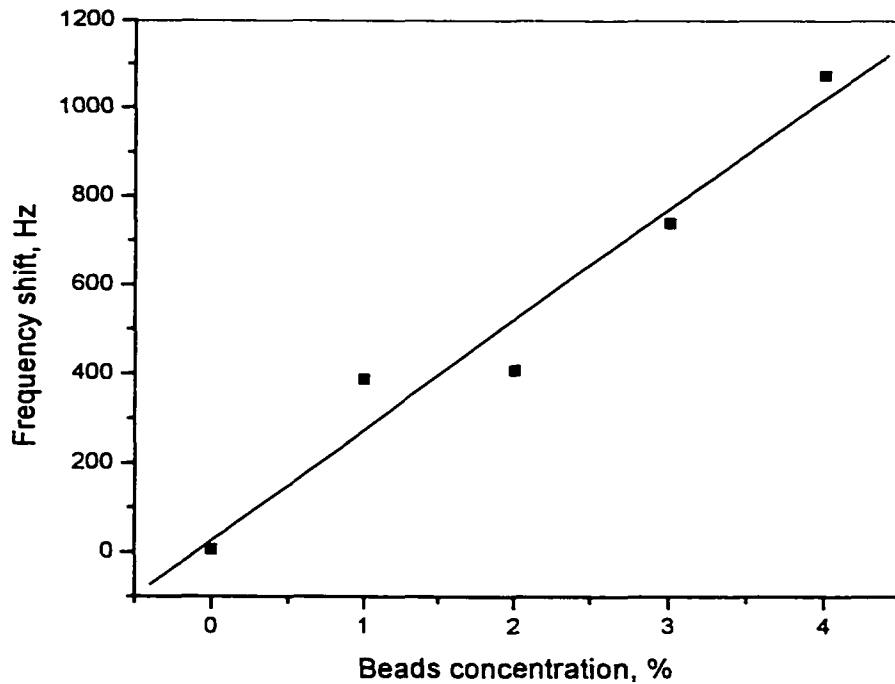
Figure 6-16 Resonance frequency shift vs. bead concentration in the HYPAN HN 50 membrane

6.3 Conclusion

Chemical sensors were prepared by coating magnetoelastic ribbons with a

chemically sensitive layer. We initially spin coated waterborne polyurethane on both

sides of the ribbon. The polyurethane layer protected the ribbon from rusting without

affecting the resonance frequency. The thickness of the polyurethane was about 4.0

micrometers.

181

HYPAN structural hydrogel polymers were used to hold pH sensitive microspheres. A typical formulation is 4% beads in 4% HYPAN polymer solution in DMSO. DMSO can pre-swell the polyurethane layer and increase the adhesion to the HYPAN membrane. PolyTCPA-VBC microspheres containing amine groups were used to monitor pH from 6.0 to 8.0. These microspheres swell at low pH and shrink at high pH. The resonance frequency increases as the pH increases. PolyVBC microspheres containing carboxylate groups were used to monitor pH from 2.0 to 8.0. These microspheres shrink at low pH and swell at high pH. The resonance frequency decreases as the pH increases.

Swelling and shrinking can affect the resonance frequency because they change the water content and elastic modulus of the sensitive membrane. It should be noted that mechanical properties of the membrane also affect the frequency. Therefore, all variables that affect the mechanical properties of the sensitive membrane, such as the HYPAN type and the ratio of the beads to the HYPAN polymer in the dry membrane, should be carefully controlled. The goal is to minimize the effects of the hydrogel membrane and maximize the effects of the pH sensitive microspheres. Another advantage of the pH sensitive ribbon is that it can be used many times when monitoring solution pH. Dried sensitive ribbons have long shelf lives without special storage requirements. Considering the convenience, cost, and other advantages of this sensor unit, magnetoacoustic sensors are expected to have a variety of applications in the future.

182

CHAPTER 7

CONCLUSIONS

PolyTCPA-VBC microspheres were prepared by dispersion polymerization. The purpose of making this copolymer is to increase the hydrophilicity and introduce porosity of the polymer material. The polyTCPA-VBC microspheres are derivatized with diethylamine to introduce pH sensitive tertiary amine on VBC groups and hydrophilic amide groups on the TCPA groups. The derivatized microsphere swell at pH lower than pH 6.0 and shrink at pH higher than pH 8.0.

PolyVBC particles were prepared by suspension polymerization. They were lightly crosslinked with DVB. A mixture of xylene and dodecane was used as the porogenic solvent. After polymerization and removing solvent, the space occupied by the porogenic becomes pore space. In order to obtain small particles by suspension polymerization, we used a new technique called SPG to prepare the monomer emulsion. In addition to the pore size in the glass membrane, many factors like applied pressure and the amount of reagents affect the sizes of emulsion droplets. The polyVBC particles are derivatized with diethyl malonate in a non-aqueous system and then hydrolyzed in 1:1 water:DMSO. The final derivatized polyVBC particles contain carboxylate groups. They are protonated at high pH and de-protonated at low pH.

Optical properties of derivatized polyVBC-TCPA and polyVBC particles were studied through turbidity measurements. These particles are entrapped in a hydrogel

183

membrane. Then the sensitive membranes were placed in different pH buffers and their turbidities were measured. The turbidities of the sensitive membrane containing derivatized polyTCPA-VBC particles increase as the pH increase, but those containing derivatized polyVBC particles decrease as the pH increase. Different hydrogels, such as PVA and different HYPAN polymers were used to prepare the hydrogel membranes. Their effects in response time and hysteresis were studied. The hydrogel membranes that contain high water content had fast response and less hysteresis. Probably the material elastic modulus is involved in the response process.

A thin layer of sensitive membrane was spin-coated on a magnetoelastic ribbon. Before that, a thin layer of polyurethane had been spin-coated on both sides of the ribbon. The polyurethane layer prevents the ribbon from rusting and increases its adhesion to the sensitive membrane. Many factors, such as viscosity of the hydrogel solution, speed of the spin-coater, and the size of the particles, affect the process of making a sensitive membrane on a ribbon. The final sensor element is a magnetoelastic ribbon coated with a layer of hydrogel membrane containing pH sensitive polymer particles. Now it is ready to monitor solution pH at a determined range in a sealed container. For example, we can put the sensitive ribbon in a Teflon cell with a pH buffer and then put the cell at the center of the pick-up coils of the Resonance Meter. If the sensitive ribbon contains derivatized polyTCPA-VBC particles, its resonance frequency increases as the pH increases from pH 6.0 to 8.0. If the coated ribbon contains derivatized polyVBC particles, its resonance frequency decreases as the pH increases from pH 2.0 to 8.0. Different HYPAN polymers were used to prepare the hydrogel membranes and their effects to the frequency responses were also studied.

184

Many factors that affect the frequency responses of the coated ribbon and many possible applications of the Resonance Meter have been studied in this thesis. These factors include ribbon length, ribbon bending, ribbon coatings, membrane thickness, membrane types, particles concentration, and so on. In addition to monitoring pH, the resonance meter can also be used for monitoring viscosity changes, mass loading, and polymerization.

Based on the above results, we can summarize as following. First, swellable microspheres can be used to make sensor elements. They can be derivatized to sense different analytes. Second, magnetoacoustic sensors provide not only new instruments but also new ideas for chemical sensing. Because they do not need any electrical connections to the sensitive elements, they have many possible applications in the future. For example, they can be used to monitor gastric pH of patients. They are ideally to be used in sealed containers or contaminated environment. However, there are still some problems that remain to be solved, such as hysteresis and determining accuracy and precision. For the swellable polymer, we need to better control particle sizes and their distribution by varying polymer formulation and improving techniques.

185

APPENDIX A

FUNCTIONS OF COMPONENT METERS IN THE

MAGNETOACOUSTIC CHEMICAL SENSOR

The following lists all components of the Resonance Meter.

1. KEPCO PROGRAMMABLE DC POWER SUPPLY
It is used to generate the DC bias current and then the desired DC field.

2. MACKLE FR M1400 PROFESSIONAL POWER AMPLIFIER
It is used to amplify the sinusoidal AC voltage from the signal generator.

3. STANFORD RESEARCH SYSTEM, MODEL SR830 DSP LOCK-IN
   AMPLIFIER
This dual-channel lock-in amplifier that tracks the signal generator frequency receive
the preamplifier voltage from the pick-up coil and then send it to the controlling
computer.

4. KEITHLEY 2000 MULTIMETER
It is used to monitor the amplified AC voltage.

5. HEWLETT PACKARD 33120A 15MHz FUNCTION/ARBITARY
   WAVEFORM GENERATOR
It is used to output a sinusoidal AC voltage that is applied to a pair of Helmhotz coils.

6. EARTH WORKS PREAMPLILIFER
It is used to amplify the voltage from the pick-up coil.

7. A HOMEMADE COMPUTER INSTALLED WITH MICROSOFT WINDOWS
   95 AND MERM 3.03 CONTROLLIONG PROGRAM
It is used to control all meters.

8. A PAIR OF AC DRIVE COILS WITH HELMHOLTZ CONFIGURATION
It is used to generate a RMS magnetic field of 55 mOe.

9. A PAIR OF DC BIAS FIELD COILS WITH HELMHOLTZ CONFIGURATION
It is used to generate a 5.5 Oe DC magnetic field.

186

10. COMPENSATED PICK-UP COIL AND BUCKING COIL

They pick up the sensor responses and feed them into a preamplifier and then a lock-in amplifier.

Note:

There used to be a Hall Probe and a Gauss Meter included in the Resonance Meter. They were used to monitor the magnitude of the magnetic field. However, they were taken away after the Resonance Meter was updated because the users usually don't need to manually adjust the Resonance Meter. On the hand, it decreases the cost of the Resonance Meter.

187

APPENDIX B

THE OPERATIONAL PANEL OF THE CONTROLLING PROGRAM

The Resonance Meter is remotely controlled with a programmed computer. The current program is MERM 3.03b.EXE, which is written by Dr. K. G. Ong in Dr. Crimes's research group. Actually this program includes two controlling methods. One is called "One Time Measurement" that only runs the measurement for one time. The other one is called "Multiple Time Measurement" that automatically run the measurements for pre-determined times. Double click this executable file and open a main window as the operational panel. The blanks in control blocks are explained as following.

The Experiment Setting Block

Start Freq: the starting frequency (kHz) in one measurement

Stop Freq: the stopping frequency (kHz) in one measurement

Points: the number of data points that will be collected in one measurement

Delay: the time interval (millisecond) between two consecutive data points

Total Run: the repeated times of measurements. The final results are averages of all measurements.

Initial AC: the starting AC voltage (Volt in rms) outputted by the signal generator. The AC voltage varies through out the experiment to stabilize the AC current.

Initial DCC: the starting DC current (A) outputted by the DC power supply. The DC current varies through the experiment to stabilize the DC field.

ACC Band: the allowed tolerance (in %) for the fluctuation of the AC field

The Peak Finding Block

Points: the number of data points that will be collected during peak finding process

188

Delay: the data interval (millisecond) between two consecutive data points

Total Run: repeated times of the peak finding process. The final results are averages of all measurements.

The Time Control Block

The functions in this block are enabled only when running "Multiple Time Measurement"

Total Set: the number of measurements that will be automatically run

Delay (Min): the time interval between two consecutive sets of measurements

File Name: the preferred file name that will be automatically saved during measurements

The Control Panel Block

Start: start running the "One Time Measurement" controlling method

Stop: stop running the "One Time Measurement" controlling method

Time Start: start running the "Multiple Time Measurement" controlling method

Time Stop: stop running the "Multiple Time Measurement" controlling method

The measuring process can be monitored through the Measurement Block, Peak Block, Progress Plot, and the Message Box. The Measuremenst Block is at the center column on the main window. It includes varying values from the signal generator, lock-amplifier, and digital multimeter. The Peak Block shows the frequency and amplitude of the final peak. The Progress Plot is at the top right of the main window. It shows the magnitude as a function of the frequency. The Message Box is at the bottom of the main window. It shows the current data point that is being measured.
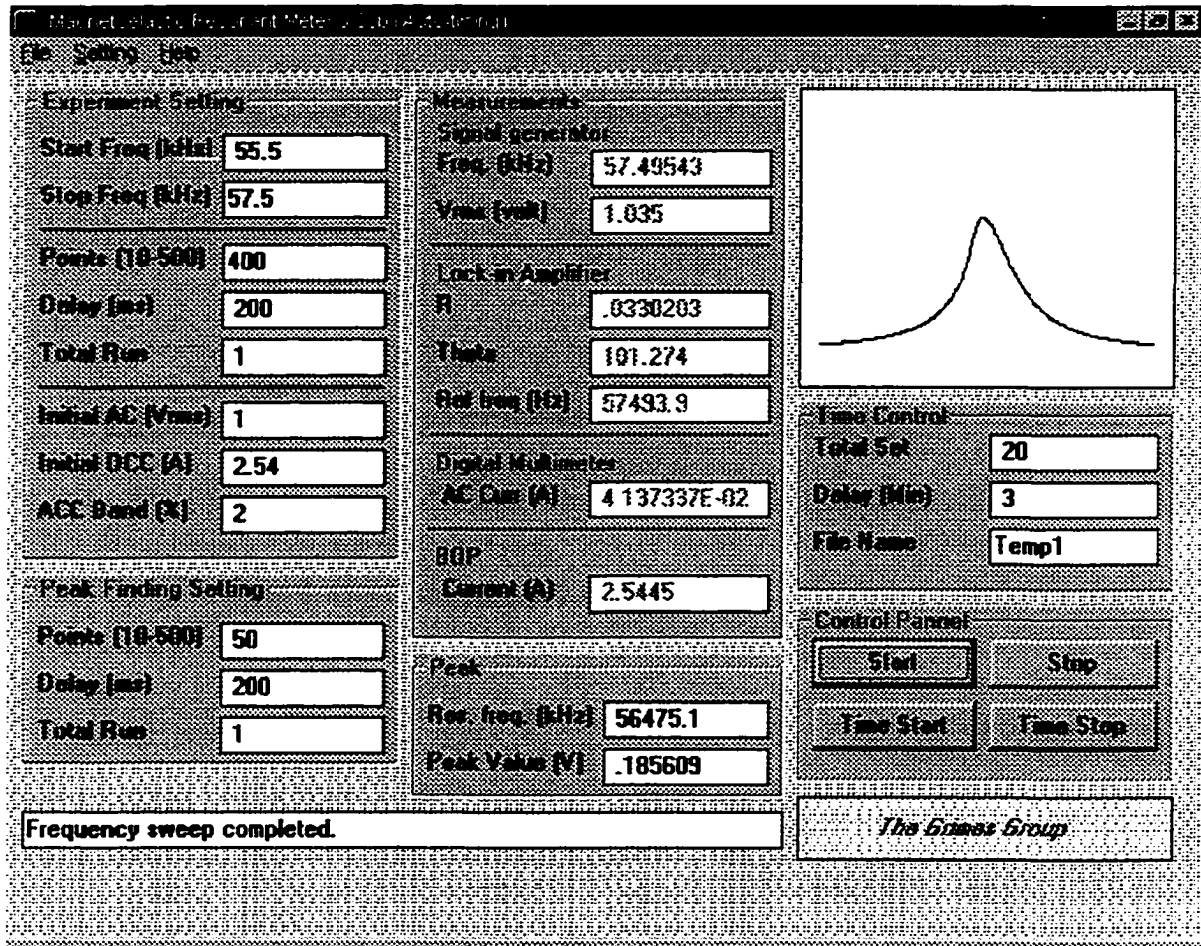
189

Figure B-1 Screenshot of the operational panel of the controlling program of the Resonance Meter

190

APPENDIX C

INSTRUCTIONS FOR OPERATING THE RESONANCE METER

The operational procedures of the Resonance Meter are summarized as following.

1. Remove all metallic parts from the workbench. Make sure no ribbons at the center of the pick-up coil.

2. Turn on all meters and allow them to warm up for 15 minutes. Put the right toggle switch of the EARTHWORKS Preamplifier to ON position.

3. Turn on the computer and open the MERM 3.03b.EXE file.

4. Set experiment setting values in the operational panel. Typically the following values need to be set: Start Freq, Stop Freq, and Points in the Experiment Setting Block; Points, Delay, and File Name in the Time Control Block. Other settings can keep the default values

5. Put the sensitive ribbon in a Teflon cell, which contains the tested solutions. This cell is put at the center of the pick-up coil.

6. In the Control Panel Block, click the "Start" button if just want to run the measurement for one time, which is "One Time Measurement". Otherwise, click the "Time Start" button to automatically run multiple measurements, which is "Multiple Time Measurement". If the measurements run very well, they will automatically stop.

7. If run "One Time Measurement", save the file after the measurements. If run "Multiple Time Measurement", a file name is needed before measurements and the file is automatically saved during the measurements.

8. After all measurements, take out samples and sensitive ribbons from the center of the pick-up coil.

9. Close the program. Turn off the computer and then all meters.

191

Notes:

1) For "One Time Measurement", the Peak Finding Routine is typically turned off because it significantly increases the experiment time. Checking it in the Setting menu if want to run it. Peak values can be read from the Peak Block, or the saved data points, or the graph after the data points are plotted using other softwares. For "Multiple Time Measurement", the Peak Finding Routine is automatically turned off. Peak values are automatically saved in the file that has been given a name before the measurements.

2) Usually all meters should be turned off at the end of the day. If it is idle for a few hours during the day, the toggle switch on the EARTHWORKS Preamplifier should be put down to STANDBY.

3) All saved files can be re-opened and analyzed using the pre-installed Kaleidagraph software. Other softewares like Microsoft Excle can also be used to analyze the saved data points.

4) It is suggested not to manually stop the running program during measurements because this may result in freezing all meters. If this happens, close the program, turn off all meters, and then restart them.

192

REFERENCES

1. Chemical Sensors and Microinstrumentation, Murray, R. W.; Dessy, R. E.; Heineman, W. R.; Janata, J.; Seitz, W. R.; Ed., American Chemical Society, Washington D. C.: **1989**

2. Fiber Optical Chemical Sensors and Biosensors, Volume I., Wolfbeis, O. S.; Ed., CRC Press, Boca Raton, FL: **1991**

3. Principle of Chemical Sensors, Janata, J.; Pleenum Press, New York, **1989**

4. Surface-Launched Acoustic Wave Sensors: Chemical Sensing and Thin-Film Characterization, Thompson, M.; Stone, D. C.; John Wiley & Sons, Inc., New York, NY: **1997**

5. Principles of Chemical and Biological Sensors, Diamond, D.; Ed., John Wiley & Sons, Inc., New York, NY: **1998**

6. Janata, J.; Josowicz, M.; Vanysek. P.; DeVaney, D. M.; *Anal. Chem.* **1998**, 70(12), 179R-208R
    Janata, J.; Josowize, M.; DeVaney, D. M.; *Anal. Chem.* **1994**, 66(12), 207R-228R
    Janata, J.; *Anal. Chem.* **1992**, 64(12), 196R-219R; **1990**, 62(12), 33R-44R.
    Janata, J.; Bezegh, A.; **1988**, 60(12), 62R-74R.

7. King, W. H.; *Anal. Chem.* **1964**, 36(9), 1735-1739.

8. Thompson, M.; Kipling, A. L.; Duncan-Hewitt, W. C.; *Analyst* **1991**, 116(9), 881-890.

9. O'Sullivan, C. K.; Guilbault, G. G.; *Biosensors & Bioelectronics* **1999**, 14, 663-670

10. Wohltjen, H.; Dessy, R.; *Anal. Chem.* **1979**, 51(9), 1458-1464; **1979** 51(9), 1465-1470

11. Carey, W. P.; Beebe, K. R.; Kowalski, B. R.; Illman, D. L.; Hirschfeld, T.; *Anal. Chem.* **1986**, 58(1), 149-153.

12. Carey, W. P.; Kowalski, B. R.; *Anal. Chem.* **1986**, 58(14), 3077-3084.

13. Albert, K. J.; Lewis, N. S.; Schauer, C. L.; Sotzing, G. A.; Stitzel, S. E.; Vaid, T. P.; Walt, D. R.; *Chem. Rev.* **2000**, 100(7), 2595-2626.

14. Grate, J. W.; *Chem. Rev.* **2000**, 100(7), 2627-2648.

15. Lucklum, R.; Behling, C.; Hauptmann, P.; *Anal. Chem.* **1999**, 71(13), 2488-2496.

16. Chance, J. J.; Purdy, W. C.; *Analytical Letters*, **1999**, 32(9), 1751-1760.

17. Grate, J. W.; Martin, S. J.; White, R. M.; *Anal. Chem.* **1993**, 65(21), 940A-948A; **1993**, 65(22), 987A-996A.

18. Martin, S. J.; Granstaff, V. E.; Frye, G. C.; *Anal. Chem.* **1991**, 63(20), 2272-2281.

19. Kanazawa, K. K.; Gordon, J. G.; *Anal. Chim. Acta* **1985**, 175, 99-105.

20. Muramatsu, H.; Tamiya, E.; Karube, I.; *Anal. Chem.* **1988**, 60(19), 2142-2146.

21. Muramatsu, H.; Tamiya, E.; Suzuki, M.; Karube, I.; *Anal. Chim. Acta* **1988**, 215, 91-98

22. Shana, Z. A.; Radtke, D. E.; Kelkar, U. R.; Josse, F.; *Anal. Chim. Acta* **1990**, 231, 317-320

23. Yang, M.; Thompson, M.; *Langmuir* **1993**, 9(3), 802-811.

24. Ji, H.; McNiven, S.; Yano, K.; Ikebukuro, K.; Bornscheuer, U. T.; Schmid, R. D.; Karube, I.; Anal. Chim. Acta 1999, 387, 39-45.

25. Harsányi, G.; *Sensors and Actuators A* **1995**, 46-47, 85-88.

26. Handbook of Chemical and Biological Sensors, Taylor, R. F.; Schultz, J. S.; Ed., Institute of Physics Publishing, Bristol, UK, **1996**

27. Haupt, K.; Mosbach, K.; *Chem. Rev.* **2000**, 100, 2495-2504.

28. Peng, H.; Liang, C.; He, D.; Nie, L.; Yao, S.; *Talanta*, **2000**, 52, 441-448.

29. Ji, H.; McNiven, S.; Ikebukuro, K.; Karube, I.; *Anal. Chim. Acta* **1999**, 390, 93-100.

30. Ji, H.; McNiven, S.; Lee, K.; Saito, T.; Ikebukuro, K.; Karube, I.; *Biosensors & Bioelectronics* **2000**, 15, 403-409.

31. Haupt, K.; Noworyta, K.; Kutner, W.; *Anal. Commun.* **1999**, 36, 391-393.

32. Cox, M. T.; Hill, L. M. R.; Gahan, L. R.; *Analyst*, **1999**, 124, 859-863.

33. Stone, D. C.; Thompson, M.; *Anal. Chem.* **1993**, 65(4), 352-362.

34. Galipeau, D. W.; Vetelino, J. F.; Lec, R.; *Sensors and Actuators B* **1991**, 5, 59-65.

35. Seitz, W. R.; Rooney, M. T. V.; Miele, E. W.; Wang, H.; Necati, K.; Zhang, L.; Doherty, S.; Milde, S.; Lenda, J.; *Anal. Chim. Acta* **1999**, 400, 55-64.

36. Conway, V. L.; Dissertation, University of New Hampshire, **1994**

37. Rooney, M. T.; Dissertation, University of New Hampshire, **1996**

38. Miele, E. W.; Dissertation, University of New Hampshire, **1999**

39. Kaval, N.; Thesis, University of New Hampshire, **1998**

40. Wang, H.; Dissertation, University of New Hampshire, **2000**

41. Zhang, Z.; Shakhsher, Z.; Seitz, W. R.; *Microchim. Acta* **1995**, 121, 41-50.

42. Rooney, M. T. V.; Seitz, W. R.; *Anal. Commun.* **1999**, 36, 267-270.

43. Pan, S.; Conway, V.; Shakhsher, Z.; Emerson, S.; Bai, M.; Seitz, W. R.; Legg, K. D.; *Anal. Chim. Acta* **1993**, 279, 195-202.

44. Conway, V. L.; Hassen, K. P.; Zhang, L.; Seitz, W. R.; Gross, T. G.; *Sensors and Actuators B*, **1997**, 45, 1-9; **1997**, 45, 11-17.

45. Seitz, W. R.; *Journal of Molecular Structure* **1993**, 292, 105-114.

46. McCurley, M. F.; Seitz, W. R.; *Anal. Chim. Acta* **1991**, 249, 373-380.

47. Shakhsher, Z.; Seitz, W. R.; *Anal. Chem.* **1994**, 66(10), 1731-1735.

48. Zhang, L.; Langmuir, M. E.; Bai, M.; Seitz, W. R.; *Talanta* **1997**, 44, 1691-1698.

49. Zhang, L.; Dissertation, University of New Hampshire, **1998**

50. Kaval, N.; Seitz, W. R.; *Proc. SPIE-Int. Soc. Opt. Eng.* **1999**, 3860 (Fiber Optic Sensor Technology and Applications), 224-231.

51. Grimes, C. A.; Ong, K. G.; Loiselle, K.; Stoyanov, P. G.; Kouzoudis, D.; Liu, Y.; Tong, C.; Tefiku, F.; *Smart Mater. Struct.* **1999**, 8(5), 639-646.

52. Stoyanov, P. G.; Grimes, C. A.; *Sens. Actuators A* **2000**, A80(1), 8-14.

53. Grimes, C. A.; Stoyanov, P. G.; Kouzoudis, D.; Ong, K. G.; *Review of Scientific Instruments* **1999**, 70(12), 4711-4714.

54. <u>Fundamentals of Polymers</u>, Kumar, A.; Gupta, R. K.; The McGraw-Hill Companies, Inc., New York, **1998**

55. Grimes, C. A.; Kouzoudis, D.; *Sens. Actuators A* **2000**, A84(3), 205-212.

56. Cai, Q. Y.; Grimes, C. A.; *Sens. Actuators B* **2000**, B71(1-2), 112-117.

57. Polymer Chemistry: An Introduction, Stevens, M. P.; Oxford University Press, New York, NY 10016, **1999**.

58. Introduction to Polymers, Young, R. J.; Chapman and Hall, New York, **1981**.

59. Ellingsen, T.; Aune, O.; *J. Chromatography* **1990**, 535, 147-161.

60. Li, W.; Stöver, H. D. H.; Hamielec, A. E.; *Journal of Polymer Science: Part A: Polymer Chemistry* **1994**, 32, 2029-2038.

61. Scientific Methods for the Study of Polymer Collides and Their Applications, Candau, F.; Ottewill, R. H.; Kluwer Academic Publishers, Dordrecht, 1990.

62. Concise Polymeric Materials Encyclopedia, Salamone, A. C.; Ed., CRC Press, New York, **1998**.

63. Yuyama, H.; Watanabe, T.; Ma. G.; Nagai, M.; Omi, S.; *Colloids Surfaces A: Physicochemical and Engineering Aspects* **2000**, 168, 159-174.

64. Omi. S.; Katami, K.; Yamamoto, A.; Iso, M.; *Journal of Applied Polymer Science* **1994**, 51, 1-11.

65. Omi. S.; Katami, K.; Taguchi, T.; Kaneko, K.; Iso, M.; *Journal of Applied Polymer Science* **1995**, 57, 1013-1024

66. "Membrane Emulsification Operation Manual", 1st Ed., Nakashima, T.; Shimizu, M.; Kukizaki, M.; Department of Chemistry Industrial Research Institute of Miyazaki Prefecture, Miyazaki-city 880, Japan, **1991**.

67. Hirotsu, T.; Katoh. S.; Sugasaka, K.; Sakuragi, M.; Ichimura, K.; Suda, Y.; Fujishima, M.; Abe, Y.; Misonoo, T.; *Journal of Polymer Science: Part A: Polymer Chemistry* **1986**, 24, 1953-1966.

68. Deb, C.; Basu, B.; *Indian Journal of Chemistry* **1992**, 31B, 131-132.

69. Radhakrishnamurti, P. S.; Patro, P. C.; *J. Indian Chem. Soc.* **1969**, 46(10), 903-908.

70. Radhakrishnamurti, P. S.; Patro, P. C.; *Indian Journal of Chemistry* **1971**, 9, 1098-1101.

71. Radhakrishnamurti, P. S.; Patro, P. C.; *J. Indian Chem. Soc.* **1971**, 48(9), 811-816.

72. Zhujun, Z.; Zhang, Y.; Wangbai, M.; Russell, R.; Shakhsher, Z.; Grant, C. L.; Seitz, W. R.; Anal. Chem. 1989, 61(3), 202-205.

73. Bao, L.; Xie, Q.; Xu, Y.; Wei, W.; *Analytical Letters* **1999**, 32(5), 885-899.

74. Shi-Hui, S.; Tie-an, Z.; De-Zhong, L.; Li-Hua, N.; Shou-Zhuo, Y.; *Analytical Letters* **1994**, 27(1), 2027-2037.

75. Kipling, A. L.; Thompson, M.; *Anal. Chem.* **1990**, 62, 1514-1519.

76. Fundamentals of Acoustics, 3rd Ed., Kinsler, L. E.; Frey, A. R.; Coppens, A. B.; Sanders, J. V.; John Wiley & Sons, Inc., New York, **1982**.

77. "Waterborne Polyurethane Coatings: One and Two Component Systems", Henderson, R. S.; Presented at *42nd Annual Technical Symposium: Waterborne Coatings*, Cleveland, Ohio, April 22-23, **1999**.

78. "The Theology of Mixing in Two-Component Waterborne Polyurethane Coatings", Dvorchak, H. B.; Hudson, K.; Hunter, J.; Presented at the *Waterborne, High Solids and Powder Coatings Symposium*, February 5-7, 1997.

79. Rosthauser, J. W.; Nachtkamp, K.; *Advances in Urethane Science and Technology* **1987**, 10, 121-162.

80. Potter, T. A.; Williams, J. L.; *Journal of Coatings Technology* **1987**, 59, 63-72.

81. "HYPAN Structural Hydrogels", HYMEDIX International, Inc., Dayton, NJ. 08810

82. "Processing of HYPAN Hydrogels", HYMEDIX International, Inc., Dayton, NJ. 08810